EXPERIMENTAL STUDY OF TUNNELS IN SQUEEZING GROUND CONDITIONS

FINAL PROJECT REPORT

by
Arora K[1]
Gutierrez M[1]
Hedayat A[1]
[1] Colorado School of Mines

Sponsorship
UTC-UTI

For

University Transportation Center for
Underground Transportation Infrastructure
(UTC-UTI)

October 5th, 2020

Disclaimer

The contents of this report reflect the views of the authors, who are responsible for the facts and the accuracy of the information presented herein. This document is disseminated in the interest of information exchange. The report is funded, partially or entirely, by a grant from the U.S. Department of Transportation's University Transportation Centers Program. However, the U.S. Government assumes no liability for the contents or use thereof.

<table>
<tr><td colspan="2">1. Report No.</td><td>2. Government Accession No.</td><td colspan="2">3. Recipient's Catalog No.</td></tr>
<tr><td colspan="3" rowspan="2">4. Title and Subtitle
Experimental study of tunnels in squeezing ground conditions</td><td colspan="2">5. Report Date
October 5th, 2020</td></tr>
<tr><td colspan="2">6. Performing Organization Code</td></tr>
<tr><td colspan="3">7. Author(s)
Ketan Arora (Orcid.org/000-0001-5854-632X)
Marte Gutierrez (Orcid.org/0000-0001-5070-8726)
Ahmadreza Hedayat (Orcid.org/0000-0002-7143-7272)</td><td colspan="2">8. Performing Organization Report No: UTC-UTI 005</td></tr>
<tr><td colspan="3" rowspan="2">9. Performing Organization Name and Address
University Transportation Center for Underground Transportation Infrastructure (UTC-UTI)
Tier 1 University Transportation Center
Colorado School of Mines
Coolbaugh 308, 1012 14th St., Golden, CO 80401</td><td colspan="2">10. Work Unit No. (TRAIS)</td></tr>
<tr><td colspan="2">11. Contract or Grant No.
69A355174711</td></tr>
<tr><td colspan="3" rowspan="2">12. Sponsoring Agency Name and Address
United States of America
Department of Transportation
Research and Innovative Technology Administration</td><td colspan="2">13. Type of Report and Period Covered
Final Project Report</td></tr>
<tr><td colspan="2">14. Sponsoring Agency Code</td></tr>
<tr><td colspan="5">15. Supplementary Notes
Report also available at: https://zenodo.org/communities/utc-uti</td></tr>
<tr><td colspan="5">16. Abstract
Squeezing rock conditions have been causing significant risks in the construction of tunnels in rock formations, especially at great depth and in weak and/or weathered rock masses. The tunnel excavation may induce a stress change with considerable deviatoric stress that can cause squeezing ground behavior. The mechanism of squeezing failure of tunnels is not clearly understood yet, and the goal of this research project is to understand better the causes leading to squeezing ground phenomena. The objectives of this research were to identify the major causes of squeezing in soft rock, quantifying the squeezing amounts and develop experimentally verified squeezing criterion for broader application to tunnels. To achieve the research objectives, a series of novel true-triaxial compression experiments with simultaneous tunneling in rock were conducted.</td></tr>
<tr><td colspan="3">17. Key Words
Squeezing ground; True-triaxial cell; Synthetic Mudstone; Miniature TBM; Longitudinal Displacement Profile; Tunnel Support</td><td colspan="2">18. Distribution Statement
No restrictions.</td></tr>
<tr><td>19. Security Classification (of this report)
Unclassified</td><td>20. Security Classification (of this page)
Unclassified</td><td>21. No of Pages
141</td><td colspan="2">22. Price

NA</td></tr>
</table>

Table of Contents

List of Figures

List of Tables

List of Abbreviations and Mathematical Symbols

A_s	Tunnel support cross-sectional area
a	Ultimate tunnel strain due to squeezing
a_b	Hoek–Brown parameters of rock mass
B	Tunnel width
b	Tunnel strain due to excavation only
b_b	Empirical exponent for SHANSEP
B_s	Tunnel span for squeezing
C^*	Support compressibility ratio
D	Disturbance factor due to excavation
d	Time-dependent parameter for the tunnel convergence
E_g	Ground's Young's modulus
E_s	Tunnel support's Young's modulus
F_c	Competency ratio
$F(n)$	Function of specific gravity
F^*	Support flexibility ratio
GRC	Ground Reaction Curve
GSI	Geological Strength Index
G_s	Specific gravity of soil solids
H	Overburden
H_p	Rock load
I_s	Moment of inertia of tunnel support
LDP	Longitudinal Displacement profile
N	Competency factor
n	Porosity of rock
N_s	Peck's stability number
OCR	Overconsolidation ratio
p_o	Isotropic stress at tunnel location
p_u	Support pressure
Q	Rock mass quality
R	Tunnel Radius
S	Squeezing number

SCC	Support Characteristic Curve
s	Hoek–Brown parameters of rock mass
S_u	Undrained shear strength
T	Thrust on tunnel support
t_s	Tunnel support thickness
u, u_a	Tunnel wall displacement
V_p	P-wave velocity of rock mass
γ	Total unit weight
γ'	Effective rock mass unit weight
σ_c	Intact rock unconfined compressive strength
σ_{cm}	Rock mass unconfined compressive strength
σ_v	Total vertical stress
σ_θ	Tangential stress
σ'	Effective stress
$\sigma'_{critical}$	Critical effective stress for squeezing
σ'_h	Effective horizontal stress
σ'_v	Effective vertical stress
σ'_y	Apparent pre-consolidation stress
ε_{cr}	Critical strain for squeezing
ε_f	Tunnel face strain
ε_θ	Tangential strain
τ_{nc}	Normalized undrained shear strength
v_g	Poisson's ratio of ground material around tunnel boundary
v_s	Poisson's ratio of tunnel support

EXCUTIVE SUMMARY

The presence of squeezing ground conditions often poses significant challenges in predicting tunnel response over time and to the design of an adequate support system to stabilize the tunnel. Over the years, many methodologies have been proposed to predict squeezing in tunnels based on tunnel depth, in situ stress, ground mineralogy, and ground strength and deformation behavior. Most of these methodologies are problem-specific and limited in scope. The study presented in this report was focused on improving the understanding of tunnel squeezing via a unique physical model test that simulated tunnel boring machine (TBM). To identify the critical parameters contributing towards squeezing, a case study of four tunnels constructed in squeezing clay-rich rock was carried out. It was established from the case studies that by combining normalized engineering behavior of rocks, Peck's stability number and Geological Strength Index (GSI), the squeezing potential for the tunnels could be determined. A squeezing number S is suggested to classify ground conditions based on the level of squeezing that the ground may experience in response to tunneling. It was demonstrated that by combining the proposed classification system and an existing classification system for squeezing ground conditions, an accurate estimate of tunnel strain could also be obtained.

Following the case studies, a novel physical model test to simulate a tunnel boring machine (TBM) excavation in squeezing ground conditions has been proposed. The physical model included a large true-triaxial cell, a miniature tunnel boring machine (TBM), a laboratory-prepared synthetic test specimen having properties similar to natural mudstone, and instrumentations to monitor deformations around the tunnel boundary during and after the excavation. The true-triaxial cell can apply principal stresses up to 13 MPa on a 300x300x300mm3 cubical rock specimen independently on the three principal planes, and this corresponds to real in-situ stress conditions. Miniature TBM can excavate a tunnel having 48-mm and maximum length 150-mm. The instrumentation and monitoring included embedded strain gauges in the form of multiple point borehole extensometer (MPBEx) and a caliper to monitor deformations around and at the tunnel boundary, respectively. The preliminary testing showed the capability of the test setup in capturing crucial features of tunnel excavation, such as tunnel advance, three-dimensional effects, and highly plastic and ductile time-dependent behavior of the ground.

The physical model was used to study the behavior of supported and unsupported tunnels at various isotropic stress levels. The deformation data were obtained from the embedded strain gauges, digital borehole caliper and strain gauges on the support system. The degree of tunnel squeezing was characterized using a classification system based on tunnel radial strain. A model for time-dependent tunnel longitudinal displacement profile (LDP) for unsupported and supported tunnels was proposed using measurements of the tunnel convergence at different times and different stress levels. The LDP parameters for both the cases were compared to account for the influence of the support system. The back-calculation of thrust forces on the support system provided an estimate of the additional effects induced in the support due to squeezing. Finally, based on the observations, a recommendation for the analysis to determine safe and economical support for the tunnel constructed in squeezing ground was proposed.

CHAPTER 1 - INTRODUCTION

1.1 Introduction

Tunnels or underground passageways are human-engineered structures mainly constructed for the purposes of mining, public works (e.g., sewage and drainage) and transportation. Every tunnel construction project is unique and may suffer from technical difficulties, financial problems and political disputes. The financial or political challenges are directly or indirectly linked with technical difficulties encountered at the construction site, which can impact the short-term and long -term stability of the tunnel. Designers and engineers, based on their field experiences, point out the geotechnical characteristics, in-situ stresses and excavation method are the main contributors to the long-term and short-term behavior of tunnels.

The geotechnical characteristics includes engineering properties of rocks and rock masses around the tunnel boundary such as strength (compressive, shear and tensile), elastic modulus, porosity, permeability, density, ductility/brittleness and flow properties of the ground material around the tunnel boundary. Higher in-situ stresses result in large stress relaxation at the tunnel boundary due to excavation, which can lead to massive convergence of the tunnel. Also, selection of the excavation method of the tunnel should be made by considering the response of the ground to the excavation because the excavation process itself can impact the existing surface structures and underground utilities around the tunnel.

In the case of unfavorable circumstances governed by the factors mentioned above, major complications can arise in tunnel construction and operation. Two examples of such problems generally occur due to high in-situ stresses and incompetent rock mass are squeezing ground conditions and rockburst. Squeezing ground condition causes gradual ductile convergence of the tunnel during and even after the construction is finished, while rockburst is the spontaneous and volatile brittle failure of the ground material. This report is focused on investigating the tunnels constructed in squeezing ground conditions.

1.1.1 Squeezing tunnels

Various definitions of squeezing have been adopted in different regions of the world (e.g., Terzaghi, 1946; O'Rourke, 1984; Singh, 1988; Aydan et al., 1996; Gioda & Cividini, 1996; and Kovari, 1998). The widely accepted definition based on the engineering behavior of rock mass was given by Barla (1995), which was adopted by the International Society of Rock Mechanics (ISRM):

"*Squeezing is the large time-dependent deformation that occurs around the tunnel and is essentially associated with creep caused by exceeding limiting shear stress. Deformation may terminate during construction or continue over a long time.*"

From the above definition, it is evident that squeezing ground conditions can impose a much higher load on the tunnel support system than expected. The ultimate tunnel support requirement in squeezing ground may be two to three times more than the same tunnel cross-section in non-squeezing ground conditions (Jethwa et al., 1984). Therefore, it is vital to estimate the

deformations due to squeezing beforehand to ensure safe, efficient and economical construction (Barla, 2001).

The inadequacy of the ground is also attributable to the presence of clay minerals in the surrounding geomaterials (Terzaghi, 1946). These clay minerals can be present in soil or with different degrees of lithification (e.g., claystone, shale or any other alteration product). Reported examples of tunnels that experienced squeezing due to high in-situ stress and the presence of clay minerals include the John Street Pumping Station Tunnel in Canada (Lo et al., 1987), the Still Water Tunnel in the United States (Phien-wej & Cording, 1991), the Uluabat Project Tunnel in Turkey (Bligin & Algan, 2012) and the Laodongshan Tunnel in China (Cao et al., 2018).

1.1.2 Methodologies to study squeezing

Numerous approaches have been proposed in the literature over the years to study squeezing, which included experimental techniques, numerical analyses, analytical methods and empirical equations. The experimental techniques include both elemental laboratory testing of the geomaterials for material characterization along with engineering properties and physical model tests for quantitative analysis (e.g., Semple et al., 1973 and Mesri et al., 1981). On the other hand, physical model tests can simulate tunnel excavation and provide an estimate of the stresses and deformation that develop around the tunnel boundary (Mesri et al., 1981). The observations from the model tests are correlated with the engineering properties of the geomaterials to develop the design criteria for a tunnel.

The numerical approaches use a time-dependent stress-strain constitutive model of the materials to simulate the exact or approximate construction sequences and processes (e.g., Dusseault & Fordham, 1993; Bonini et al., 2009; Barla et al., 2012). On the other hand, the analytical approaches incorporate the laws of physics along with the material properties and boundary conditions to derive an equation for the convergence of a tunnel with time (e.g., Pan & Dong 1991; Gioda & Cividini 1996; Singh et al., 2018).

The empirical solutions for tunnels in squeezing ground are purely based on the field experiences of the engineers and are not necessarily universally applicable (e.g., Terzaghi, 1946; Barton et al., 1974; Singh et al., 1992; Goel et al., 1995; and Arora et al., 2020a). All the proposed methodologies can be characterized based on the principle item investigated such as the ground material properties, critical stresses and strains, material flow properties and field correlations (Arora et al., 2020a).

As per the International Society of Rock Mechanics (ISRM) (1994), the most appropriate method for the design of tunnels in squeezing ground conditions should incorporate field observations along with numerical techniques and conventional closed-form solutions. The time-dependent convergence of a tunnel should be used along with the rock mass creep parameters for the forecasting of squeezing.

1.2 Gap in the Literature and Motivation

Despite the commendable efforts of researchers over the years who studied tunnels in squeezing ground conditions, designers continue to encounter many engineering surprises (Wang et al., 2019). The lack of a definite progress in this area is primarily due to the critical assumptions and

limited applicability of the approaches discussed in Section 1.1.2. For example, the physical models proposed to date have not been able to three-dimensionally simulate the tunneling effect, the advancement of the tunnel and the excavation at in-situ stress together (Meguid et al., 2008).

The current analytical methods generally associate squeezing with the creep behavior of the rock and assume no volumetric changes (e.g., Pan & Dong 1991; Gioda & Cividini 1996). However, several past researchers observed that during creep, rock experiences significant volumetric changes (e.g., Kranz & Scholes, 1977 and Fabre & Pellet, 2006). Similarly, the numerical methods also require a reliable constitutive model for the time-dependent behavior of the rock derived with minimum assumptions (Bonini et al., 2009).

The present empirical methods for the design of tunnels in squeezing ground conditions were derived from limited field observations (e.g., Schmidt, 1974; Attwell, 1978; O'Reilly & New, 1982; and Mair et al., 1993). Field monitoring of tunnel response under squeezing conditions remains not only difficult but also a perilous undertaking. Due to the high loads and extreme deformations, field sensors, just like the tunnel support system themselves, are under extreme environments and often fail before meaningful data can be obtained once the squeezing has started. Without reliable field data, it is difficult to validate methods to predict the response and design a tunnel in squeezing ground.

From the limitations of the different approaches discussed above, it is quite evident that the squeezing phenomena has been extensively studied. An applicable reliable criterion for squeezing would not only improve our understanding but, more importantly, could guide the tunnel engineers in the design of squeezing-resilient support systems.

As in-situ monitoring is limited in squeezing conditions, physical model tests without any major limitations is considered a viable option. The aim of this research was to advance the understanding of the gradual time-dependent convergence of tunnels due to the squeezing characteristics of clay-rich rock such as mudstone. This study involved the development of an advanced laboratory-scaled physical model to improve forecasting of squeezing ground conditions around tunnels excavated in clay-rich rocks by studying the post-construction long-term three-dimensional impact of the tunnel construction.

1.3 Research Objectives

The primary goals of this report were to achieve an improved understanding of tunnels in squeezing ground conditions through well controlled laboratory experiments and to develop a robust criterion to predict tunnel squeezing. To achieve these goals, the following specific objectives were pursued:

1. Carry out case studies to identify the major causes of squeezing in tunnels excavated in clay-rich rocks.
2. Design and fabricate an experimental setup that is capable of simulating tunnel squeezing in cubical rock specimens subjected to true-triaxial stress state at a laboratory scale.
3. Develop a synthetic rock material for laboratory model study with mechanical behavior comparable to naturally occurring squeezing mudstone and characterize the behavior of the material.

4. Perform a series of laboratory-scale physical simulation of tunnel squeezing under different conditions based on data from the tunnels experienced squeezing.
5. Analyze and synthesize model test results to develop an improved and reliable procedure to predict tunnel squeezing.

A rational approach for the tunnel analysis and design in difficult squeezing ground conditions was obtained. This new approach will allow for a more scientific, data driven, and logical evaluation of the interaction between the tunnel support system and the squeezing ground.

1.4 Research Tasks

The objectives of this report which were discussed in Section 1.2, were pursued through an experimental testing program and an extensive and detailed analysis of the experimental data. The tasks that were performed to accomplish the research objectives are described in the following sub-sections.

1.4.1 Tasks related to "Objective 1"

- Conduct an extensive literature review of the methodologies proposed over the years to study tunnels in squeezing ground conditions and characterize them.
- Collect the geotechnical and geological data of different tunnels constructed in squeezing clay-rich rocks and analyze to identify the major causes of squeezing.

1.4.2 Tasks related to "Objective 2"

- Design and fabricate a miniature tunnel boring machine (TBM) compatible with the existing true-triaxial cell at the Colorado School of Mines.
- Determine an adequate instrumentation and monitoring system to monitor damages and deformation in the rock specimen during the tests.
- Perform experiments to check the capability of the test setup in simulating the three-dimensional effect of tunnel excavation in squeezing ground condition.

1.4.3 Tasks related to "Objective 3"

- Identify the commercially available suitable materials for producing a synthetic mudstone based on the mineralogical composition of the naturally occurring mudstone.
- Perform multiple trials to determine the correct final mixture for the synthetic mudstone preparation based on its stress-strain behavior in the uniaxial compression test (UCT).
- Characterize the prepared synthetic mudstone to determine the physical and mechanical properties and compare it with the naturally occurring mudstone.

1.4.4 Tasks related to "Objective 4"

- Perform experiments to monitor the convergence of the tunnel with time at multiple isotropic stress levels.
- Conduct a convergence-confinement study in an experiment to determine the interaction between the tunnel and the support system in squeezing ground conditions.

1.4.5 Tasks related to "Objective 5"

- Develop experimentally verified criteria for the LDP of tunnels constructed in squeezing ground conditions.
- Develop criteria for the load considerations on the support system of the tunnels in squeezing ground conditions from the convergence-confinement study.

1.5 Report Outline

This is a manuscript-based report where the majority of the main chapters have been published, accepted or are undergoing revisions with peer-reviewed international journals and conferences. The main chapters of this report, are similar to the originally published or submitted individual manuscripts. Each of the main chapters has its specific abstract, introduction, main body text, results, discussions, conclusions and acknowledgments. All the references in the development of the report are presented at the end of the document. The report consists of seven chapters in total, with the five main chapters being Chapters 2 through 6.

The remainder of the report proceeds as follows.

Chapter 2 presents the literature review and case-studies of tunnels in squeezing clay-rich rocks.

Chapter 3 presents the physical model setup designed to study tunnels in squeezing ground conditions.

Chapter 4 discusses the laboratory-prepared synthetic mudstone specimen for physical model studies, including its preparation, characterization and comparison with natural mudstone.

Chapter 5 addresses the time-dependent behavior of the tunnels in the ground and introduces a model for time-dependent LDP using measurements of the tunnel convergence at different times and different stress levels during an experiment.

Chapter 6 focuses on the rock-support interaction for the tunnels in squeezing ground conditions.

Chapter 7 presents the primary findings, major conclusions and contributions of this report.

CHAPTER 2 - TUNNELS IN SQUEEZING CLAY RICH ROCKS

2.1 Abstract

Squeezing ground conditions, which can lead to severe loads in tunnels, have historically been associated with the presence of clay minerals in the ground. Over the years, many methodologies have been proposed to predict squeezing in tunnels based on tunnel depth, in situ stress, ground mineralogy, and ground strength and deformation behavior. This chapter presents a comprehensive review of methodologies to predict tunnel squeezing in clay-rich rocks. A new methodology is proposed where ground conditions and squeezing potential are assessed based on the SHANSEP (Stress History and Normalized Soil Engineering Property) approach adapted to clay-rich rocks, Peck's stability number and Hoek & Brown's (1997) Geological Strength Index (GSI). A squeezing number *S* is suggested to classify ground conditions based on the level of squeezing that the ground may experience in response to tunneling. Finally, it is demonstrated that by combining the proposed classification system and an existing classification system for ground squeezing condition, an accurate estimate of tunnel strain can also be obtained. The proposed method is applied to four case studies of tunnels in squeezing ground in shale and mudstone.

2.2 Introduction

During and after excavation, the tunnel converges, and the excavated area reduces. In some cases, the ground around the tunnel yields, undergoes plastic deformation and tunnel convergence may continue even after excavation. If the tunnel keeps on substantially converging over a time period, the tunnel is deemed to be in a squeezing ground condition (Barla, 1995). Several other definitions of tunnel squeezing have been proposed including those by Gioda (1982), O'Rourke (1984), Kovari (1988) and Aydan et al. (1993). A full review of the different definitions is given in Barla (2001) and below.

In case of squeezing ground condition, the tunnel walls undergo large plastic deformation and the primary governing factor that leads to such high deformation is the ratio of the ground shear strength and in-situ stresses at the tunnel level. Squeezing condition defines the boundary between stable and unstable excavations. Consider a typical cross-section along the alignment of a circular tunnel having isotropic field stresses of σ_o as illustrated in Figure 2-1. When the tunnel is excavated, the stresses around the boundary are redistributed and during this redistribution of stresses and depending on the applied internal support, some regions around the tunnel boundary may fail. The boundary that separates the elastic and inelastic zones is considered as the plastic zone boundary. The extent of the plastic zone, shown in Figure 2-1, depends on the strength of the ground material, ground heterogeneities, radius of the tunnel, in-situ stresses, groundwater condition, etc.

Squeezing ground condition can lead to much higher deformation of the tunnel support system than anticipated, and the ultimate support requirement can be up to two to three times higher than calculated for the same amount of final tunnel convergence (Jethwa et al., 1984). The main problem that can be encountered in the construction of the most difficult tunnels is squeezing ground. For example, the Yacambu-Quibor is a 23.3 km long, 5-m diameter water conveyance tunnel designed to carry water through the Andes from the Yacambu dam in the wet tropical Orinoco basin to the semi-arid but fertile Quibor basin in western Venezuela. The tunnel

excavation was carried out in silicified and graphitic phyllite with the maximum depth of overburden of 1270 m. The project was initiated in 1965, and it took 32 years to determine and resolve the ground-squeezing problem in this tunnel. Hoek & Guevara (2009) studied the squeezing in this tunnel and observed that the strength of rock mass was almost one-tenth of the in-situ stresses due to the extreme thickness of cover above the tunnel. This led to squeezing ground conditions with up to 30% maximum strain in the ground. Also, such high magnitude of ground strain causes lot of problems in the design of the tunnel support system and resulted in long and expensive delays in the project.

There are many methodologies proposed over the years for the design of tunnels in squeezing ground conditions. The first part of this chapter discusses the popular methods that have been proposed to study tunnels in squeezing ground conditions along with their applicability and limitations. Each of the discussed methodologies is further classified based on different categories on. The International Society of Rock Mechanics (ISRM) suggested methods for tunnel construction in squeezing ground conditions are also discussed in this chapter. In the second part of the article, a new methodology is proposed that can be widely applicable to tunnels excavated in squeezing clay and clay-rich rock. The method is based on Peck's (1969) stability number, the SHANSEP (Stress History and Normalized Soil Engineering Properties) approach by Ladd & Foott (1977), and Hoek-Brown's (1997) Geological Strength Index (GSI). The proposed methodology is tested on the four tunnel projects, and the results are compared with the field observations to validate the method. Based on the case studies of four different tunnels using the suggested methodology, a new parameter 'Squeezing number' is introduced in this work.

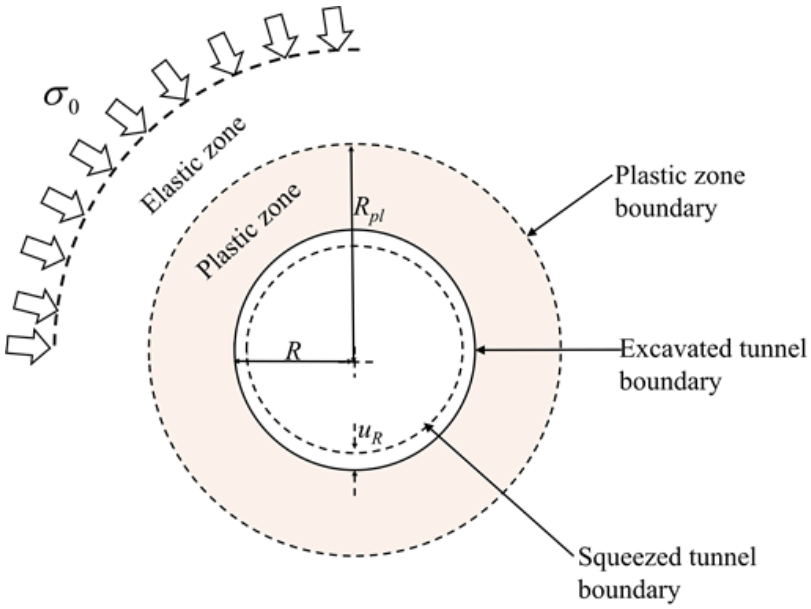

Figure 2-1 Cross-section of a circular tunnel in isotropic in situ stress field and squeezing ground condition. R is the radius of tunnel, R_{pl} is radius of plastic zone and u_R is the tunnel convergence.

2.3 Methodologies to Characterize Tunnels in Squeezing Ground

2.3.1 Classification based on the Ground Material Properties

One of the important factors for the occurrence of squeezing conditions is the behavior of ground. Terzaghi (1946) associated the existence of ground squeezing in tunnels with the presence of micaceous or clay minerals and sub-microscopic particles with a low swelling capacity having plasticity index PI less than 15%. Tunnels tend to show squeezing when clay is present particularly in the form of claystone, shale or any other alteration products. Terzaghi (1946) found that the squeezing rock formation slowly converges into the tunnel without perceptible volume change and the amount of advance depends on the clay mineralogy. He proposed a parameter called 'rock load' H_p which is defined as the load per unit length of the tunnel on the roof of the tunnel support system. Based on the rock mass condition and magnitude of H_p, Terzaghi (1946) proposed a classification system for the tunnels which range from class 1 to 9. Class 1 represents hard and intact rock mass condition with H_p equal to zero, whereas class 9 represents poor ground conditions due to swelling rock and high magnitude of H_p.

Rose (1982) revised Terzaghi's classification system by incorporating the rock quality designation RQD. It was found that any change due to RQD does not apply to the special case of squeezing rock, and Terzaghi's proposed criteria adequately provides a preliminary assessment of squeezing in tunnels. Woods (1972) studied the main characteristics of three road tunnels in Britain based on the nature of the ground in which they were excavated. It was observed that the problem of squeezing in soft ground arose due to the low strength of the material. A factor known as 'competency ratio' F_c, given in below, was proposed. F_c is the ratio of the unconfined compressive strength σ_c of the ground material and the net overburden pressure, both at the tunnel level.

$$F_c = \frac{\sigma_c}{\gamma H} \tag{2-1}$$

where γ is the total unit weight of the ground material, and H is the depth of tunnel from the ground surface up to crown level. Woods (1972) found that when the value of F_c is less than 2, the ground will be over stressed immediately after excavation and squeezing condition may exist. However, in the case of tunnel excavation in a competent ground (i.e., hard rock), the competency ratio along with the stress-strain behavior govern the behavior of ground.

Jaeger and Cook (1976) used elasto-plastic analytical solution for the rock mass to determine the tangential stress σ_θ in terms of earth pressure coefficient k at the tunnel boundary. It was proposed that if σ_θ is greater than the unconfined compressive strength of the rock mass σ_{cm} at the tunnel depth, the ground will experience squeezing.

Jethwa et al. (1984) evaluated the ultimate rock pressure for tunnel lining under squeezing condition for the tunnels in Himalayan regions. A semi-empirical method based on rock-mass quality Q (Barton et al., 1974) and the overburden H was proposed to predict the squeezing potential of tunnels. For preliminary assessments of the squeezing potential, a competency factor N similar to competency ratio F_c proposed by Woods (1972) was used. The only difference was that unconfined compressive strength of intact rock σ_c in Eq. 2-1 was replaced by the unconfined compressive strength of the rock mass σ_{cm}. It was observed that for the magnitude of N greater than 2, the ground behaviour would be non-squeezing. Based on field observations and analysis

of results, Jethwa et al. (1984) concluded that in a squeezing ground, ultimate support pressure requirement could be 2 to 3 times that of the initial support pressure.

Verman (1993) use the ground reaction curves (GRC) proposed by Pacher (1964) in the field study and instrumentation of nine Himalayan tunnels. Based on the empirical correlation and ground reaction curves, a design chart was developed to classify the ground as self-supporting, non-squeezing (elastic) and squeezing (elasto-plastic). The ground condition depends on the height of overburden H, tunnel span B and rock mass quality Q. The tunnel span B_s that the ground can support without squeezing is given as

$$B_s = 3.2Q^{0.4} \tag{2-2}$$

where Q is the rock mass rating in the Q rock mass classification system (Barton et al., 1974). Based on the actual span and span given in Eq. 2-2, ground is: (a) self-supporting if B-$B_s < 0$, (b) non-Squeezing if $H(B - B_s)^{0.1} < 483Q^{\frac{1}{3}}$, and (c) squeezing or rock burst if $H(B - B_s)^{0.1} > 483Q^{\frac{1}{3}}$.

2.3.2 Classification based on critical stresses and strain

Labasse (1949) for the first time incorporated the application of rock-mass support interaction to quantify tunnel wall deformation due to squeezing. Using Mohr-Coulomb yield criterion and zero cohesion of the material, the average volumetric strain in the plastic region around the tunnel was determined and then the tunnel wall displacement u_a due to ground squeezing was determined.

Saari (1982) quantified the amount of squeezing in tunnels based on the tunnel tangential strain. Based on the elastic-visco-plastic response of the ground, a threshold value of 1% tangential strain ε_θ was proposed. This threshold value differentiates between squeezing and non-squeezing ground. However, this model does not consider the reduction in strength of the ground due to strain softening. Later, Tanimoto (1984) used the strain softening elasto-plastic behavior of the ground to explain the phenomenon of squeezing. According to the proposed model, when the ground is strained up to residual plastic (flow) state, the ground will squeeze. However, the ground will be heavily squeezed at this state, and the prosed threshold value can be very high (Aydan et al., 1996).

Sakurai (1997), based on his observations from field measurements, proposed a critical strain (ε_{cr}) value to study the deformations due to squeezing in tunnels. The critical strain value can be determined in the laboratory by performing standard unconfined and confined compressive tests. It was found that the critical strain is not influenced by the environmental factor such as water content, temperature, etc. The stability of tunnels was assessed by comparing the field results and the critical strain obtained in the laboratory.

Aydan et al. (1996), from their field observation on tunnels in Japan and laboratory experiments, made a significant contribution to the literature. A model based on deformation-time degradation was proposed. The preliminary examination of the squeezing ground was carried out by determining the competency ratio F_c (Eq. 2-2). The fundamental concept was based on observing the stress-strain response of specimen in the laboratory loaded uniaxially and triaxially and comparing it with the tangential stress-strain response around the tunnel. The stress-strain plots were divided into five regions: (1) elastic (no squeezing), (2) strain hardening (light squeezing),

(3) strain softening (fair squeezing), (4) strain softening at higher rate (heavy squeezing), and (5) residual-flow state (heavy squeezing).

Similar to the work of Aydan et al. (1996), Hoek (1998) used the competency ratio in Eq. 2-1 to determine the squeezing potential. Later, Hoek & Marinos (2000), using finite element analysis (FEA) results and various numerical case studies, proposed criteria based on the tunnel strain ε_t and face strain ε_f as follows:

$$\varepsilon_t(\%) = \left[0.15\left(1-\frac{p_u}{p_0}\right)\frac{\sigma_{cm}}{p_o}\right]^{-\frac{\left(\frac{3p_u}{p_o}+1\right)}{\left(\frac{3.8p_u}{p_o}+0.54\right)}} \quad (2\text{-}3)$$

$$\varepsilon_f(\%) = \left[0.1\left(1-\frac{p_u}{p_0}\right)\frac{\sigma_{cm}}{p_o}\right]^{-\frac{\left(\frac{3p_u}{p_o}+1\right)}{\left(\frac{3.8p_u}{p_o}+0.54\right)}} \quad (2\text{-}4)$$

For different $\frac{p_u}{p_o}$ ratios, plots of ε_t versus $\frac{\sigma_{cm}}{p_o}$, and ε_f versus $\frac{\sigma_{cm}}{p_o}$ were made for tunnels in Venezuela, Taiwan and India. Results were compared with Aydan et al. (1996) and the following squeezing levels were defined in terms of support problems: (1) small support problems ($\varepsilon_t < 1\%$), (2) minor squeezing ($1\% < \varepsilon_t < 2.5\%$), (3) severe squeezing ($2.5\% < \varepsilon_t < 5\%$), (4) very severe squeezing ($5\% < \varepsilon_t < 10\%$), and (5) extreme squeezing ($\varepsilon_t > 10\%$).

For a preliminary analysis of squeezing, Singh et al. (1992) observed that squeezing will occur when the relationship $H > 350Q^{1/3}$ is achieved. Later, Singh et al. (2007) studied critical strains to quantify the squeezing. They found that critical strain that defines a threshold value for squeezing is an anisotropic property and depends on the intact properties of the rock and joints. Value of critical strain was redefined as the empirical value of tangential strain at the periphery of the opening at which jointed rock mass fails under uniaxial compression loading.

Based on 348 tunnel sections and 45 case studies, Majumder et al. (2017) developed a novel multiple-graph technique for the preliminary estimation of the ground condition and probable hazards due to excavation in tunnelling. The technique incorporates parameters such as rock mass shear strength parameters, competence factor F_c, and the ground conditions of the rock mass. A new ground condition classification was also presented for both soft rock mass and hard rock mass.

Recently, Vrakas et al. (2018) studied squeezing in Gothard base tunnel and five other projects using an elasto-plastic Mohr-Coulomb (MC) model. The study was based on: (a) triaxial experiments on rock and joint, (b) a revised MC model that incorporates hardening, (c) GRC for a material satisfying strain hardening soil models, and (d) selection of appropriate operational deformation modulus from triaxial test results. It was concluded that, if an appropriate value of elastic deformation modulus E_{MC} is incorporated in MC model, the phenomenon of squeezing can be studied for any soil or rock.

2.3.3 Classification based on material flow properties

At a great depth, the redistribution of stresses in response to excavation leads to non-reversible deviatoric creep strains. The creep strain develops over time at constant and eventually increasing

rates, namely secondary and tertiary creep, respectively (Dusseault & Fordham, 1993). To study deformation of tunnels in squeezing ground condition, Gioda & Cividini (1996) considered the ground as a single-phase media having elastic, plastic and viscous properties. The finite element method (FEM) was selected to model the viscous behavior of rock under deviatoric stress state. The loss in strength of the rock with an increase in deviatoric stress (without considerable volumetric changes) was studied. By incorporating primary, secondary and tertiary creep, they were able to calculate large time-dependent deformations and hence, able to quantify squeezing.

Further work was carried out by Sterpi & Gioda (2009) who developed a constitutive relation that defines viscous, elastic and plastic behavior of the rock mass. The focus of the developed two-dimensional plane strain finite element model was to study the influence of an excavation advancing on the tunnel closure and the stress redistribution around it. They considered the deformation due to primary creep (visco-elastic), secondary creep (visco-plastic) and tertiary creep. The finite element results showed that the influence of tertiary creep is quite significance in the short-term closure of the tunnel and could have a notable negative effect in case of TBM driven tunnels.

Bonini et al. (2009) studied the mechanical behavior of clay shales (CS) from Apennines, Italy to study the tunnelling in difficult conditions. Two constitutive models, namely, the visco-elastic plastic model (CVISC) and elastic visco-plastic Lemaitre's model (VILPA) were found appropriate to study the large time-dependent convergence of tunnels. The time-dependent behavior of CS was shown as a significant factor to be taken into consideration for the assessment of tunnels in response to swelling and squeezing. Furthermore, Debernadi & Barla (2009) developed stress hardening elastic viscous plastic (SHELVIP) model for CS for the design analysis of tunnels in squeezing condition. The model couples general elasto-plasticity and a time-dependent component. Barla et al. (2011) carried our finite element and finite difference numerical analysis to study squeezing in Lyon-Turin railway project tunnel using time-dependent model for rock mass namely SHELVIP and three-stage creep (3SC) model. Elastic, plastic and viscous properties of the rock mass were calculated from the field observations using a back-analysis procedure.

Manh et al. (2015) proposed a three-dimensional semi-empirical approach that considered the time-dependent and anisotropic behavior of the rock mass to investigate squeezing behavior. The developed model was based on the observations in Lyon-Turin railway project tunnel. The proposed model was implemented into the finite difference code FLAC3D (Itasca Consulting Group 2013). It was observed that the numerical simulation results align well with the field observations. However, like all other creep models, the effect of tunnel support system with the ground was not considered in determining large time-dependent deformation.

2.3.4 Other methods

Mercier-Langevin & Hadjigeorgiou (2011), based on their observations from LaRonde Mine in Canada and other mining operations, proposed a hard rock squeezing index (HRSI) for the preliminary assessment of squeezing in hard rocks. HRSI was based on the observed foliation spacing of the rock mass and stress to the strength of intact rock ratio. This work also considered the influence of excavation orientation on the structure. However, the proposed HRSI index was calibrated based on the observations at one mine only.

Gutierrez & Xia (2009) developed an empirical correlation to assess the condition of ground containing clay or clay-rich rocks. The method incorporates the stability ratio *N* proposed by Peck (1969) – see below - and the normalized undrained shear strength and apparent over consolidation ratio OCR of the ground. The proposed equation determines the critical value of effective vertical stress, and if the value of in-situ vertical effective stress at tunnel level is more than the critical effective vertical stress, the tunnel is in squeezing ground.

2.4 ISRM Suggested Methods for Squeezing Tunnel Design

Design of tunnels in squeezing ground conditions using conventional closed-form solutions and numerical methods involves high degree of complexity particularly for preliminary design (Barla, 2001). In squeezing ground conditions, these analyses can gain importance if complemented with field observations and monitoring. According to the International Society of Rock Mechanics (ISRM, 1994) suggested methods, observations and monitoring during tunnel excavation in squeezing ground conditions should become an integral part of the tunnel design scheme along with analytical and numerical solutions. The field observations are classified into primary observations and instrumented observations. Primary observations include ground material and geological characteristics, whereas instrumented observations comprise of measurement of displacement, deformation, pore pressure, and other important features around the tunnel boundary. The type of instrumentation selected for the tunnel project depends on the ground conditions and method of tunneling adopted.

The observations and monitoring of the test tunnel should be carried out to: 1) identify and quantify the squeezing behavior using the competency ratio F_c (discussed below); 2) include in-situ monitoring of deformation around the tunnel boundary; 3) compare predicted and observed performance of test tunnel; 4) analyze tunnel response during face advance; and 5) iterate and improve on the initial design of support system

The ISRM suggested methods also considers time-dependent response as an important aspect of ground behavior that contributes to squeezing as manifested in the continued deformation and convergence of the tunnel following completion of an excavation stage. This time-dependent behavior can be responsible for a significant part of squeezing. Special care should be devoted during performance monitoring of tunnels to the evaluation of the time-dependent behavior of the ground material around tunnel boundary. Additionally, rock mass creep parameters in the constitutive models to be used in predicting tunnel response must be evaluated experimentally.

Figure 2-2 shows the timeline of the different methodologies developed over the years to study tunneling in squeezing ground. The methodologies are based on field observations and monitoring of different tunnels constructed in squeezing ground conditions all around the world.

From the brief review of the proposed methodologies to study tunnels in squeezing ground conditions, it can be observed that most of the methodologies are based on statistical data obtained from the field observations and does not consider all the critical factors together (ground competency, creep behavior and overburden) that governs the squeezing ground conditions. This chapter presents new procedures to estimate squeezing potential of tunnels excavated in clay or clay-cemented rocks using normalized shear strength behavior, unconfined compressive strength

and seismic velocity. Based on the case studies of four different tunnels using the suggested methodology, a new parameter 'Squeezing number' is also introduced in this work.

2.5 Tunnel squeezing in Clay-Rich Rocks

2.5.1 Method based on SHANSEP

Terzaghi (1946) associated squeezing mainly with clay-rich rocks. Consistent with Terzaghi's original description, the focus of this chapter is on tunnels in clay-rich rocks such as claystone, clay shale, mudstone and shale. Peck (1969) proposed a stability number *N* for tunnels in clays. *N* is expressed as the ratio between the total vertical stress σ_v corresponding to the tunnel location and the undrained shear S_u of the cohesive soil:

$$N = \frac{\sigma_v}{S_u} \tag{2-5}$$

Based on the value of *N* and tunnel behavior observed in the field, Peck (1969) proposed the classification system presented in Table 2-1. According to this classification system, tunnels with *N*>5 are subjected to high degrees of rapid squeezing. Higher values of *N* >7 indicate potential for general shear failure and large tunnel displacements close to the tunnel heading.

Table 2-1 Stability criteria for tunnels in cohesive soils (Peck 1969).

N	**Field observations**
1-5	Tunnelling without unusual difficulties.
5-6	Clay may squeeze rapidly into shield void.
6-7	Shear failure ahead of tunnel causes ground
>7	General shear failures and ground movements around tunnel heading cause shield contact to become difficult; shield tends to dive.

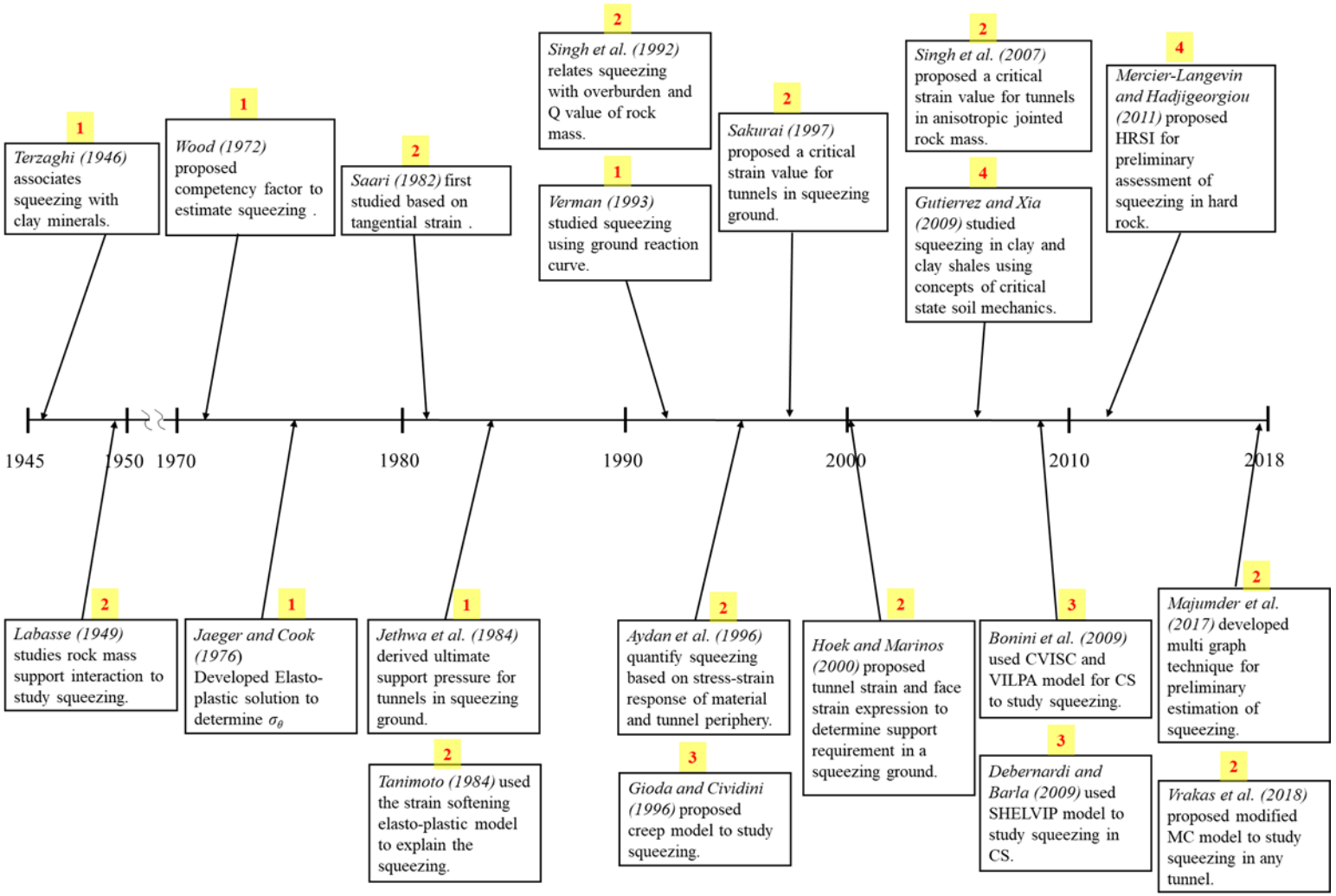

Figure 2-2 Timeline of the methodologies developed to study tunnels in squeezing ground conditions with reference number on the top of each box representing methodology based on, 1: ground material; 2: critical stresses and strains; 3: material flow properties; and 4: other methods.

A widely used method to estimate the undrained shear strength of clays is the SHANSEP (Stress History and Normalized Soil Engineering Properties) procedure developed by Ladd & Foott (1977). According to this procedure, the undrained shear strength S_u of normally consolidated (NC) clays normalized with respect to the current effective vertical stress σ_v' is unique, and approximately S_u/σ_v'=0.22 for many clays. For overconsolidated OC clays, the relationship between normalized undrained shear strength and overconsolidation ratio *OCR* is represented as:

$$\frac{S_u}{\sigma_v'} = \left(\frac{S_u}{\sigma_v'}\right)_{nc} (OCR)^b \tag{2-6}$$

where $(S_u/\sigma_v')_{nc}$ is the normalized undrained shear strength of NC clay, i.e. S_u/σ_v' for *OCR* =1.0 and *b* is an empirical exponent.

Numerous studies in the literature have shown the applicability of SHANSEP in representing the undrained shear strength of many types of clays and for clays with some degree of cementation (Steiger & Leung, 1991; Gutierrez et al., 1996; Bo et al., 2003; Indraratna et al., 2008). Steiger & Leung (1991) conducted investigations on the applicability of SHANSEP to shales and found that SHANSEP could adequately represent the undrained shear strength of the shale. However, the applicability of SHANSEP to strongly cemented materials like shales and other clay-rich rocks has not been not fully established.

To determine the validity of SHANSEP to clay-rich rocks, Gutierrez et al. (1996) created a database of clay-rich rocks with different stress histories and diagenesis from non-mechanical compaction including cementation. They found that undrained strength can be correlated with its physical properties and stress history and diagenesis similar to the SHANSEP procedure for uncemented clays. Using triaxial data for 25 different types of clay-rich rocks, Gutierrez et al. (1996) determined that an "apparent *OCR*" can be defined for clay-rich rocks:

$$OCR = \frac{\sigma_y'}{\sigma_v'} \tag{2-7}$$

where σ_y' is the "apparent pre-consolidation stress" corresponding to the effective vertical stress at which yielding can be observed from the experimental consolidation stress-strain curve. This "apparent pre-consolidation stress" accounts not only for mechanical pre-consolidation as in clays but for other diagenetic pre-consolidation effects such as cementation. Similar to the power function given in Eq. 2-6, results showed the following linear relationship between $\log(S_u/\sigma_v)$ and $\log(OCR)$:

$$\frac{S_u}{\sigma_v'} = 0.37(OCR)^{0.87} \tag{2-8}$$

Gutierrez & Xia (2009) demonstrated the use of the above empirical relation to predict the squeezing potential of tunnels in clay-rich rock.

To facilitate the evaluation of squeezing potential, correlations of the apparent pre-consolidation with the unconfined compressive strength (UCS) and seismic P-wave velocity, to calculate *OCR* in Eq. 2-8, were established. It was observed that σ_y' has a strong correlation with the UCS (σ_c) and seismic compression wave velocity (V_p), and the following relations were obtained to estimate the apparent pre-consolidation:

$$\sigma_y' = 5.4(\sigma_c)^{0.73} \tag{2-9}$$

$$\sigma_y' = 1.08 \times 10^{-8}(V_P)^{2.5} \tag{2-10}$$

where σ_y' and σ_c are in MPa, and V_P is in m/sec. A value of critical effective vertical stress given below was derived by incorporating Eqs. (2-8), (2-9) and (2-10) in Eqs. (2-5) and (2-6).

$$\sigma_{critical}' = \left(\frac{F(n)}{\tau_{nc}N}\right)^{\left(\frac{1}{b}\right)} \sigma_y' \tag{2-11}$$

where $F(n)$ is a function of the specific gravity of soil solids G_s and porosity n. The expression of $F(n)$ is given as:

$$F(n) = \frac{\gamma}{\gamma'} = \frac{\sigma_v}{\sigma_v'} = \frac{G_s(1-n)+n}{(G_s-1)(1-n)} \tag{2-12}$$

where γ and γ' are total and effective unit weight of the material respectively. σ_v and σ_v' are total and effective vertical stresses at tunnel location, respectively.

If the value of effective vertical in-situ stress at the tunnel location is higher than the critical effective vertical stress in Eq. 2-12, i.e., $\sigma_v' > \sigma_{critical}'$, then the ground will squeeze in response to tunnelling. Gutierrez & Xia (2009) compared their results with field data from Broms & Bennermark (1967) and Bhasin (1991), and the empirical correlation proposed by Singh et al. (1992) and showed the predictive capability of the above equations.

2.5.2 Accounting for Discontinuities

The methodology proposed by Gutierrez & Xia (2009) for tunnels in clay-rich rocks does not account for large-scale discontinuities. The proposed methodology is extended to account for the effects of joints and the use of rock mass properties instead of intact rock properties. Hoek et al. (2002) provided an estimate of the strength of the rock mass based on the Geological Strength Index (*GSI*) developed by Hoek & Brown (1997). UCS of the rock mass is obtained from equation:

$$\sigma_{cm} = \sigma_c s^a \tag{2-13}$$

where *s* and *a* are Hoek and Brown parameters calculated using the following equations:

$$s = \exp\left(\frac{GSI - 100}{28 - 14D}\right) \tag{2-14}$$

$$a = \frac{1}{2} + \frac{1}{6}\left(\exp\left(\frac{-GSI}{15}\right) - \exp\left(\frac{-20}{3}\right)\right) \tag{2-15}$$

where *D* is the disturbance factor of the rock mass, which is 0 for undisturbed in situ rock mass and 1.0 for the disturbed rock mass (Hoek et al., 2002). According to Hoek et al. (2002), the effects of heavy blast damage and stress release due to overburden or excavation are examples of the cause disturbance of the rock mass. In all these cases, rock mass is highly disturbed and disturbance factor *D* close to 1.0 is more appropriate.

2.6 Analysis of Case Histories of Tunnel Squeezing

2.6.1 Application to Case Histories

The methodology for clay-rich rocks described above, based on a combination of the Gutierrez and Xia (2009) procedure and GSI, are applied to four different tunnels that have undergone some level of squeezing. These four tunnels are: (1) the John Street Pumping Station Tunnel in Canada, (2) the Laodongshan Tunnel in China, (3) the Uluabat Tunnel in Turkey, and (4) The Stillwater Tunnel in USA. Most of the geological unit encountered along the alignment of these four tunnels are clay-rich rocks. Table 2-2 presents a summary of the main geological unit and the intact and rock mass properties for the four tunneling projects. Analysis of the squeezing potential for these tunnels is discussed in the following sections.

John Street Pumping Station Tunnel in Canada

The John Street Pumping Station Tunnel was built in 1925 for the supply of water in downtown Toronto, Canada. During the 1980's a new 1.5 m diameter tunnel was proposed to help with the supply water along with the existing tunnels. According to Czurda et al. (1973), the tunnel site is located on land reclaimed from Lake Ontario. The tunnel goes through the Georgian Bay formation sandwiched between maroon-colored Queenstone shale above and black Collingwood shales below. The formation consists of a thick sequence of thinly bedded or laminated shales, calcareous mudstones, siltstones and very occasionally sandstones with interbeds of siliceous or argillaceous limestone (Robinsky & Morton, 1973). Majority of the tunnel alignment passes through the weak clay shales.

Lo et al. (1987) performed various field and laboratory tests on the overburden material above the John Street Pumping Station Tunnel. Routine split-spoon sampling techniques were used to collect sample of soils and rocks at regular interval. From the field measurements, it was observed that the horizontal stress is 13 to 30 times more than the vertical stress. Therefore, despite the low overburden of 10 to 35 m, the ground shows large time-dependent squeezing behavior in response to tunnelling.

Lo et al. (1987) performed time-dependent deformation tests on the specimen of clay shales to determine the horizontal and vertical deformations of 17 different specimens obtained from 17 tunnel locations. In this analysis, these 17 locations are considered as tunnel stations along the alignment to compare the Lo et al. (1987) observation with the present analysis.

Table 2-2 presents the intact rock and rock mass properties of the clay shales obtained from the laboratory investigation by Lo et al. (1987). Some values are taken directly whereas some are calculated based on the condition of rock mass provided by the author. Values of the parameters *a* in Eq. 2-15 and *b* in the Eq. 2-11 are taken as 0.37 and 0.87, respectively, as in Eq. 2-8.

Table 2-2 Intact rock and rock mass properties from various tunneling projects.

Project	**Geological unit**	**Intact rock**					**Rock mass**		
		***w* (%)**	**G_s**	**γ_{dry} (kN/m^3)**	**γ_{sat} (kN/m^3)**	**UCS (MPa)**	***n* (%)**	***GSI***	**UCS (MPa)**
John Street pumping station tunnel, Canada	Clay Shale	3.75	2.70	23.89	25.05	10 to 20	11.5	15	0.03 to 0.30
Laodongshan tunnel, China	Mudstone	5.01	2.70	23.33	24.70	1 to 13	13.6	5 to 50	0.30 to 0.51
Uluabat project tunnel, Turkey	Mudstone	4.75	2.70	23.87	25.05	1 to 96	11.6	5 to 45	0.24 to 1.00
Stillwater tunnel, USA	Clay Shale	4.35	2.70	23.75	24.95	50 to 92	12.03	15 to 55	0.02 to 0.20

Notes: w=water content, G_s=specific gravity of solids, γ_{dry}=dry unit weight, γ_{sat} = saturated unit weight, UCS=unconfined compressive strength, n=porosity, GSI= Geological Strength Index

Using Eqs. (2-5) to (2-11), the critical effective stress is obtained. As already mentioned, in this case, horizontal stresses are 13 to 30 times higher than the vertical stresses. Hence, more squeezing will occur due to the horizontal stress in comparison to vertical stress. Figure 2-3a presents the ground and tunnel elevation along the 17 tunnel stations. Figure 2-3b presents the critical effective stress for squeezing and actual effective horizontal stress at the same tunnel stations. In this case, the critical effective stress will be horizontal ($\sigma_v' < \sigma_h'$) and defined as critical effective vertical stress (Eq. 2-11) times the coefficient of lateral earth pressure which is considered as 20 on an

average as per the observations of Lo et al. (1987). At any given station, when the value of actual effective horizontal stress is higher than the critical effective vertical stress for squeezing, the ground has reached its critical state, and then the tunnel may be in a squeezing ground condition.

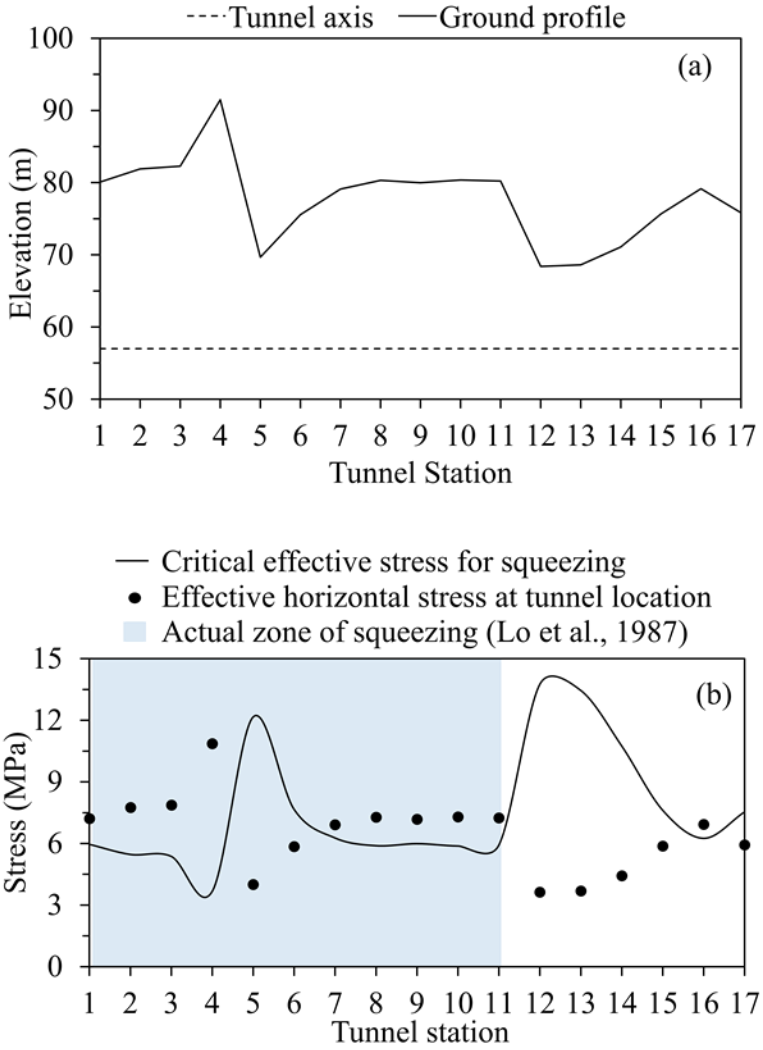

Figure 2-3 John Street pumping station: (a) Ground and tunnel elevation; (b) Critical effective stress for squeezing and actual effective horizontal stress at 17 tunnel stations.

Lo et al. (1987) observed high time-dependent horizontal deformation on the specimen procured from the tunnel stations 1-4, 6, and 8-9 whereas, smaller horizontal time-dependent deformation where observed for tunnel stations 5, 7, 10 and 11. The methodology of Gutierrez & Xia (2009) predicts squeezing ground or high deformation at tunnel stations 1 to 4, 7 to 11 and 16 (Figure 2-3b). The model appears to be able to predict squeezing at 9 out of 11 tunnel stations where it occurred. Hence, Gutierrez & Xia (2009) model show almost 80% accuracy in this case.

Laodongshan Tunnel in China

The Laodongshan Tunnel is a part of Guangtong-Kunming railway in China, which experienced squeezing failure in its early tunneling stage (Cao et al. 2018). The tunnel is 7,578 m long and was excavated in the zone of maximum overburden of 370 m. The start and the end points of this tunnel are located at chainage 947+555 km and 955+133, respectively. During the field exploration 14 boreholes with a total length of 1360.42 m were drilled (Cao et al. 2018). From the field investigation, it was found that at the tunnel location along the alignment geology of this area contains mudstone, sandstone and marl. As per the rock mass rating (RMR) proposed by Bieniawski (1969), the rock mass grades were in a range from type III, which is a fair grade of the rock mass to type V, which is a very poor grade of the rock mass. Tunnelling along the mudstone was found to be most problematic due to high overburden and very poor rock mass condition.

The squeezing potential evaluation involves the study of 33 critical sections along the tunnel alignment of Laodongshan tunnel. A critical section is selected based on the presence of grade V mudstone at tunnel location. Various parameters such as overburden, intact rock and rock mass properties are obtained from the study of Cao et al. (2018). Table 2-2 presents the properties of the intact and jointed mudstone encountered at the tunnel level in this project. The intact mudstone specimen is very weak with an unconfined compressive strength ranging from 1 MPa to 13 MPa. The *GSI* listed in Table 2-2, represents grade III to grade V rock mass.

However, in this analysis only grade V rock mass is taken into consideration as it represents the most critical case. There were no evidence that horizontal in-situ stresses are higher than vertical in-situ stresses. Hence, the in situ vertical effective stress at tunnel location prior to excavation is considered as governing value for ground squeezing condition. Figure 2-4a presents the ground elevation profile and tunnel location throughout the alignment of Laodongshan tunnel. Figure 2-4b represents the actual effective vertical stress and critical effective vertical stress along the alignment of the tunnel at which mudstone is encountered. Like the previous case, when the actual effective vertical stress is higher than critical effective vertical stress, the tunnelling may experience squeezing conditions.

Cao et al. (2018) observed maximum horizontal deformation and crown settlement in grade V mudstone of 402 mm and 275 mm, respectively. Tunnelling was very difficult, and this led to very high support requirement. From Figure 2-4b, the results of this analysis also predict the squeezing in grade V mudstone and the results align well with the field observations.

Uluabat Project Tunnel in Turkey

The Uluabat Project Tunnel is located in the southern part of Uluabat-Bursa (Apolyont) Lake. A power tunnel of 11.465 km length was proposed, and the excavation started in 2002. Initially, conventional tunnelling method and support systems were used in this project.

However, after one year due to excessive roof deformation, sometimes as large as one meter, the construction was halted until June 2006 (Bligin & Algan, 2012). Finally, the excavation resumed from chainage 11.465 to 1.792 km. The geology of Uluabat area contains the Karakya and Akçakoyun formations. The tunnel route within chainages 11.465 km to 7.750 km and 6.000 km to 1.792 km consisted of Karakaya formation. Karakaya formation is made up of Triassic aged metadetritic rocks like fine-grained meta-claystone, meta-siltstone, meta-sandstone and graphitic schists.

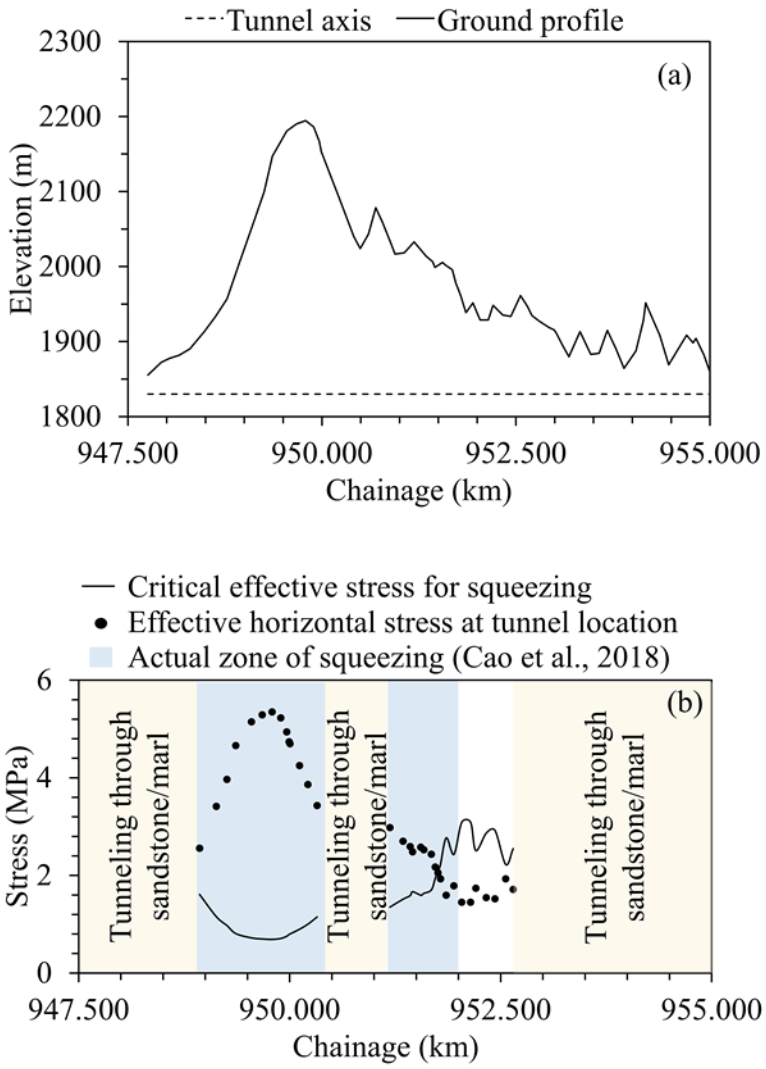

Figure 2-4 Laodongshan tunnel in China: (a) Ground and tunnel elevation; (b) Critical effective stress for squeezing and actual effective horizontal stress along the alignment.

Squeezing potential is examined only through Karakaya formation, which predominantly consists of mudstone. The properties of mudstone of Karakaya formation are given in Table 2-2. UCS of the rock in Karakaya formation is between 1 and 96 MPa, and the condition of the rock mass is varying from grade III to grade V. Properties are directly taken from Bligin & Algan (2012). The corresponding GSI for rock mass of grade V, IV and III is found to be varying from 5 to 45. This analysis provides a preliminary estimate of squeezing ground condition while tunnelling through grade III to grade V Karakaya formation.

To determine the squeezing potential of the ground, Bligin & Algan (2012) carried out the analysis by dividing the tunnel alignment into 18 galleries. Figure 2-5a presents the ground and tunnel elevation along the 18 tunnel galleries of the Uluabat project. The variation in an overburden at these 18 galleries can be clearly understood from Figure 2-5a. Critical effective vertical stress calculated by the empirical relation of Gutierrez & Xia (2009) and in-situ effective vertical stress at these 18 tunnel galleries are shown in Figure 2-5b. Bligin & Algan (2012) determine the

squeezing index for the 17 tunnel galleries out of the 18 observed. The squeezing index was found to vary from 13.1 kN h/m to 90.1 kN h/m with a mean value of 42.9 kN h/m among 17 tunnel galleries. Squeezing ground conditions were observed in all the tunnel galleries. The methodology proposed by Gutieerez & Xia (2009) is found to predict squeezing in all the 18 tunnel galleries. Hence, in this case, the methodology aligns 100% with the field observation.

Stillwater Tunnel in the USA

Stillwater tunnel is a 13 km long, and 3.5 to 4-m excavated diameter tunnel in the state of Utah, USA. The tunnel is a part of trans-mountain Strawberry Aqueduct of the Central Utah project of the US Bureau of Reclamation. Excavation of the tunnel initiated in 1976, and it was the second tunnel-boring machine (TBM) excavation in rock in the history of US (Phien-wej & Cording, 1991). The excavation encountered undesirable and unanticipated ground response, which led to severe damage to the TBM and the concrete segments. After extensive investigations, it was found that the prime cause of the problem was the unforeseen squeezing of the shale mass at such a depth due to its dominant plastic and viscous behavior (Morton & Provost, 1979).

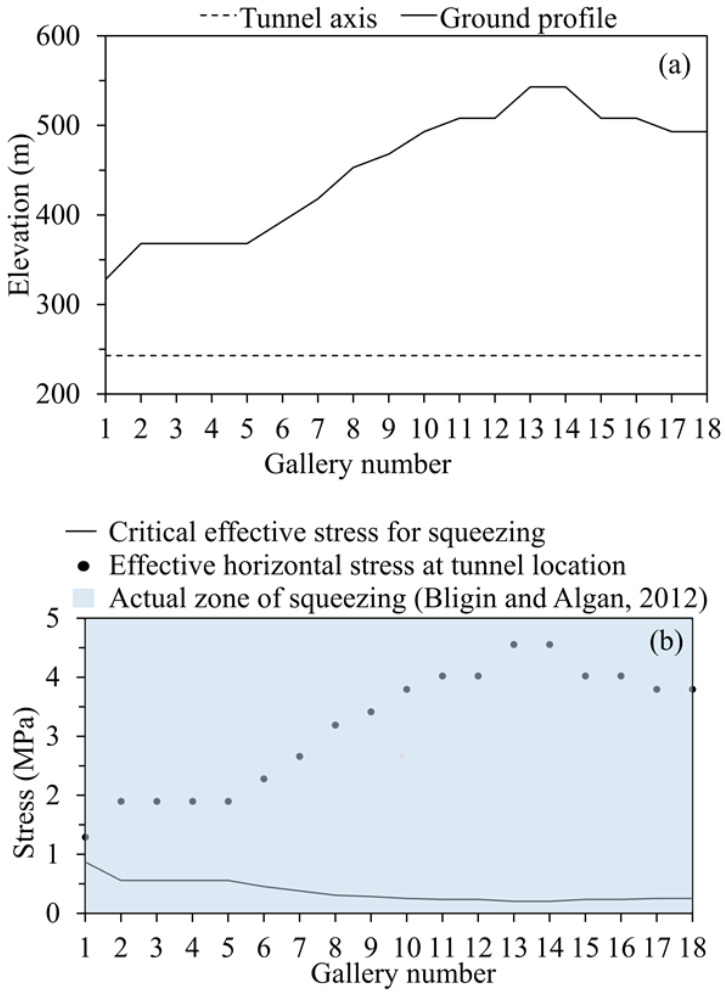

Figure 2-5 Uluabat project tunnel: (a) Ground and tunnel elevation; (b) Critical effective stress for squeezing and actual effective horizontal stress at 18 tunnel galleries.

Stillwater tunnel is located on the south western side of the Uinta mountain range of the Rocky Mountains system. The inlet portal of the tunnel penetrates sandstone and argillite of the Precambrian Uinta Mountain group for first 600 m. The tunnel alignment encounters 70 m wide disturbed zone of steeply dipping South Flank fault. After the fault, the tunnel alignment passes through red pine shales. This formation consists of a dark grey to black, medium to hard, thinly bedded to laminated, well-indurated shale with numerous thin (few centimetres to meters) inter-beds of sandstone and siltstone (Phien-wej & Cording, 1991). The overburden along the two-third length of this tunnel varies from 600 to 780 m.

Tunnelling is examined for squeezing ground condition only through the red pine shales. Phien-wej & Cording (1991) classified these shales into the following three groups: (a) class II which is moderately jointed; (b) class III for rock mass with tight shears spaced less than 0.3 m, and (c) class IV for rock mass with sheared or fault zones containing large amount of clay gauge. The properties of the shale encountered along the alignment of Stillwater tunnel are presented in Table 2-2. The strength of intact rock ranged from 50 to 92 MPa and *GSI* varying from 15 to 55.

Figure 2-6a presents the ground profile and tunnel axis along the alignment of Stillwater tunnel. Most of the alignment between chainage 2.790 km and 10.665 km encounters class II and class IV shale at tunnel location. Figure 2-6b presents the critical effective vertical stress for squeezing and in-situ vertical effective stresses along the alignment of tunnel in shale materials.

Phien-wej & Cording (1991) observed that approximately 26% of the tunnel length experienced light squeezing (up to 2% tunnel closure) to moderate squeezing (up to 5% tunnel closure). Moderate squeezing was observed in class IV shale only. However, Phien-wej & Cording (1991) did not explicitly mention the zone of light squeezing. As shown in Figure 2-6b, the current study based on the procedure by Gutierrez & Xia (2009) predicts squeezing in class IV shale throughout the alignment, whereas squeezing is predicted in some of the class II shale. Hence, the results of Phien-wej & Cording (1991) are comparable with the present analysis results.

2.6.2 Squeezing Number

In the previous section, it is observed that the Gutierrez & Xia (2009) methodology provides a good estimate for the preliminary assessment of the squeezing condition in the ground containing cemented clays. The methodology calculates critical effective vertical/horizontal stress for squeezing ($\sigma'_{critical}$). If the value of in-situ vertical/horizontal effective stress (σ') at tunnel level is higher than $\sigma'_{critical}$, the tunnel is in a squeezing ground condition. However, for lightly to very highly squeezing ground, σ' will be higher than $\sigma'_{critical}$. Based on the observations a squeezing number (S) is proposed given by Eq. 2-16.

$$S = \frac{\sigma'}{\sigma'_{critical}} \tag{2-16}$$

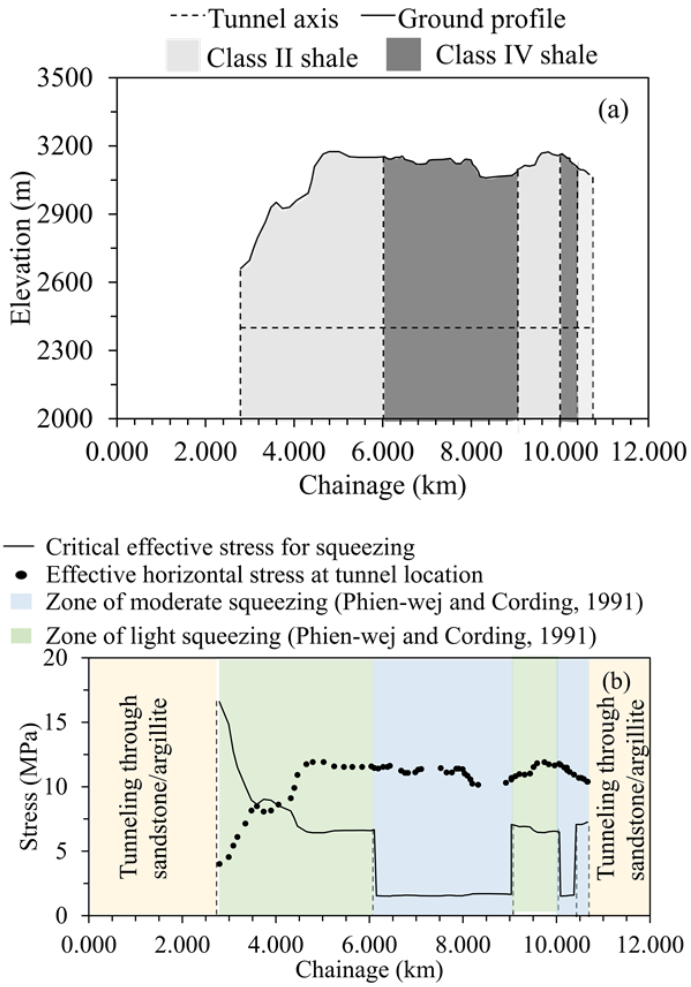

Figure 2-6 Stillwater tunnel, USA (a) ground and tunnel elevation; (b) Critical effective stress for squeezing and actual effective horizontal stress along the alignment.

According to Gutierrez and Xia (2009), σ' is the vertical effective stress at the tunnel location. However, in many cases horizontal effective stress can be greater than the vertical effective stress stress will contribute more towards tunnel wall displacement and hence, σ' is the maximum value among effective horizontal or vertical stress at tunnel location, i.e. among horizontal or vertical effective in-situ stress, a higher value will govern the squeezing ground condition.

If the value of *S* at a cross-section of the tunnel is greater than one, that tunnel section is in a squeezing ground condition. Figures 2-7a to 2-7d present the value of squeezing potential along the alignment of four tunnels considered in this study. In the case of John Street pumping station in Canada, the value of *S* varies from 0.26 to 2.97 as shown in Figure 2-7a and for this range of *S*, the present study predicts no squeezing to moderate squeezing (Figure 2-7a). Lo et al. (1987) observed moderate time-dependent deformations in the tunnel due to high horizontal in-situ stresses.

For Laodongshan tunnel in China, *S* is varying from 0.47 to 7.78 and the present study predicts no squeezing to high squeezing for this tunnel as shown in Figure 2-7b. From their field

measurements, Cao et al. (2018) observed that the maximum horizontal convergence and crown settlement were 402 mm and 275 mm, respectively. Hence, it is a case of high squeezing ground conditions.

In case of Uluabat project tunnel in Turkey, *S* varies from 1.48 to 22.32 and therefore according to the present study, it is a case of low to very high level of squeezing as shown in Figure 2-7c. Bligin & Algan (2012) reported maximum tunnel wall convergence of 1.2 m and corresponding tunnel closure of 14%. This presents a case of very highly squeezing ground conditions. As already stated, Bligin & Algan (2012) determined the squeezing potential of ground for TBM performance by introducing a parameter called 'squeezing index'. In the zone of moderate squeezing, the value of *S* is found to be between 3.40 and 7.01. Whereas, in the zone of high squeezing value of *S* is observed in the range of 10.30 to 17.10.

For Stillwater tunnel in the USA, the value of *S* is observed in a range of 0.24 to 7.55 and hence, as per the present study, no to high squeezing is observed in the tunnel (refer to Figure 2-7d). As already mentioned, moderate squeezing was observed in class IV shale (Phien-wej & Cording, 1991) and the corresponding *S* value range from 5.94 to 7.55. Whereas, light to no squeezing was observed in case of class II shale and the corresponding *S* value range from 0.24 to 1.85 (Phien-wej & Cording, 1991). Combining all the results, it can be concluded that when *S* is less than one, very low or no squeezing is observed in the ground containing cemented clays. When the value of *S* is between one and two, low squeezing in observed in the ground. If the value of *S* is between two to seven, fair to high squeezing is observed in the ground and for *S* values from 7 to 17, ground shows high to very high squeezing behavior. Finally, if the value of *S* is greater than 17, extremely high levels of squeezing is observed in the ground. Table 2-3 presents the summary of the relation between the value of *S* and squeezing conditions in the ground.

The proposed range of squeezing number (*S*) for a different level of squeezing is presented along with the observation of Hoek & Marinos (2000) in Table 2-3. Together, the proposed squeezing number along with the squeezing classification of Hoek & Marinos (2000), can give a fair estimate of the ground condition. Considering the case of Uluabat project, where the maximum value of *S* obtained is 22.32, and the observed tunnel strain was 14 %. It can be observed that the proposed classification system as well as the Hoek & Marinos (2000) classification system can predict very high squeezing ground condition.

2.7 Conclusions

A comprehensive review of existing methodologies for the evaluation of tunnel squeezing was presented in this chapter. The methods were classified based on the nature of ground material, stress-strain behavior and the material flow properties.

A methodology was proposed to predict the level of squeezing conditions in tunnels constructed in squeezing clay-rich rocks. The method is based on the SHANSEP model, Peck's stability number and Hoek-Brown's GSI. The proposed methodology provides an estimate of critical effective principal stress $\sigma'_{critical}$ at tunnel location. The $\sigma'_{critical}$ profile is determined for four different tunnels constructed in cemented clays. If $\sigma'_{critical}$ is less than major effective principal stress σ' at tunnel location, the tunneling is in squeezing ground conditions. Based on the ratio of

σ' and $\sigma'_{critical}$, a squeezing number *S* is proposed to predict the level of squeezing for tunnels in clays and cemented clays.

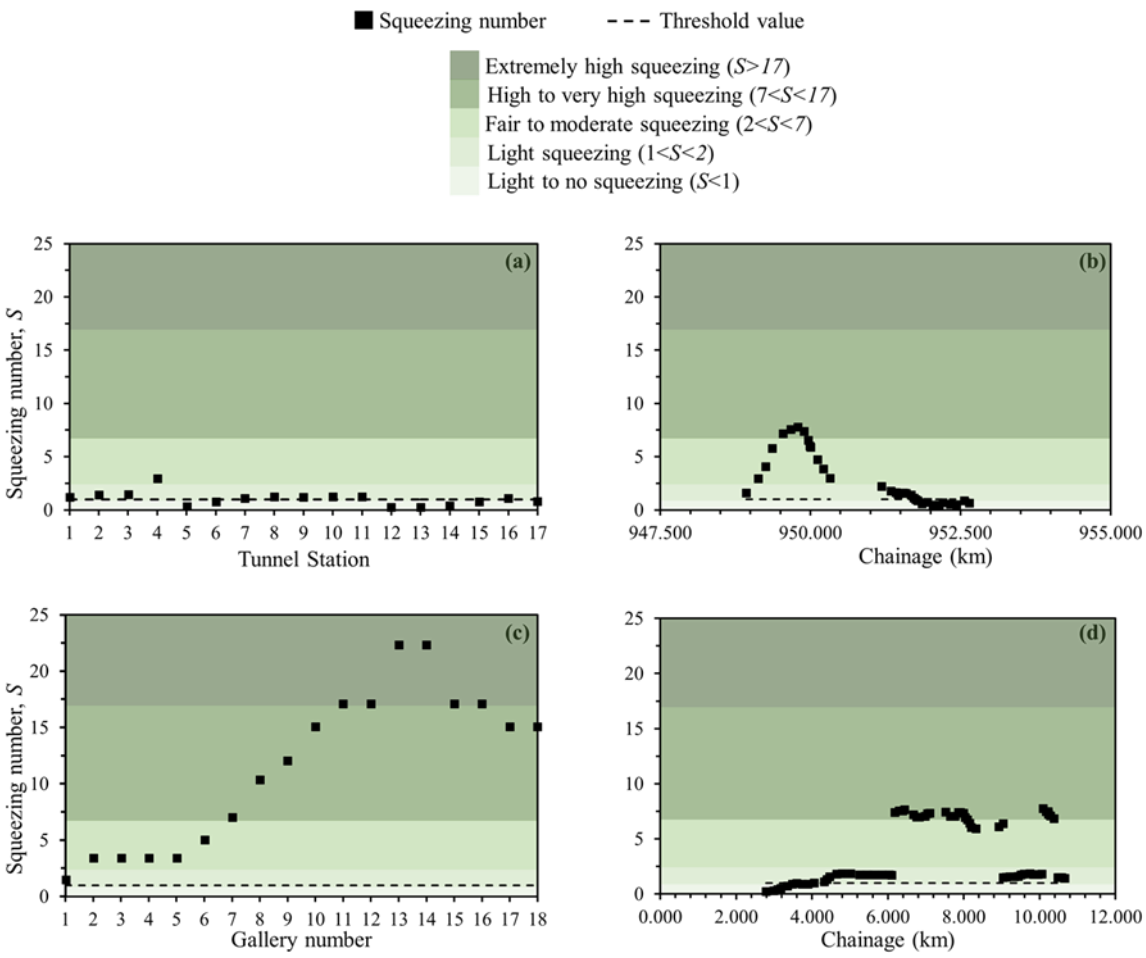

Figure 2-7 Squeezing number along the alignment of different tunnels (a) John Street pumping station tunnel in Canada, (b) Laodongshan tunnel in China, (c) Uluabat project tunnel in Turkey, and (d) Stillwater tunnel in United States.

It is observed that when the value of *S* is less than 1, the tunnel will experience no or very light squeezing and the tunnel strain will be less than 1%. If the value of *S* lies between 1 and 2, then the tunnel will experience light squeezing and the corresponding tunnel strain will be between 1.5% and 2%. For the value of *S* between 2 and 7, then the tunnel will experience fair to moderate squeezing and the tunnel strain will be 2.5% to 5%. Any value of *S* between 7 and 17, corresponds to high to very high squeezing condition and tunnel strain will be 5% to 10%. The value of *S* higher than 17 reflects very high squeezing ground conditions and tunnel strain can be expected to be more than 10%. The proposed methodology provided great agreement with the existing field data and proved efficient in the quick assessment of squeezing ground conditions.

Table 2-3 Description of the squeezing level for different value of squeezing number

Class number	**Squeezing number, *S***	**Squeezing level**	**Hoek and Marinos (2000)**	
			Squeezing level	**Tunnel strain (%)**
1	$S < 1$	Light to no squeezing	Few support problem	$\varepsilon_t < 1.0$
2	$1 < S < 2$	Light squeezing	Minor squeezing	$1.0 < \varepsilon_t < 2.5$
3	$2 < S < 7$	Fair to moderate squeezing	Severe squeezing	$2.5 < \varepsilon_t < 5.0$
4	$7 < S < 17$	High to very high squeezing	Very severe squeezing	$5.0 < \varepsilon_t < 10.0$
5	$S > 17$	Extremely high squeezing	Extreme squeezing	$\varepsilon_t > 10$

CHAPTER 3 - NEW PHYSICAL MODEL TO STUDY TUNNELS IN SQUEEZING CLAY-RICH ROCKS

3.1 Abstract

Squeezing ground conditions in tunnels are often associated with rock mineralogy, strength, ductility, excavation sequence, and the magnitude of in-situ stresses. Numerous methodologies and empirical correlations have been proposed in the past to determine the level of ground squeezing conditions in tunnels, but most of them are problem-specific and limited in scope. This chapter presents a fundamental study of tunnel squeezing using a novel experimental approach to simulate tunnel boring machine (TBM) excavation in squeezing ground conditions. The proposed experimental setup employs a cubical specimen of synthetic mudstone with each dimension being 300 mm, which the six faces subjected to a true-triaxial state of stress with different magnitudes of principal stresses and stress levels that correspond to realistic in situ conditions. A miniature TBM was designed, engineered and used to excavate a tunnel into the host rock (specimen) while the rock was subjected to a true-triaxial state of stress. Embedded strain gages and acoustic emission (AE) sensors, which were coupled on the surface of the tunnel liner, were also used to monitor the tunnel's response during the excavation stage. The results from the experiment confirmed the capability of the physical model to provide a better understanding of tunnel squeezing and to delineate the damage and the deformation that occurs during instant stress release and creep behavior of rock around the tunnel boundary during tunnel excavation.

3.2 Introduction

Many underground projects, such as tunnels and mining excavations, are constructed in the severest of ground conditions (high in-situ stresses and weak rock mass) that can arise to major excavation issues, including rockburst and squeezing ground conditions. Rockburst phenomenon involves violent ejection of rock from the surface of a tunnel during the excavation stage (Ortlepp & Stacey, 1994), while squeezing phenomenon is characterized by gradual convergence of the tunnel boundary during and even after the excavation stage (Panet, 1996).

Over the years, engineers have faced momentous challenges during the construction of tunnels in squeezing ground conditions due to large unforeseen deformations. Squeezing or gradual deformation of the tunnel boundary is mainly attributed to the deformation, creep and consolidation behavior that may occur when clay minerals at very high in-situ stress are present (Terzaghi, 1946). Projects that are known to have experienced these phenomena are the Yacambu-Quibor water supply tunnel in Venezuela which was identified as the most challenging tunnel construction ever by Hoek & Guevara (2009); the John street pumping station tunnel in Canada (Czurda et al., 1973; Lo et al., 1987); the Laodongshan railway tunnel in China (Cao et al., 2018); the Uluabat project tunnel in Turkey (Bilgin & Algan, 2012); and the Stillwater tunnel in Utah in the United States (Phien-wej & Cording, 1991).

Over the last seven decades, based on field observations and laboratory testing, researchers have proposed various methodologies to study tunnels in squeezing ground conditions, many of which were also based on the properties of the ground material (Terzaghi, 1946; Rose, 1982; Wood, 1972; Jaegar & Cook, 1976; Jethwa et al., 1984; Verman, 1993). Various researchers have defined the critical cut-off value of tangential stress or strain for a tunnel to be in a squeezing ground condition

(Labasse, 1949; Saari, 1982; Sakurai, 1997; Aydan et al., 1996; Hoek & Marinos, 2000; Singh et al., 1992 & 2007; Majumder et al., 2017; Vrakas et al., 2018).

In the last three decades, many researchers shifted their focus to develop a methodology to study the tunnel in squeezing ground conditions considering the elastic, plastic, and viscous (creep) behavior of the material (Dusseault & Fordham, 1993; Barla, 1995; Gioda & Cividini, 1996; Sterpi & Gioda, 2009; Bonini et al., 2009; Debernadi & Barla, 2009; Barla et al., 2011; Manh et al., 2015).

From the literature, it is quite evident that the problem of squeezing is associated with the complexities of ductile and altered ground material and is mainly encountered in clay-rich rocks having poor deformability and strength properties. The problem of squeezing produces an inevitable effect not only on the short-term stability of the tunnel but on its long-term stability as well. Real-time monitoring of the tunnel wall stresses and displacements could help provide a better understanding of tunnels in squeezing ground conditions. However, since the in-situ tests are necessarily limited in time and cost, physical model tests now are considered a viable option for to improve the understanding of the stability and failure of geotechnical structure (Lin et al., 2015).

Many researchers have developed and implemented physical models to simulate the tunnel excavation process in soft ground in order to study the stability of lined and unlined tunnels (Terzaghi, 1936 & 1946; Love, 1984; Park et al., 1999; Adachi et al., 1995; Chambon, 1991; Kamata & Mashimo, 2003; Atkinson et al., 1975; Sharma et al., 2001). Examples of such physical models include the two-dimensional and three-dimensional trapdoor model (Lin et al., 2015; Terzaghi, 1936), a rigid tube with a flexible and rigid face as a lining element (Chambon, 1991; Kamata & Mashimo, 2003), an excavation tool such as an auger (Love, 1984), and a miniature shield TBM that can operate under centrifuge condition (Nomoto et al., 1999). Meguid et al. (2008) provided an extensive review of the developed physical models used in soft ground tunneling.

Laboratory scale models under 1g conditions can accurately simulate the excavation process, but they do not simulate the in-situ conditions. On the other hand, centrifuge testing simulates the in-situ stress state, but the excavation process must be simplified. Hence, a physical model test that can simulate tunnel excavation at in-situ stress conditions could provide a better understanding of tunnels in squeezing ground conditions.

This chapter introduces a novel physical model experimental setup that can simulate tunnel excavation in squeezing ground conditions using TBM at in-situ stress state at laboratory scale. Unlike other proposed physical models, the proposed setup simulates the tunnel excavation process and advancement at an in-situ stress level without any simplification in the excavation process. The proposed model also studies the three-dimensional effects of tunnel excavation on the ground deformation that occurs at and around the tunnel boundary. The design, fabrication and experimental work, along with our observations from the proposed physical model are discussed in this chapter.

3.3 Experimental Setup

The goal of the study presented in this chapter is to advance the investigation of the problem of squeezing in tunnels by developing a novel laboratory scale physical model. The key features of the proposed experimental setup are as follows:

The experiment is designed in such a way that it simulates a TBM excavation in a cubical rock specimen loaded at field stress level in a true-triaxial cell. The designed setup allows temporal monitoring of the TBM parameters (torque, thrust, and advance rate) and deformation at multiple points around the tunnel boundary during and after the excavation stage as well as damage monitoring using acoustic emission (AE) sensors.

Figure 3-1 illustrates the overall experimental arrangement of the proposed physical model, which has four major components: 1) a true-triaxial cell, 2) a miniature TBM, 3) a cubical rock specimen, and 4) a monitoring unit. The design and function of each component are discussed in the following sections.

3.3.1 True-triaxial Cell

A large number of true-triaxial equipment have been designed over the years which are still widely utilized in geomechanics research (e.g., Pater et al., 1994; Mogi, 2007; Kwasniewski & Takahashi, 2013; Frash et al. 2014). A typical true-triaxial cell accommodates a rectangular specimen, and loading is applied through rigid platens, flexible bladders, and passive confinement. The proposed physical model incorporates the use of a true-triaxial cell developed by Frash et al. (2014) at Colorado School of Mines. This apparatus, as shown in the schematic diagram in Figure 3-2, applies the load with the help of a mixed semi-flexible bladder flat jack and a passive confinement system. For each loading direction, one face of the cubical rock specimen (defined as the active face) comes in direct contact with the flat jack while the other face (defined as the passive face) supports the opposing reaction from the flat jack with a rigid plane, as shown in Figure 3-2.

The active face of the rock specimen has the following components: 1) one active hydraulic jack, 2) 300 mm diameter circular steel platens on both faces of the flat jack, and 3) a 300 x 300 mm^2 rectangular steel platen between the specimen and the circular steel platen. As shown in Figure 3-2, the rigid passive platen is fixed and made up of a plate on concrete. With this arrangement, the apparatus is capable of applying three independently controlled principal stresses up to 13 MPa to a 300 mm cubical rock specimen. The steel top lid of the true-triaxial cell is furnished with two ports 63 mm and 75 mm in diameter. The 63 mm diameter port provides a pass-through for the sensor cable and hydraulic lines while the 75 mm port at the center of the top lid provides access to the surface of the rock specimen for the tunnel excavation using the miniature TBM. More details about this true-triaxial apparatus can be found in Frash et al. (2014).

3.3.2 Miniature TBM

TBMs are quite popular in the modern tunneling industry not only due to their rapid excavation rate and circular tunnel profile but also their proven ability to reduce the damage to the surrounding ground, buildings, and utilities (Meguid et al., 2008; Ebrahim & Rostami 2009). TBMs cut through the rock with a rotary cutter head, which is equipped with either a disk cutter (for hard rock) or a tungsten carbide cutter bit (for soft ground). The selection of an appropriate TBM is governed by the existing geotechnical conditions and in-situ stresses (Shahriar et al., 2008). The problem of

squeezing ground is very common in clay-rich rocks, which are generally weak and highly deformable. Hence, a cutter head with a tungsten carbide bit is appropriate for squeezing ground conditions.

The proposed physical model further incorporates a miniature soft ground open face TBM, which is mounted on the top of the existing true-triaxial cell. One of the significant challenges faced was designing the high cutter head thrust and torque requirements (equivalent to in-situ requirements) at laboratory scale. Figure 3-3a presents the conceptual diagram of the miniature TBM designed and fabricated at the Colorado School of Mines. The miniature TBM was mounted on the top of a true-triaxial cell while the cubical rock specimen is loaded in a true-triaxial stress state.

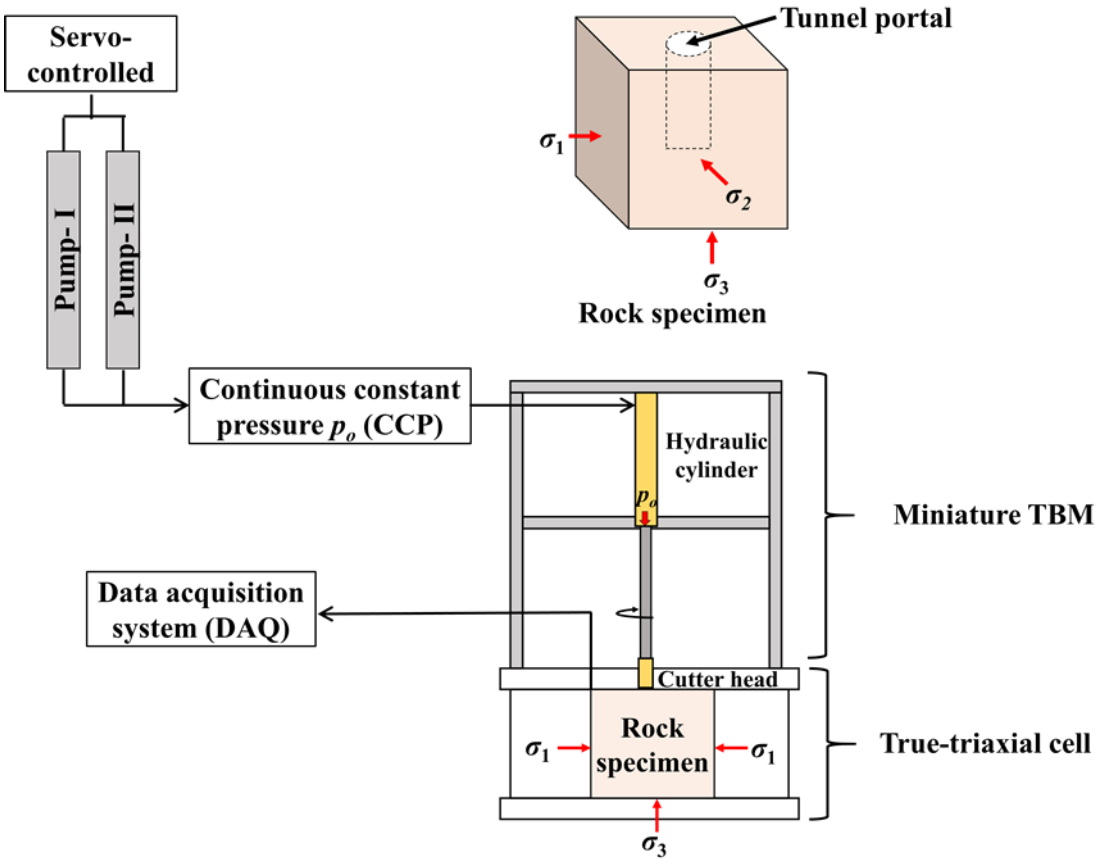

Figure 3-1 Schematic diagram of the proposed physical model with cubical rock specimen loaded in true-triaxial cell and tunnel is excavated using miniature tunnel boring machine.

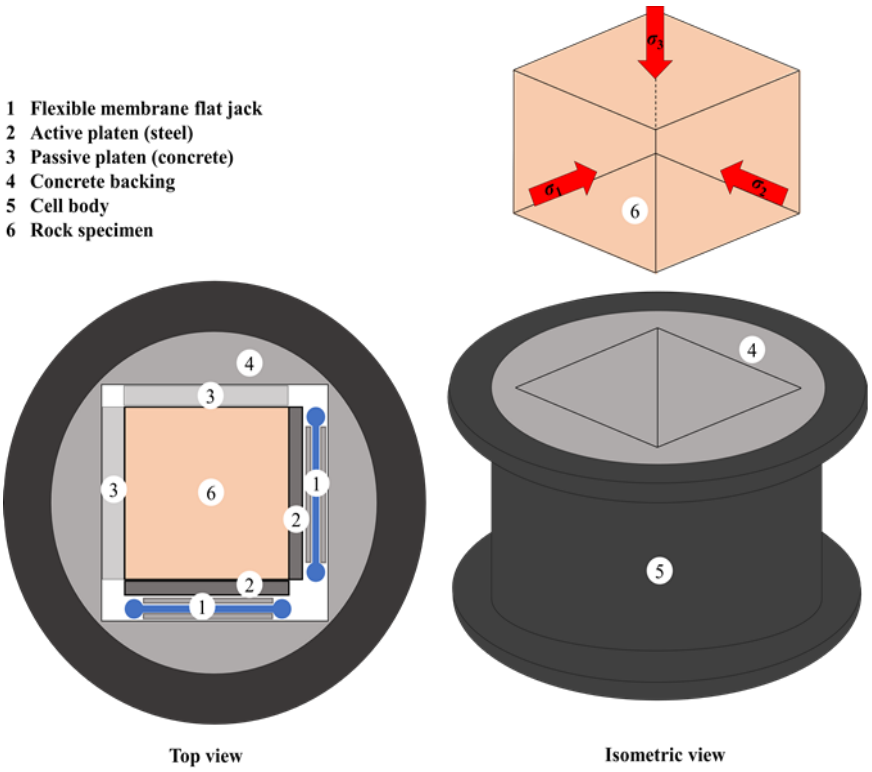

Figure 3-2 Schematic diagram of the true-triaxial loading setup at Colorado School of Mines (modified from Frash et al. 2014).

The required thrust in the miniature TBM is provided by a hydraulic jack controlled by a pair of ISCO syringe pumps, and the torque is provided by a constant speed alternating current (AC) motor. There are four components of the miniature TBM, which are discussed in the following section: a) thrust unit, b) torque unit, c) cutting unit, and d) supporting unit.

Thrust Unit

The thrust unit consists of a hydraulic jack, a pair of servo-controlled pumps, and a thrust bearing. As shown in Figure 3-3a, the hydraulic jack provides the required thrust to the cutter head, and a pair of servo-controlled syringe pumps control the jack. The hydraulic jack was manufactured by Enerpac and is globally available with the product code 'RC108'. The maximum operating pressure of this jack is 10 MPa, and the equivalent force is 101 kN.

The collapsed length and the extended length of this jack are 298 mm and 501 mm, respectively. Hence, the jack can provide a maximum stroke of 200 mm. This parameter governed the maximum length of the tunnel that can be excavated using this setup. The body of this hydraulic jack is steel, and the total weight of the jack is about 5.4 kg.

The hydraulic jack is controlled by a pair of D-series pumps manufactured by Teledyne ISCO and commercially available as the "65D Syringe Pump." Both pumps are controlled by a pump controller and a LabVIEW program, which maintains the continuous constant pressure (CCP) in the hydraulic jack. The pumps can maintain a CCP with an accuracy of ± 0.1 %.

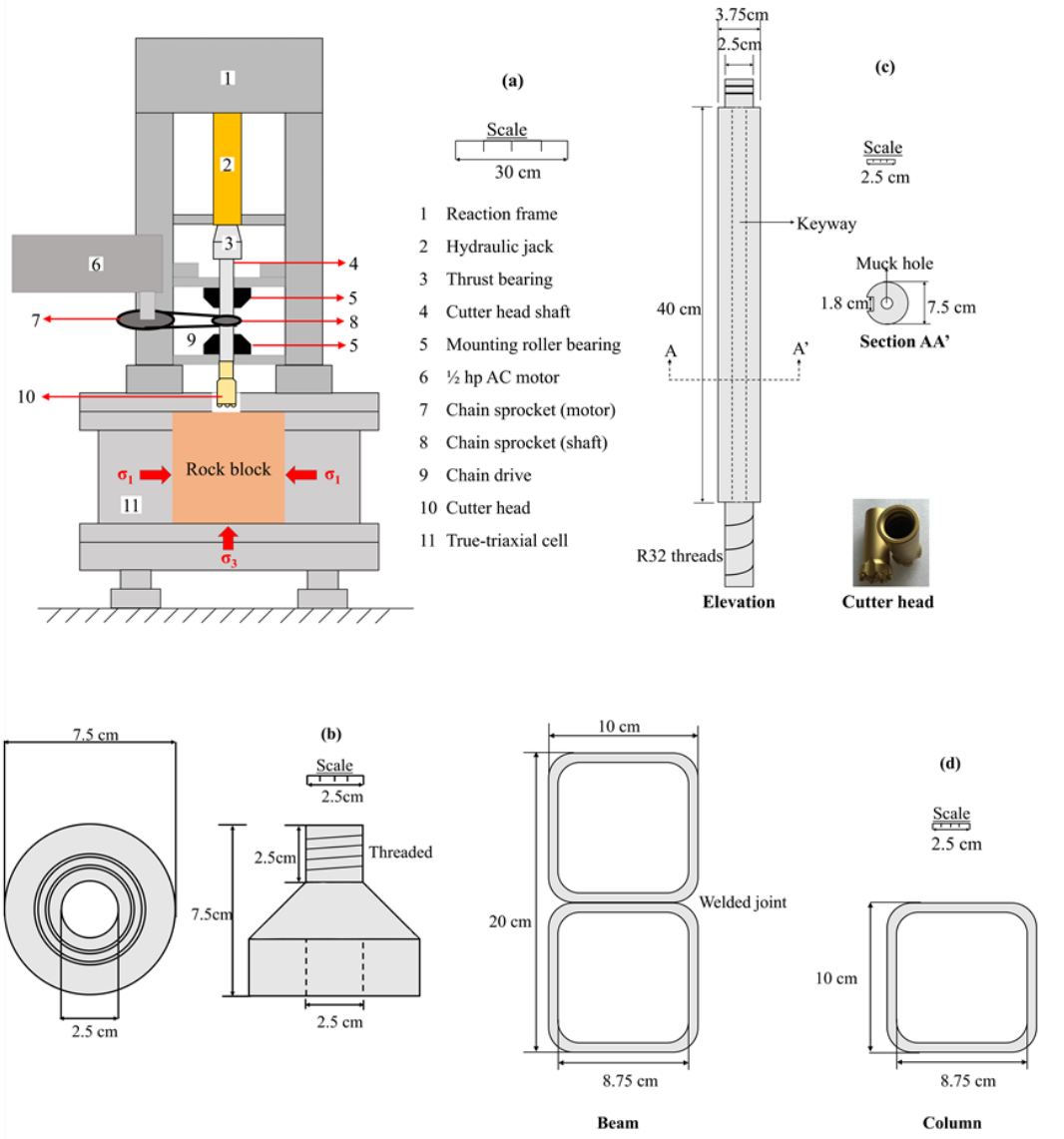

Figure 3-3 (a) Detailed schematic diagram of the proposed physical model with its key components (miniature TBM mounted on top lid of true-triaxial cell), (b) plan (left) and elevation (right) of the thrust bearing connecting plunger of hydraulic jack and cutter head shaft, (c) conceptual drawing of the cutter head shaft along with the cutter head and (d) cross-section of the beam (left) and column (right) of the reaction frame.

The plunger of the hydraulic jack has internal threads, which makes it flexible enough to connect to any size shaft using a step-up or step-down adapter. The thrust bearing was designed to do the following: 1) transfer the thrust force from the hydraulic jack to the rotation shaft, and 2) transfer zero or the least possible amount of torque from the rotating shaft to the plunger of the hydraulic jack. A "steel shield thrust ball bearing" was press-fit into a steel adapter that connects the 37.5 mm diameter plunger and the 37.5 mm diameter cutter head shaft. The conceptual drawing of this

assembly is shown in Figure 3-3b. The bearing can withstand dynamic thrust up to 31 kN and maximum rotational speed of 3,800 revolutions per minute (rpm).

Torque Unit

The torque unit consists of a constant speed alternating current (AC) motor, two chain sprocket gears (one at the axle of the motor and the other at the cutter head shaft), and a chain. A 0.5 hp, 115V, single-phase constant speed AC motor is used, which provides the torque required by the cutter head shaft via the chain drive. The motor rotates at a constant speed of seven revolutions per minute by varying the torque required to maintain the constant speed. The motor can provide a maximum torque of 400 N-m, and the motor is supported by the reaction frame shown in Figure 3-3a.

A roller chain, which has proven to be a very efficient method of power transmission over time was the choice for the drive chain to transfer rotational power from the motor to the cutter head shaft as shown in Fig 3-3a. One of the two sprocket gears is attached to the shaft of the motor and the other to the cutter head shaft. Power is transmitted from the motor's sprocket gear to the cutter head sprocket gear via the roller chain. The number of teeth on the sprocket gear of the motor is twice that of the teeth on the sprocket gear of the cutter head shaft. Hence, the rotational speed of the cutter head shaft is twice that of the motor. The cutter head shaft slides axially along the sprocket.

Cutting Unit

As shown in Figure 3-3a, the cutting unit has a shaft with a cutter head connected at one end. The other end of the shaft is coupled with a hydraulic jack using a thrust bearing. The cutter head shaft was fabricated from machinable steel, and its overall length of 500 mm was divided into three parts. One end of the shaft fits into the thrust bearing, which is 25 mm outer diameter and 25 mm in length. The other end of the shaft is 75 mm long, with R32 threads on the surface that screw in the drill bit. The remaining 400 mm length of the shaft has an outer diameter of 37.5 cm with a keyway 18 mm wide and 18 mm deep. The technical drawing of the cutter head shaft is shown in Figure 3-3c.

As already discussed, the miniature TBM was designed for excavation in soft rock (e.g., mudstone) and hence has a drill bit with a cutter head having nine button type tungsten carbide bits (see Figure 3-3c). The diameter of the cutter head is 48 mm, and the overall length of the drill bit is 125 mm. The shank of the bit has R32 female threads and can be easily attached to a shaft having similar male threads. The cutter head was manufactured and supplied by Epiroc in the United States and by Atlas Copco in other countries.

Supporting Unit

The cutter head shaft has a very high length to diameter ratio of 6.67 so there is a high possibility that the shaft could buckle during the drilling. However, the shaft is prevented from buckling by two "mounting roller bearings" with a four-bolt flange installed as shown in Figure 3-3a. The mounted roller bearings are further supported by the reaction frame and can support a shaft of 375 mm diameter under a dynamic radial load of 1,200 N-m.

The reaction frame of our miniature TBM supports the entire assembly of the heavy equipment hydraulic jack, the AC motor, and the mounting roller bearing. The reaction frame has two square columns, one rectangular beam and four rectangular bracings welded together, as shown in Figure 3-3a. The frame is constructed of ASTM A500 structural steel. A cross-section view of the beam and column is shown in Figure 3-3d.

3.3.3 Cubical rock specimen

The objective of study is to investigate the tunnel construction in squeezing "clay-rich" rocks (mudstones). The mudstone specimen is composed of fine-grained detrital sediments and more than 50 percent of the particles were smaller than 62 μm (Potter et al., 2005). Unconsolidated sediments are known as mud (or clay), whereas its lithified equivalents are known as mudstone (Potter et al., 2005). There is a difference in the mechanical behavior (strength and deformation properties) of mud and mudstone. For example, the typical shear strength of soft clay has been observed to be less than 25 kPa while mudstones are on the order of few megapascals depending on the degree of weathering (Chandler, 1969; Miura et al., 2001; Horpibulsuk, 2005; Saadeldin & Siddiqua, 2013).

This study required cylindrical and cubical mudstone specimens for material characterization and physical model tests, respectively. Due to the soft nature of mudstone, it was difficult to obtain continuous and homogenous regular-shaped specimens from the field. Therefore, a significant effort was made to develop a suitable synthetic model material in the laboratory that has properties similar to naturally occurring mudstone. Johnston & Choi (1986) developed a homogeneous and isotropic synthetic mudstone, named "Johnstone," for laboratory physical model studies by mixing pulverized natural mudstone, cement, and water in defined proportions.

The addition of cement is a well-established technique to increase the shear strength of clays. Over the years, researchers have tested the resilience of clay-cement mixes at different water to cement ratios, w/c_m, and cement content, C (Gallavresi, 1992; Lee et al., 2005; Horpibulsuk et al., 2010; Seng & Tanaka, 2011; Lu et al., 2012; Zhang et al., 2013; Chian et al., 2015). Various empirical correlations, based on laboratory studies, have been suggested over the years to describe the effects of different combinations of water to cement ratio w/c_m, and cement content C to the strength gain of the clay-cement mix.

The model material was designed according to empirical correlations proposed by Chian et al. (2015) based on their laboratory experience with Singapore marine clay. Based on their model, the unconfined compressive strength (UCT or q_u) for different w/c_m and soil to cement ratio (s/c) is given in Eq. 3-1.

$$q_u = \frac{a_c + b_c(s/c)}{Y^{(w/c_m)}} ln(t) \qquad (3\text{-}1)$$

where, a_c and b_c are the clay strength parameters and can be determined experimentally.

Methodology

The synthetic mudstone is prepared in the laboratory by mixing type I/II cement, clay, and water in defined proportions shown in Table 3-1. A description of each mix ingredient follows.

Clay: Commercially available standard dry clay with the label "Goldart Clay" supplied by Laguna Clay Company, California, USA, was used in the preparation of the artificial mudstone. Chemically, this clay is hydrous aluminum silicate and has a granular appearance and an earthy color. According to the datasheet provided by the supplier, this clay is non-volatile and slightly soluble in water and has a specific gravity of G_{sc} of 2.60. The clay we used contained 10-30% crystalline silica by weight, cristobalite 0.075 mg/m^3, tridymite 0.05 mg/m^3 and quartz 0.125 mg/m^3. The plasticity index of the clay was 13.02%, with the liquid limit of 48.45% and the plastic limit of 35.43%.

Cement: The cementing agent used in this mix was commercial grade type I/II Portland cement manufactured by Quikrete, which meets the requirements of ASTM C150. The specific gravity of the cement, G_{scm} was 3.15. After choosing cement as the bonding material, the next step was to find the correct proportion of cement. The amount of cement to add to the mix is defined by the parameter cement content, C, which is given as the weight of the cement to the total weight of its solids (cement and clay). After performing various trials, we determined that a cement content of 30% (C = 0.3) would provide the required adhesion to the mix.

Water: The amount of tap water required can be quantified in terms of the water to cement ratio by weight w/c_m. For a fixed cement content C, a very high w/c_m can lead to a long setting time and a low mix density. On the other hand, a small w/c_m can lead to stronger and more brittle specimens than naturally occurring mudstone. Therefore, an optimum amount of w/c_m is very important when preparing a representative specimen of mudstone. A w/c_m of 1.5 was found to be adequate for preparing the model material. Distilled water was used instead of tap water to eliminate the effects of the minerals in tap water, which might affect the hydration of the cement and the properties of the clay minerals.

Additives: A superplasticizer was added to increase the workability of the mix. The correct proportion of superplasticizer depends on the type and grade of the superplasticizer used. BASF MasterGlenium 7920 was used as a water-reducing agent for concrete mix. It can be added with the initial batch of water or after wet mixing; however, its maximum effects are generally obtained with the delayed addition. It was determined that the appropriate amount of this admixture was 60 ml/kg cement.

Table 3-1 Mix proportion for the synthetic mudstone prepared in the laboratory.

Component (unit)	Cement content, C	Water to cement ratio by weight, w/c	Quantity required for 1 m^3 of the mix			
			Clay (kg)	Cement (kg)	Water (kg)	Superplasticizer, MasterGlenium 7920 (litres)
Quantity	0.3	1.5	859.79	368.48	552.72	45

Material Characterization

Cylindrical specimens, 51 mm in diameter and 102 mm in length were prepared to determine the physical and mechanical properties of the rock specimen. Each cylindrical specimen was cured in water for 28 days to reach complete hydration of the cement in the mix. The tested cylindrical specimens met the dimensions and shape tolerance as per ASTM D4543-19. Unconfined compressive tests (UCT) were carried out to determine the unconfined compressive strength (UCS), σ_c, and the elastic modulus, E_{50}, of the rock specimen as per ASTM D7012. Undrained triaxial tests were performed on the cylindrical rock specimen using a Hoek cell according to the method suggested by Hoek & Franklin (1970) to determine the confined compressive behavior of the rock specimens. The triaxial tests were performed on the rock with confining pressure, σ_3 varying from 1 to 6 MPa. Both the UCT and triaxial tests were displacement-controlled with a constant axial strain rate of 10^{-5} s^{-1}. The axial stress-strain plot obtained from the UCT (σ_3 = 0 MPa) and triaxial tests at different confining pressure (σ_3 varying 1 MPa to 6 MPa) are shown in Figure 3-4a. Physical and mechanical properties of 28 days cured synthetic mudstone are given in Table 3-2.

From the 10 UCT tests on the cylindrical rock specimens, the mean UCS and tangential elastic modulus (at 50% of peak stress), E_{50} were found to be 4.47 MPa and 0.67 GPa with standard deviations of 0.15 MPa and 0.02 GPa, respectively; and from the measurement of the axial and radial strain, the Poisson's ratio (ν) was determined as 0.13. For each plot shown in Figure 3-4a, using the peak deviatoric stress (σ_1 - σ_3) achieved at each σ_3, the Mohr-circles were plotted to determine the failure envelope (refer to Figure 3-4b). The Mohr-Coulomb failure criterion was found to provide a good estimate of the failure envelope in a confining pressure range of 0 MPa to 6 MPa. As shown in Figure 3-4b, using the Mohr-Coulomb linear fit, the undrained cohesion *c*, and friction angle ϕ were found to be 2.06 MPa and 10°, respectively.

To characterize the strain-rate sensitivity of the synthetic mudstone, 15 triaxial compression tests at a constant confining stress of 1 MPa, three each at the axial strain rates, $\dot{\varepsilon}_1$, approximately 5 x 10^{-6} s^{-1}, 1.3 x 10^{-5} s^{-1}, 1.7 x 10^{-5} s^{-1}, 2.3 x 10^{-5} s^{-1} and 1.5 x 10^{-4} s^{-1} . It can be seen from Figure 3-4c and 3-4d that the maximum value of the deviatoric stress and the elastic tangential modulus, given by the tangential slope of the linear portion of the stress-strain curve, increased with increases in the strain rate, respectively.

Table 3-2 Physical and mechanical properties of synthetic mudstone after 28 days of curing.

Property	Saturated unit weight, γ_{sat} (kN/m^3)	Dry unit weight, γ_{dry} (kN/m^3)	Void ratio, *e*	Water content, w_w (%)	At strain rate = 10^{-5} s^{-1}		
					UCS, σ_c (MPa)	Elastic modulus, E_{50} (GPa)	Poisson's ratio, ν
Value	18.12	12.93	1.20	45	4.47 ± 0.15	0.65 ± 0.02	0.13

The strain rate dependency of the material's strength can be represented by the power-law relationship in Eq. 3-2 (Katsuki & Gutierrez 2011)

$$\sigma_d = \sigma_{dS} + \sigma_{dVR}\dot{\varepsilon}_1^m \quad (3\text{-}2)$$

where σ_{dS} is the static component of the material strength, σ_{dVR} is a material parameter for the strain rate sensitive material strength, and m represents the strain rate sensitivity parameter for material strength at σ_3 = 1 MPa. Based on the experimental observations of Katsuki & Gutierrez (2011), it is assumed that material does not show significant rate sensitivity for $\dot{\varepsilon}_1 \leq 1 \times 10^{-5}$ s^{-1}. Hence from the triaxial test data ($\dot{\varepsilon}_1 = 1 \times 10^{-5}$ s^{-1}), the value of σ_{dS} could be taken as 4.51 MPa at σ_3 = 1 MPa. The best fit for Eq. 3-2 is shown in Figure 3-4c as a dotted line, was obtained by taking σ_{dVR} = 187.39 MPa and m = 0.65. The value of strain rate sensitivity m = 0.65 suggests that the response could be intensified approximately (at σ_3 = 1 MPa) 4, 20, and 89 times higher as the strain rate increased 10^1, 10^2, and 10^3 times, respectively.

3.3.4 Monitoring System

The proposed experimental setup includes continuous monitoring of: a) the TBM output (thrust and torque); b) the energy release associated with rock damage using acoustic emission (AE); and c) deformation around the excavation using the multiple points borehole extensometer (MPBEx). As shown in Figure 3-1, the thrust of the TBM was controlled by a pair of the servo-controlled pumps under continuous constant pressure (CCP) mode, which allowed the TBM to apply constant thrust at the excavation face. The change in advance rate of the TBM was back-calculated from the change in flow rate Q with time t of the servo-controlled pumps. The torque provided by the TBM was continuously monitored by a separate data acquisition unit (DAQ) that recorded the power output from the constant speed alternating current (AC) motor.

The AE events were monitored using the Physical Acoustic Corporation (PAC) AE monitoring system with six WSα sensors and three PCI-2 cards mounted in the Micro-II chassis. Six AE sensors were used because, in case we do not get high-quality data from two or three sensors, there should be high-quality data from the minimum number of sensors required for geophysical characterization. As shown in Figure 3-5a, six AE sensors were placed on the test specimen surfaces and were attached directly to the face of the specimen using a thin layer of vacuum gel for coupling. The six AE sensors were able to collect direct AE signals with minimal reflection, surface interference, sensor orientation error, or attenuation effects. The use of six sensors also enabled the application of moment-tensor analysis to classify recorded AE events according to their location and failure modes, which were either tensile dominated, shear dominated, or mixed-mode.

Strain gauges were embedded in the cubical specimen of mudstone to monitor the strains around the excavation. Due to the very high-water content of the synthetic mudstone, there was improper adhesion between the strain gages and mudstone. Hence, the strain gauges cannot be directly embedded in the specimen. A miniature multiple point borehole extensometer (MPBEx) was prepared using a thin, flexible Teflon material in this work and an array of strain gauges as shown in Figure 3-5a. These techniques ensured adequate adhesion of the strain gauges to the Teflon sheet and was an indirect way to measure strain at multiple points in the rock specimen. Our methodology was validated by embedding an axial strain gauge in a cylindrical specimen loaded

in uniaxial compression and then comparing the observations with the strain gauge results on the surface. The strain gauge, glued on a 1 mm thick 10 x 10 x mm^2 Teflon sheet, was embedded longitudinally in the cubical synthetic mudstone specimen as shown in Figure 3-5b. The specimen was loaded with a compressive load and the strains from the embedded strain gauge were compared with the strains from a linear variable differential transformer (LVDT) that was monitoring in the same direction. It can be seen from Figure 3-5b that the strains from the embedded strain gauges were well within 5% difference to the strains recorded by LVDT. Hence, this technique was shown to be entirely instrumental in determining strain at a point inside the synthetic mudstone specimen.

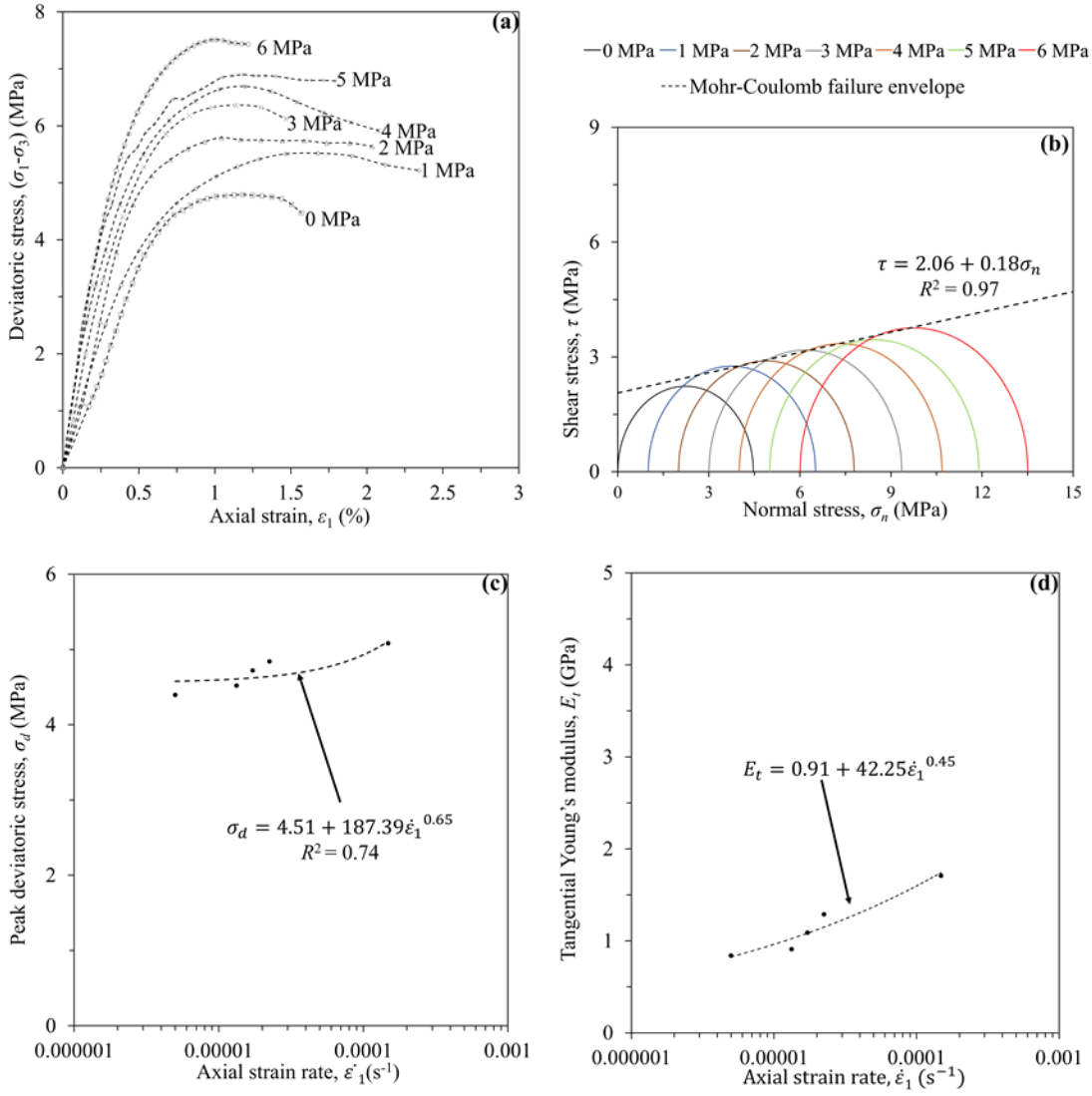

Figure 3-4 (a) Uniaxial compression test and triaxial tests axial stress-strain plot with σ3 varying from 0 MPa to 6 MPa, (b) shear stress τ- normal stress σ_n plot with Mohr-Coulomb failure envelope, (c) change in peak deviatoric with axial strain rate $\dot{\varepsilon}_1$ with σ_3 = 1MPa, and (d) change in tangential elastic modulus (E_t) with axial strain rate ($\dot{\varepsilon}_1$) at σ3 = 1MPa.

3.4 Experimental Observations and Discussions

Figure 3-6 is a photo of the assembled proposed physical model designed and fabricated at the Colorado School of Mines. The designed miniature TBM is mounted on the top of the existing true-triaxial cell. This setup can simulate TBM excavation at maximum stress of 13 MPa, which is equivalent to tunnel excavation at around 500 m depth for clay-rich rocks.

A test was carried out to validate the capability of the designed physical model. A 300 x 300 x 300 mm^3 synthetic mudstone specimen was prepared with six AE sensors on the surface of the specimen (Figure 3-5) and four embedded MPBEx (M1, M2, M3, and M4). Each MPBEx strip had four strain gauges that monitored radial strain at multiple locations and at 50 mm from the center of the tunnel. The geometrical locations of the four MPBEx and the strain gauges are shown in Figure 3-7. Due to the homogenous and isotropic behavior of the rock specimen, the response of the material was axisymmetric.

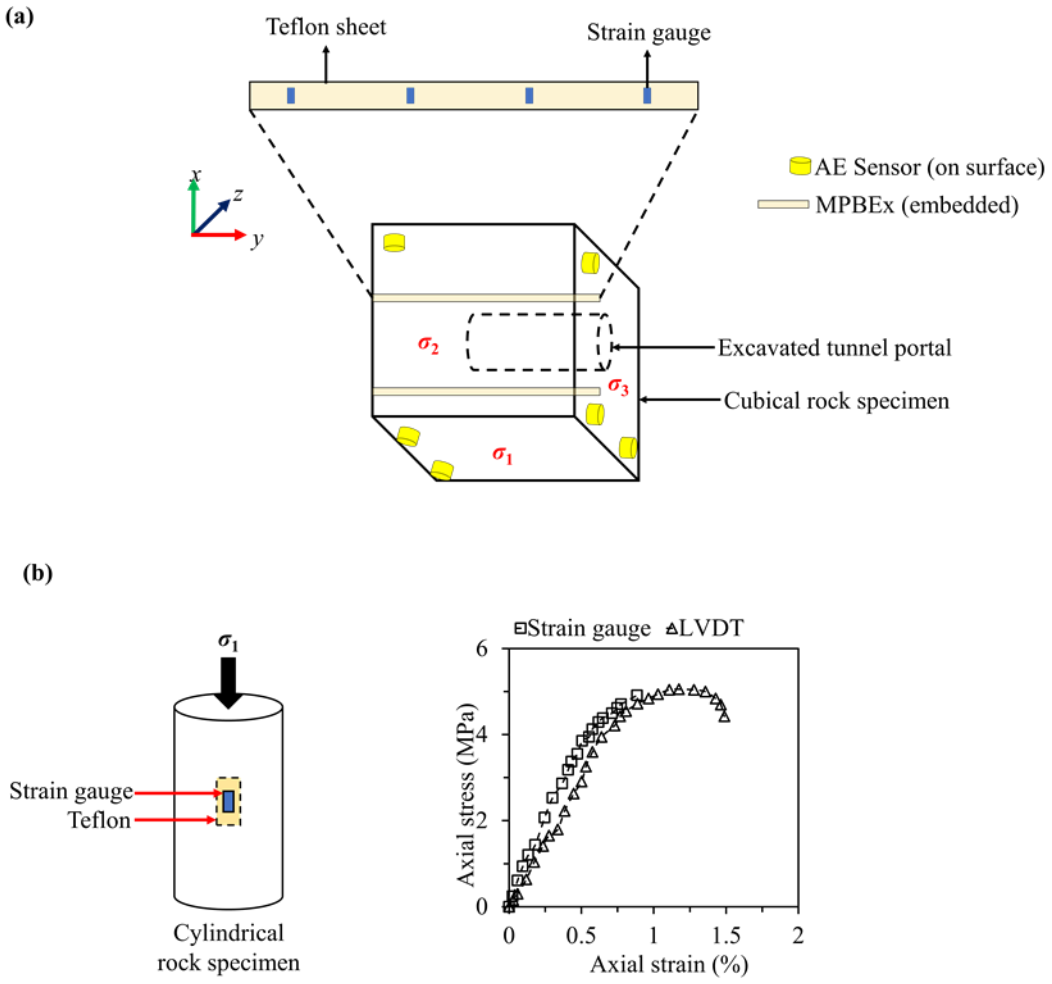

Figure 3-5 (a) MPBEx embedded in the cubical synthetic mudstone specimen along with AE sensors on the surface, and (b) validation of the embedded strain gauge technique.

Hence, the strains obtained from the MPBEx M1 and M3 represent strain fields that were represented by MPBEx M2 and M4, respectively (Figure 3-7), which mathematically cab be expressed as

$$\varepsilon_{C1i} = \varepsilon_{C2i} \quad (3\text{-}3)$$

$$\varepsilon_{S1i} = \varepsilon_{S2i} \quad (3\text{-}4)$$

where i is an integer between 1 and 4, and ε_{C1i}, ε_{C2i}, ε_{S1i}, and ε_{S2i} represent the strain measurements from strain gauges C_{1i}, C_{2i}, S_{1i}, and C_{1i}, respectively.

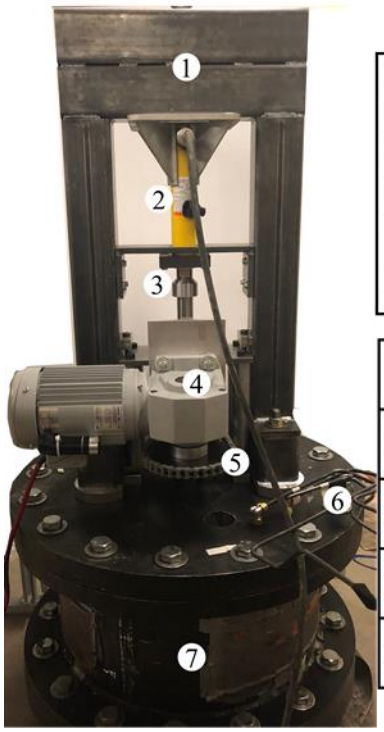

1 Reaction frame for TBM
2 Hydraulic cylinder
3 Cutter head shaft
4 Constant speed AC motor
5 Chain drive
6 Hydraulic and sensor lines
7 True-triaxial cell

TBM parameter	*Value*
Cutter head diameter	50 mm
Maximum stroke (mm)	160 mm
Maximum TBM thrust	100 kN
Maximum TBM torque	400 N-m

Figure 3-6 Physical model to study tunnels in squeezing ground conditions designed and fabricated at Colorado School of Mines.

It can be argued that only two MPBEx (either of M1 or M2 and M3 or M4) are sufficient to obtain the required strain measurement. However, the success rate of the measurement from the embedded strain gauges was around 70 %, hence, four MPBEx were used for an extra precaution. The prepared cubical rock specimen was cured in water for 28 days to allow complete hydration of the cement in the mix. After curing the specimen was loaded in a true-triaxial cell with principal stresses of σ_1 = 10.84 MPa, and σ_2 = σ_3 = 5.42 MPa. While the rock specimen was loaded in the true-triaxial stress state, a 50 mm diameter tunnel was excavated in the rock specimen using the miniature TBM. The experimental observations are discussed in the following sections.

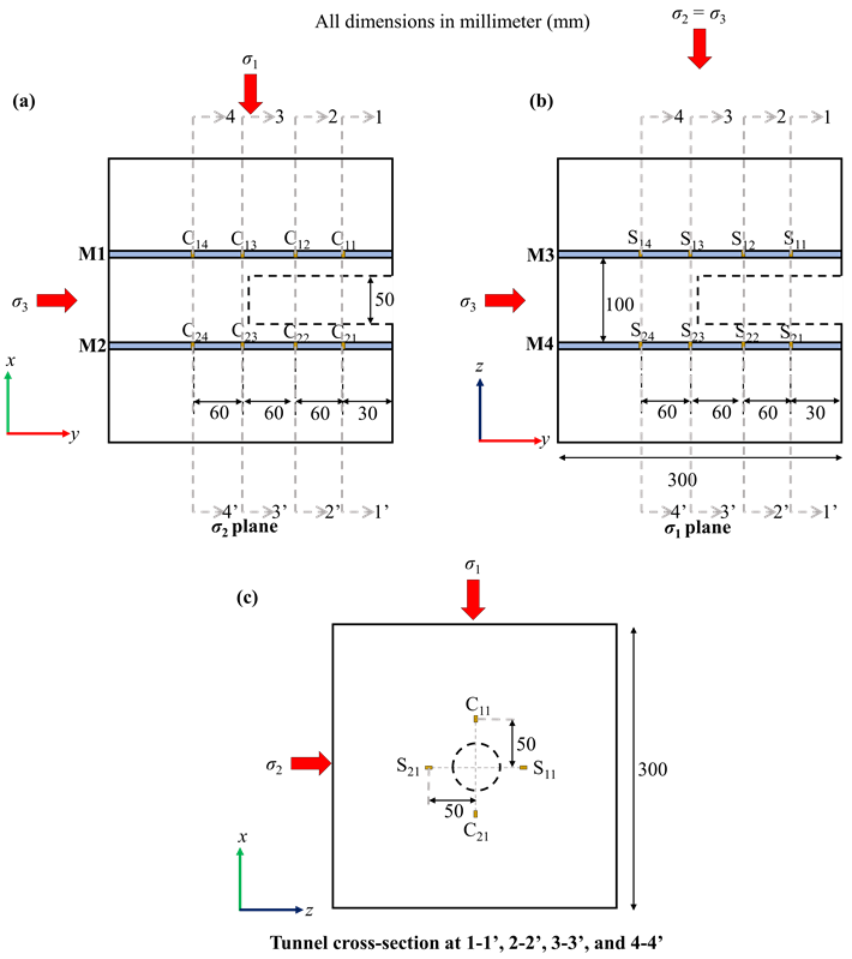

Figure 3-7 (a) Orientation of the MPBEx M1 and M2 on the σ_1-σ_3 plane, (b) orientation of the MPBEx M3 and M4 on the σ_2-σ_3 plane, and (c) tunnel cross-section with the location of four strain gauges from four MPBEx.

3.4.1 Performance of Miniature TBM

The TBM parameters were continuously monitored during the excavation stage. The operator-controlled parameters were the TBM face pressure applied through the servo-controlled pump and the rotational speed of the shaft using a single-phase constant speed AC motor. Figure 3-8 a illustrates the applied TBM face pressure over time during the excavation stage while the rpm of the cutter head was maintained constant at 14 using a constant speed AC motor. The changes in the shaft torque, provided by the motor via a chain drive, are shown in Figure 3-8 b. The miniature TBM advance rate and the advance achieved throughout the excavation phase are shown in Figure 3-8c and 3-8d.

The excavation of a 120 mm long tunnel with a diameter of 50 mm was completed in about 28 hours. The advance rate was observed to be highly dependent on the face pressure (thrust) applied at the cutter head (Figure 3-8).

Due to its low strength properties, the rock around the excavation experienced high squeezing when it encountered the cutter head shaft (Figure 3-9). As the rock contacted the cutter head shaft, a high amount of energy was required by the system to keep the rotational speed constant at the same face pressure. This additional energy was required to overcome the resistance resulting from the interaction between the cutter head shaft and the rock. As shown in Figure 3-8b, the average torque from the motor increased by 8% over 15 hours after the commencement of the excavation stage. This increase in torque from the motor provided a reasonable estimate of the level of squeezing experienced by the excavated tunnel.

Miniature TBM Face and Shaft Resistance

As the squeezed tunnel boundary met the rotating cutter head shaft, the torque required to maintain a constant rotational speed with the constant cutter head thrust increased. This additional torque was required to overcome resistance to the shaft from the squeezed tunnel boundary. It therefore was essential to evaluate the torque requirements of the cutter head at the tunnel face and the cutter head shaft at different thrust levels and isotropic stresses. In this study, the former was identified as face-resistance, and the latter was identified as shaft-resistance. Figure 3-9a shows the schematic diagram of the miniature TBM cutter head and shaft excavating in isotropic stress p_o with the thrust of P.

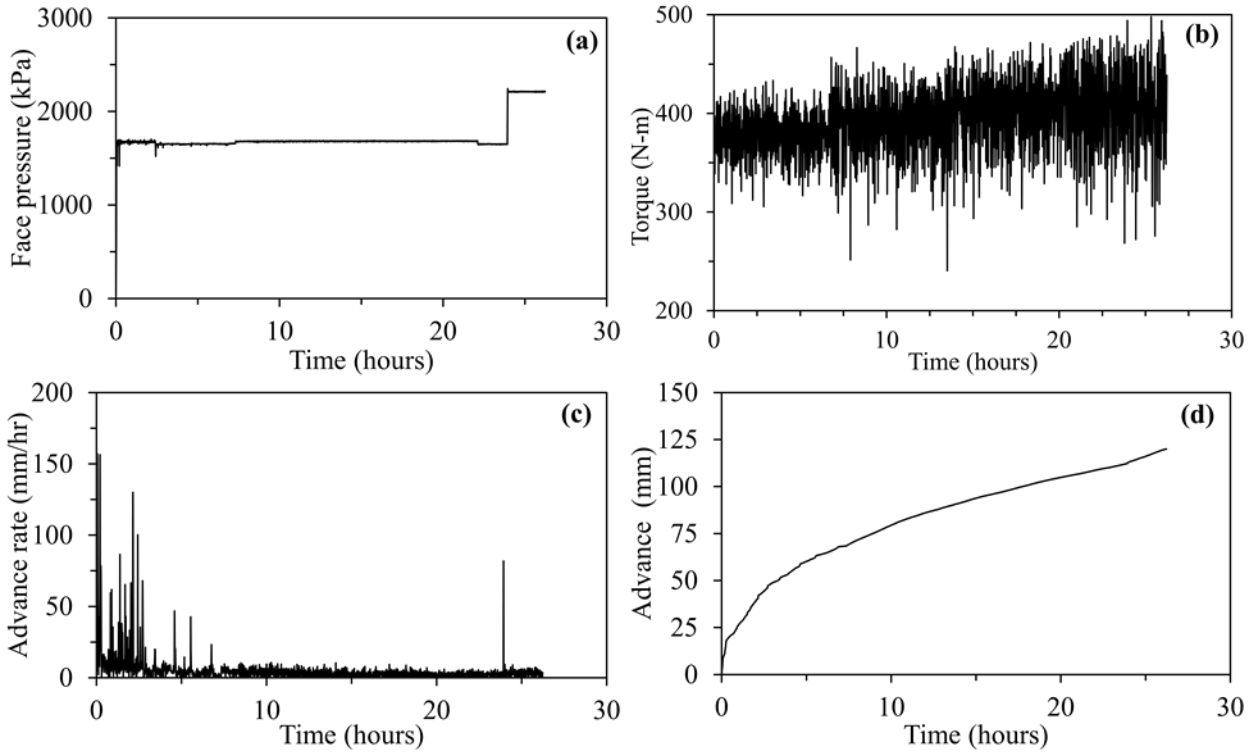

Figure 3-8 Monitoring of miniature TBM parameters during the excavation stage (a) face pressure (thrust), (b) advance rate, (c) cutter head torque, and (d) TBM advance.

The face-resistance was estimated by applying different levels of TBM face pressure on the cutter head and zero true-triaxial stress on the cubical rock specimen. The changes in the cutter head torque were continuously monitored along with the changes in the cutter head thrust. Theoretically,

the face-resistance experience by the cutter head can be expressed as the contact force between the cutter head and the tunnel face times the coefficient of friction at this interface. The expression for torque T required to drive the shaft under cutter head thrust force P was derived as follows.

Consider contact area A between the cutter head and tunnel face to be circular and to have an average contact friction coefficient as μ_f. As shown in Figure 3-9b, taking a small element at a radial distance r from the center of contact area, having area dA and the torque required to drive this small element against face resistance with no isotropic stress (p_o = 0) can be expressed as given in Eq. 3-5.

$$dT_f = \mu_f \, p \, dA \, r \tag{3-5}$$

The area of this small element subtending small-angle $d\theta$ at the center of the contact area between the cutter head and the tunnel face is given by Eq. 3-6.

$$dA = r \, d\theta \, dr \tag{3-6}$$

Combining Eq. 3-5 and 3-6,

$$dT_f = \mu_f \, p \, r^2 \, d\theta \, dr \tag{3-7}$$

The total torque required to drive the cutter head at a constant rotational speed was derived by double integration of Eq. 3-7 as given below.

$$T_f = \mu_f \, p \int_0^R r^2 dr \int_0^{2\pi} d\theta \tag{3-8}$$

Integrating Eq. 3-8 and applying the boundary conditions, the expression for the torque required to drive the cutter head against face resistance is given by Eq. 3-9.

$$T_f = \frac{2\pi}{3} \mu_f R^3 p \tag{3-9}$$

It can be inferred from the above equation that for a constant cutter head radius R, there is a linear relationship between the torque required to overcome face resistance T_f and cutter head pressure p. Figure 3-9d presents the plot of T_f and p obtained by monitoring the torque required to overcome face resistance at a different level of face pressure (thrust). The value of μ_f was determined as 0.332 based on the best linear fit.

The torque required to overcome frictional resistance due to the interaction between the cutter head shaft and the squeezed tunnel boundary only (P = 0) was calculated using equilibrium equations. This required torque can be expressed as a multiple of the contact force between the shaft surface and tunnel boundary F_s, the radius of shaft R, and the coefficient of friction μ_s. The final expression is given in Eq. 3-10.

$$T_s = 2\pi \, R^2 \, L \, \mu_s \, p_o \tag{3-10}$$

Similarly, there is a linear relationship between the torque required to overcome shaft resistance T_s and isotropic triaxial stress p_o. Figure 3-9e shows the plot of T_s and p_o obtained by monitoring

the torque required to overcome the shaft resistance at a different level of face pressure (thrust). The value of μ_s was determined as 0.09 through the best linear fit.

3.4.2 Rock Damage and Deformations

In this experiment, the competency ratio, F_c, i.e., ratio of the UCS of rock to the major principal stress, σ_1 was around 0.41. Due to the incompetent rock specimen, the excavated tunnel experienced very high convergence, due to the elastic, plastic and viscous behavior of the rock. Hence, the miniature TBM shaft could not be retracted without damage while the rock specimen was loaded in the true-triaxial cell. However, upon unloading the tunnel wall elastic component of the tunnel wall convergence improved and the shaft was easily retracted without any damage to the rock specimen. Figure 3-10 shows the miniature TBM shaft in the rock specimen during the loaded and unloaded stages.

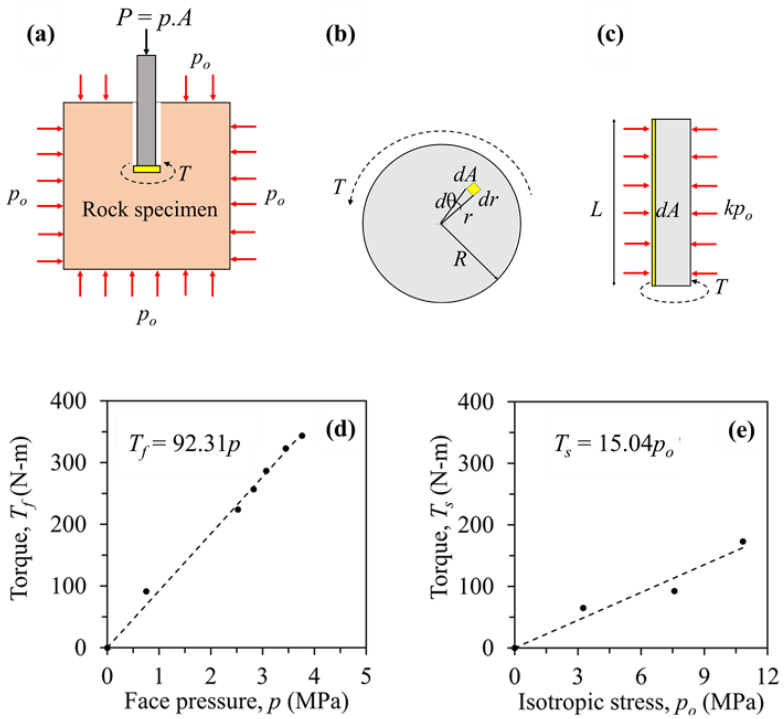

Figure 3-9 (a) Miniature TBM excavating in isotropic stress-state (po), thrust ($P = p.A$) and torque T, (b) Cutter head and tunnel face interaction (face-resistance), (c) cutter head shaft and tunnel boundary interaction (shaft-resistance), (d) Cutter head and tunnel face interaction (face-resistance) with $p_o = 0$, and (e) cutter head shaft and tunnel boundary interaction (shaft-resistance) with $p = 0$.

Since the miniature TBM shaft was stuck in the excavated tunnel during the loading stage, direct measurements of the tunnel wall deformations were not possible. However, after the rock specimen was unloaded, the shaft was retracted, and the non-recoverable convergence of the tunnel wall could be measured. This section of the chapter discusses the capability of the proposed physical model to capture time-dependent damages and deformation in tunnels in squeezing ground conditions.

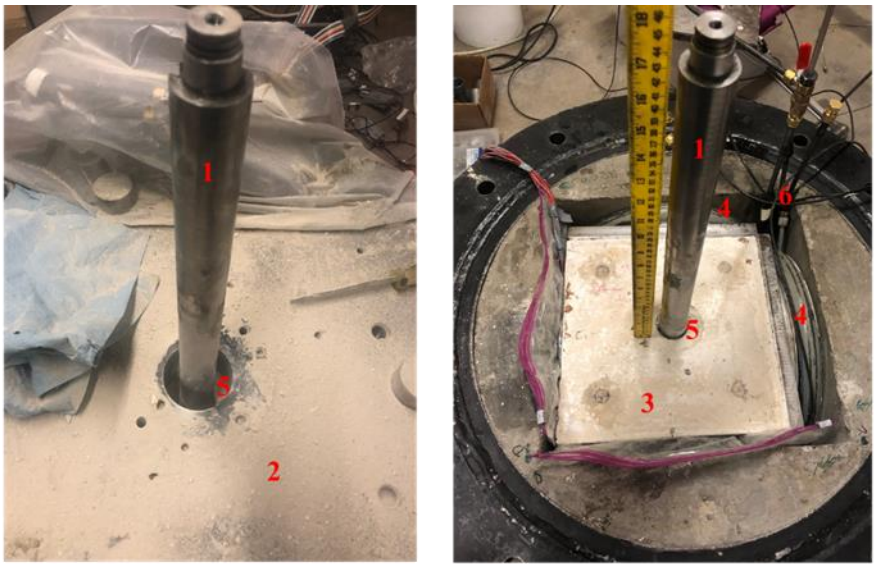

(a) Post-excavation loaded stage **(b) Post-excavation unloaded stage**

1 Cutter head shaft	4 Hydraulic jack for loading
2 True-triaxial cell	5 Tunnel portal
3 Rock specimen	6 Hydraulic and sensor lines

Figure 3-10 (a) Miniature TBM shaft inside excavated tunnel in the rock specimen while loaded in true-triaxial stress state, and (b) miniature TBM shaft inside excavated tunnel after unloading the rock specimen.

Damage Monitoring

An AE data collection system produced by MISTRAS Group, Inc. was used throughout all acoustic material characterization and tunneling tests. MISTRAS PCI-2 system consisted of 3 PCI-2 boards for a maximum of six signal inputs. WSα sensors had an operating frequency range of 100-1000 kHz and a resonance of 125 kHz. Six AE sensors were placed on the surface of the rock specimen to monitor the damage with time in the rock around the tunnel boundary.

Prior to the test, the rock specimen characterization was performed using the AE system to document the material's wave velocity and attenuation. Active and passive AE testing was performed using Auto-Sensor Tests (ASTs) and pencil lead break tests, respectively. ASTs sequentially created pulses emanating from each sensor located on the surface of the rock specimen. The pulsing sensor and all remaining sensors acted as receivers, and with a computer-controlled and initiated event time for each signal, highly accurate directional wave velocities were measured.

After performing the characterization tests, the cubical rock specimen was subjected to the true-triaxial stress state and the tunnel was excavated using the miniature TBM. Damage during and after the excavation was continuously monitored using six AE sensors. In the AE monitoring, each micro-crack (event) was detected by a minimum of four AE sensors and identified as an event.

The results are presented in the form of cumulative AE hits and events over time and events were located in the cubical rock specimen (Figure 3-11).

In our analysis, the AE hits and events collected during the first 28 hours should be considered as excavation damage-induced because of the tunnel excavation using the miniature TBM. The hits and events after the excavation stage (i.e., after 28 hours) are indications of physical damage due to the time-dependent behavior of the material. The true-triaxial stresses on the rock specimen were kept constant during and after the excavation stage as shown in Figures 3-11a and 3-11b. AE events due to true-triaxial loading are not presented in these results.

Figure 3-11a shows the cumulative AE events and hits during the excavation stage. As the excavation period was relatively short (only 28 hours) for squeezing to occur, the AE hits and events recorded during the excavation stage solely resulted from the excavation of the tunnel in the rock specimen and the damage in the rock specimen around the tunnel boundary. As shown in Figure 3-11a, a total of 1,588 AE events were recorded in the rock specimen during the 28 hours of tunnel excavation using the miniature TBM. As shown in Figure 3-11b, most of the recorded events were located along the path of the excavated tunnel.

The damage due to the time-dependent behavior of the material was studied by logging the cumulative AE event counts over time after the excavation stage. Figures 3-11c and 3-11d show the cumulative AE events during the time interval of 28 hours to 168 hours. The recorded AE events were solely considered due to the time-dependent behavior of the rock specimen. As presented in Figures 3-11c and 3-11d, 947 AE events were recorded during this stage, which was an approximately 60% increase after the excavation stage. The 60% increase in the AE events after the excavation stage provided a qualitative estimate of the amount of squeezing the tunnel experienced after the excavation stage.

Deformation Monitoring

Unlike damage monitoring using AE, deformation monitoring of the rock around the tunnel boundary provided a quantitative estimate of the amount of squeezing that the tunnel experienced. This experiment involved radial strain monitoring at radial distance, r which was 50 mm from the center of the excavated tunnel at four tunnel cross-sections (Figures 3-12a and b). The radius of the excavated tunnel, R, was 25 mm and the ratio of r to R was2. Figure 3-12a shows four tunnel cross-sections 1-1', 2-2', 3-3', and 4-4' located at the longitudinal distance of 30 mm, 90 mm, 150 mm, and 210 mm from the tunnel portal, respectively.

As already discussed, there were four strain gauges at each of these tunnel cross-sections for monitoring radial strain during and after the excavation stage. Of the four, two of them monitored the radial strain along the direction of major principal stress, σ_1, and the other two along the direction of the major principal stress σ_3, with $r/R = 2$. Strains due to true-triaxial loading are not presented in these results.

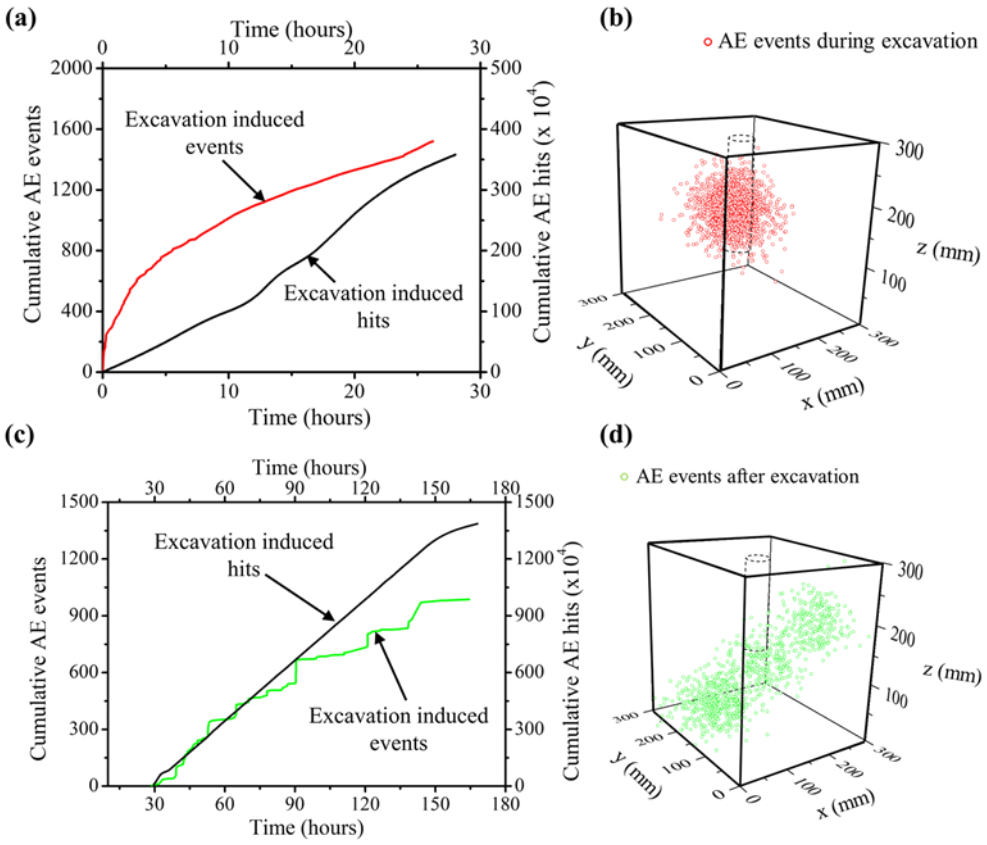

Figure 3-11 Cumulative AE hits and events with time during excavation stage, (b) location of AE events due to tunnel excavation, (c) cumulative AE hits and events with time after excavation stage, and (d) location of AE events after tunnel excavation.

Figure 3-12c shows the increase in radial strain over time along with the orientation of σ_1 and σ_3 in tunnel cross-section 1-1'. In this test, the miniature TBM reached this cross-section in 1.30 hours, and the radial strain recorded at that time along the σ_1 and σ_3 directions were 0.05% and 0.03%, respectively. The total excavation stage lasted for 28 hours, and the radial strain recorded at that time was 0.28% and 0.13%, respectively. After the excavation stage, while the specimen was loaded in the same stress-state for 168 hours, the radial strain increased to 0.38% and 0.18%. Hence, the time-dependent behavior of the rock specimen led to an approximately 35% increase in the radial strain (at $r/R = 2$) at this cross-section.

Similar monitoring results were obtained at tunnel cross-sections 2-2', 3-3', and 4-4' as shown in Figures 3-12c, d and e, respectively; and the time-dependent increment in the radial strain at these sections was approximately 55%, 40% and 10%, respectively. As discussed earlier, the total length of the excavated tunnel was 120 mm and sections 3-3' and 4-4' were at a longitudinal distance of 150 mm and 210 mm from the tunnel portal (or 30 mm and 90 mm from the tunnel face), respectively. Thus, there was no tunnel at sections 3-3' and 4-4' and the influence of the tunnel excavation decreased while going from section 3-3' to 4-4'. All the radial strain observations in these sections are summarized in Table 3-3. The observed time-dependent change in radial strain was at $r/R = 2$ and it is expected to increase with decreases in r/R with maximum at $r/R = 1$. After 168 hours, the rock specimen was unloaded, and the shaft was retracted from the tunnel. The

longitudinal profile of the tunnel was measured using the extensometer to obtain an estimate of non-recoverable convergence, *u* of the tunnel due to the plastic and viscous behavior of the rock. The non-recoverable longitudinal displacement profile of the tunnel is presented in Figure 3-13. The vertical axis represents the ratio of the non-recoverable tunnel convergence, *u* and radius of the excavation *R* while the horizontal axis represents the longitudinal distance, *X* measured from the face of the tunnel normalized with the radius of the tunnel *R*.

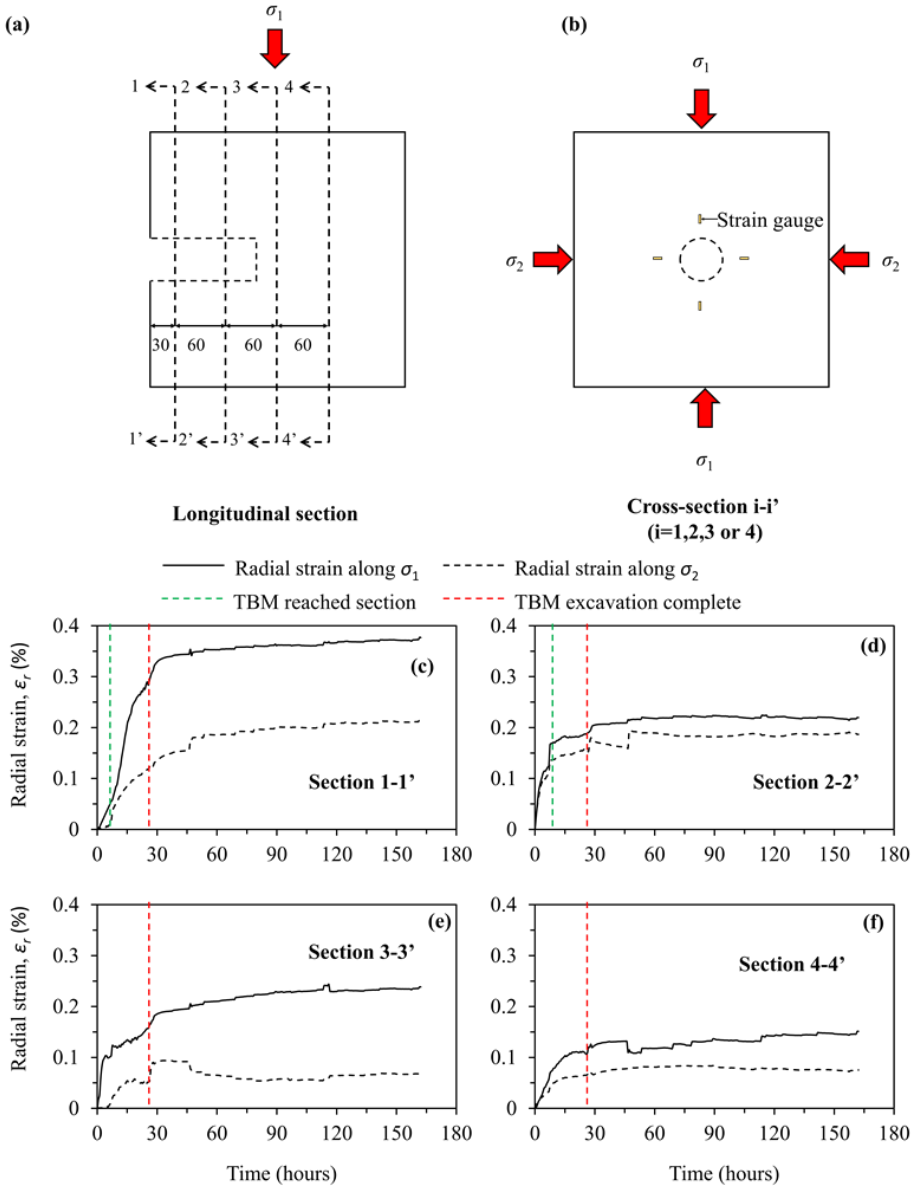

Figure 3-12 (a) Longitudinal section of the rock specimen with location of the embedded strain gauges (MPBEx), (b) tunnel cross-section i-i' (i=1, 2, 3 and 4), (c) radial strain with time at section 1-1', (d) radial strain with time at section 2-2', (e) radial strain with time at section 3-3', and (f) radial strain with time at section 4-4'.

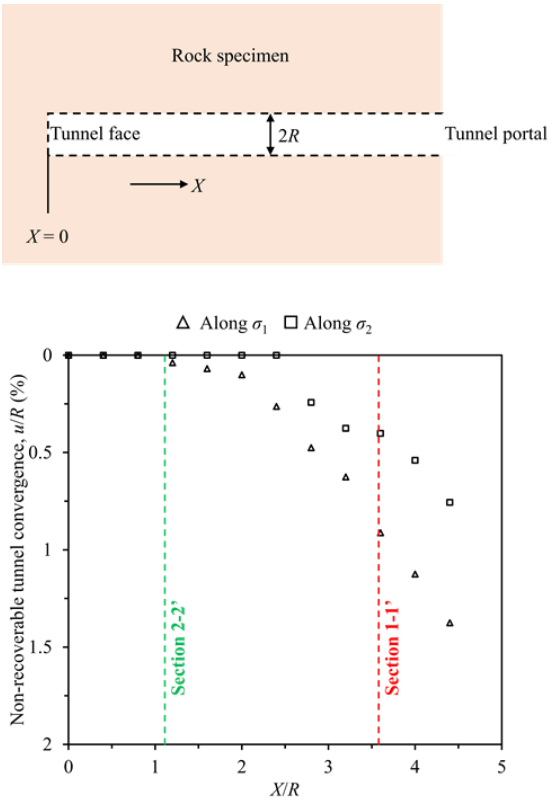

Figure 3-13 Longitudinal displacement profile of the excavated tunnel after unloading the rock specimen.

Table 3-3 Summary of the radial strain observation from MPBEx.

Tunnel cross-section	Radial distance, R (mm)	Longitudinal distance, X (mm)	Radial strain, ε_r (%)					
			TBM reached cross-section		TBM excavation complete		After 168 hours of loading	
			Along σ_1	Along σ_2	Along σ_1	Along σ_2	Along σ_1	Along σ_2
1-1'	50	30	0.05	0.03	0.28	0.13	0.38	0.18
2-2'		90	0.15	0.11	0.18	0.15	0.24	0.19
3-3'		150	N/A	N/A	0.16	0.05	0.20	0.09
4-4'		210	N/A	N/A	0.10	0.05	0.13	0.06

The measurements were taken along the direction of major principal stress, σ_1 as well as minor principal stress, σ_1 (Figure 3-13). The maximum non-recoverable convergence of the tunnel wall was 1.45% at the farthest point from the face of the tunnel in the direction of major principal stress.

It can be seen that that the damage and deformation around the excavated tunnel boundary over time provided qualitative and quantitative estimates of the influence of the time-dependent behavior of the rock and the level of squeezing experienced by the tunnel. This chapter discussed only our preliminary test observations using the proposed physical model to study tunnels in squeezing clay-rich rocks. However, a detailed analysis of the tunnels in squeezing clay-rich rocks will be carried out in the future by embedding more sensors at multiple locations and different orientations. Also, instrumentation will be done on the miniature TBM shaft to study shaft-tunnel boundary integration over time and account for the level of tunnel squeezing experienced.

3.5 Conclusions

This chapter introduced a novel physical model designed and fabricated to simulate the effects of full-scale TBM excavation in squeezing ground conditions. The experimental setup was shown to simulate the excavation of unlined tunnels in squeezing ground conditions. By incorporating adequate monitoring methods, the experimental system can provide a fair estimate of the damage and deformation that occurs around the tunnel. The physical model is capable of monitoring important TBM parameters, such as thrust, rotational speed, and torque with tunnel advance. The torque required to drive the TBM cutter head at constant rotational speed was found to increase as the tunnel wall convergence increased. We also used the proposed setup to study TBM cutter head and rock interaction properties as well as the TBM shaft and rock interaction properties.

The damage monitoring using AE sensors indicated that the damages around the tunnel boundary increased by 60 % due to the time-dependent behavior of the material in just 140 hours. However, the MPBEx showed that at $r/R = 2$ the radial strain increased by 35 % in just 140 hours. The high magnitude of non-recoverable tunnel convergence ($u/R = 1.45$ %) further quantified the amount of squeezing the tunnel experienced over the studied period.

The proposed physical model was shown to be quite capable of capturing the time-dependent behavior of rock around a tunnel boundary during the excavation stage and for a long time thereafter. An even more detailed analysis of tunnels in squeezing ground conditions can be carried out by introducing a larger number of embedded sensors at different locations and orientations and further incorporating additional monitoring techniques for the post-analysis and synthesis of test results. The results will be beneficial in validating the existing criteria or developing new criteria for the design of tunnels in squeezing ground conditions.

CHAPTER 4 - CHARACTERIZATION OF SYNTHETIC MUDSTONE FOR PHYSICAL MODEL STUDIES

4.1 Abstract

The complex problem of squeezing tunnels in clay-rich rocks has led to support design problems in many civil engineering tunnels. The laboratory investigation of clay-rich squeezing rocks has been limited due to the difficulties encountered in obtaining regularly-shaped homogenous and isotropic specimens of such rocks. Preparing s, yet representative, mudstone specimens in the laboratory for physical model studies can overcome this challenge. In the study presented in this chapter, synthetic mudstone was prepared by mixing "Goldart" clay as the main ingredient, type I/II cement as the binding agent, and water in defined proportions. During the mixing process, admixtures such as high range water reducer and accelerator were added to increase the workability and decrease the set time of the mix, respectively. Uniaxial compression tests and triaxial tests are conducted on the laboratory prepared 51 mm diameter and 102 mm long cylindrical specimen to determine strength, modulus, Poisson's ratio and plastic properties. The strain-rate sensitivity to strength and the modulus of the synthetic mudstone was determined by conducting triaxial tests at different strain-rates and confining pressure equal to 1 MPa. Three unconfined compressive creep tests were conducted at different stress levels to determine the creep properties of the synthetic mudstone specimens. Based on experimental observations, an empirical correlation was developed to describe the performance of the synthetic mudstone as an engineering material. The synthetic mudstone was found to be homogenous, isotropic, and reproducible, and its properties were similar to natural mudstone.

4.2 Introduction

Squeezing ground conditions exhibit large time-dependent deformation that often can lead to support design problems in large diameter tunnels (Bonini et al., 2009). Squeezing ground conditions are often associated with the presence of clay minerals in geomaterials (Terzaghi, 1946). The engineering behavior of clay-rich rocks can be very complex and has many factors, such as mineralogy, depositional characteristics, weathering, and age. For soft rocks such as mudstone, it is often difficult to obtain continuous and homogenous regular-shaped specimens from the field to study these problems (Johnston and Choi, 1986). Hence, laboratory-prepared synthetic specimens of clay-rich rocks would be useful in physical model studies.

Physical models are constructed and employed in geotechnical engineering for two purposes: (i) to achieve geometry similarity in order to provide mainly qualitative information or (ii) for quantitative analysis in order to develop a model that satisfies the conditions of "similitude" (Stimpson, 1970). For the second class of physical models, it is often difficult to attain perfect similitude; however, sufficient quantitative information can be obtained to better understand the behavior of the phenomenon under investigation. When a synthetic material correctly scales the primary features of the prototype material, similar observations can be made in the model and its prototype (Moncarzand and Krawinkler, 1981). Therefore, selecting the appropriate synthetic material is of paramount importance in physical model studies. Stimpson (1970) provided an extensive review of various types of model geomaterials used to simulate several rock mechanics problems including rock slope stability, underground construction, dam and pile foundation.

The relationship between the ideal synthetic material and the relevant prototype geomaterial can be explained by the theory of scale model similitude. The key physical parameters include unit weight γ, elastic modulus E, cohesion c, and internal friction ϕ (Hobbs, 1966; Jeon et al. 2004).

The main objective of the study presented in this chapter was to develop a representative laboratory prepared synthetic mudstone for a physical model study of the squeezing phenomena. For this purpose, a synthetic mudstone specimen was prepared in the laboratory by mixing clay, cement and water. The physical and mechanical behavior of the synthetic mudstone then was characterized by performing, uniaxial compressive strength tests, triaxial tests, strain-rate tests and creep tests.

4.3 Mudstone and Synthetic Materials

Mudstone is typically composed of fine-grained detrital sediments with more than 50 percent of the particles smaller than 62 μm (Potter et al., 2005). Unconsolidated sediments are known as mud (or clay), whereas their lithified equivalents are known as mudstone (Potter et al. 2005). There is a difference in the mechanical behavior (strength and deformation properties) of mud and mudstone. For example, the typical shear strength of soft clays is less than 25 kPa while mudstones are on the order of a few megapascals depending on the degree of weathering (Chandler, 1969; Miura et al., 2001; Horpibulsuk, 2005; Saadeldin and Siddiqua, 2013).

The addition of cement is a well-established technique to increase the shear strength of clays. Over the years, researchers have tested the resilience of clay-cement mixes at different water to cement ratios (w/c_m) and cement content (Gallavresi, 1992, Lee et al., 2005, Horpibulsuk et al., 2010; Seng and Tanaka, 2011; Lu et al., 2012; Zhang et al., 2013; Chian et al., 2015). Various empirical correlations, based on laboratory studies, have been suggested over the years to describe the effects of different combinations of w/c_m and cement content to the strength gain of the clay-cement mixtures.

The synthetic material in this study was designed according to empirical correlations proposed by Chian et al. (2015) using Singapore marine clay. Based on their model, the unconfined compressive strength (UCT or q_u) for different w/c_m and soil to cement ratio (s/c) is given as follows:

$$q_u = \frac{a_c + b_c(s/c)}{\gamma(w/c_m)} ln(t) \qquad (4\text{-}1)$$

where a_c and b_c are the clay strength parameters and can be determined from the experiments.

4.4 Model Constituents

The synthetic mudstone was prepared in the laboratory by mixing type I/II cement, clay, and water. A description of each mix ingredient follows.

4.4.1 Clay

Commercially available standard dry clay with the label “Goldart clay” supplied by Laguna Clay Company, California, USA, was used in the preparation of the synthetic mudstone. This clay is a hydrous aluminum silicate and has a granular appearance and an earthy color. According to the

datasheet provided by the supplier, this clay is non-volatile and slightly soluble in water and has a specific gravity of *Gsc* of 2.60. The clay contained 10-30% crystalline silica by weight, cristobalite 0.075 mg/m^3, tridymite 0.05 mg/m^3 and quartz 0.125 mg/m^3. The plasticity index of the clay was 13%, with a liquid limit of 48% and the plastic limit of 35%.

4.4.2 Cement

The cementing agent used in this mix was commercial grade type I/II Portland cement manufactured by Quikrete which meets the requirements of ASTM C150. The specific gravity of the cement, *Gscm* was 3.15. The amount of cement to add to the mix is defined by the parameter cement content, *C*, which is given as the weight of the cement to the total weight of its solids (cement and clay). After performing various trials, we determined that a cement content of 30% (C = 0.3) would provide the required shear strength to the mix.

4.4.3 Water

The amount of water required can be quantified in terms of the water to cement ratio by weight w/c_m. For a fixed cement content *C*, a very high w/c_m can lead to a long setting time and a low mix density. On the other hand, a small w/c_m can lead to stronger and more brittle specimens than naturally occurring mudstone. Therefore, selecting a proper w/c_m is very important when preparing a representative specimen of mudstone. After several trials in this study, the w/c_m of 1.5 was found to be adequate for preparing the synthetic material. Distilled water was used instead of tap water to eliminate the effects of the minerals in tap water, which might affect the hydration of the cement and the properties of the clay minerals.

4.4.4 Additives

In this study, a high range water reducer (superplasticizer) was added to increase the workability of the mixture. The correct proportion of water reducer depends on the type and efficiency of the chemical. It can be added with the initial batch of water or after wet mixing; however, its maximum effects are generally obtained with the delayed addition. BASF MasterGlenium 7920 was used as the water reducer for this mix and it was determined that the appropriate amount of this admixture was 60 ml for every kg of cement.

The cement content C, water to cement ratio w/c_m and quantity of material required to prepare 1m^3 of mix are shown in Table 4-1. Cylindrical specimens measuring 51 mm in diameter and 102 mm long were prepared to determine the mechanical behavior of the material by conducting uniaxial compression tests (UCT) and conventional triaxial tests at a confining pressure ranging from 1 to 4 MPa. Each cylindrical specimen was cured in water for 28 days to reach complete hydration of the cement in the mix. The tested cylindrical specimens met the dimensions and shape tolerance as per ASTM D4543-19. Figure 4-1 shows the representative cylindrical synthetic mudstone specimen prepared for UCT and triaxial tests.

4.5 Material Properties

4.5.1 Physical and Mechanical Properties

Unconfined compressive tests (UCT) were carried out to determine the unconfined compressive strength σ_c, and the elastic modulus, E_{50}, of the rock specimen as per ASTM D7012. Undrained triaxial tests were performed on the cylindrical rock specimen according to the method suggested by Hoek and Franklin (1970) to determine the confined compressive behavior of the rock specimen. The triaxial tests were performed with confining pressure, σ_3, varying from 1 to 4 MPa. Both the UCT and triaxial tests were displacement-controlled with a constant axial strain rate of 10^{-5} s^{-1}. The axial stress-strain plot obtained from the UCT (σ_3 = 0 MPa) and triaxial tests at different confining pressure (σ_3 varying 1 to 4 MPa) are shown in Figure 4-2a. The changes in volumetric strain ε_v, with the change in the axial strain ε_1, for all the UCT and triaxial tests are shown in Figure 4-2b where it can be seen that with an increase in the confining pressure, the material tended to be less dilative.

Table 4-1 Mix proportion for the synthetic mudstone prepared in the laboratory

Component (unit)		**Quantity**
Weight of cement to solids, C_s		0.3
Water to cement ratio by weight, w/c_w		1.5
Quantity required for 1 m^3 of the mix	Clay (kg)	859.79
	Cement (kg)	368.48
	Water (kg)	552.72
	Superplasticizer, MasterGlenium 7920 (litres)	45

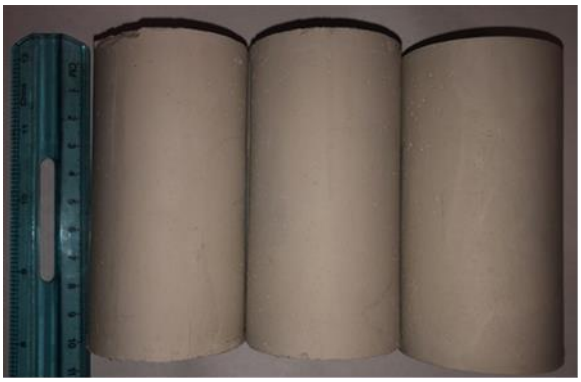

Figure 4-4-1 Laboratory prepared cylindrical specimen of synthetic mudstone for UCT and triaxial testing.

Based on the results of ten UCT tests on the cylindrical rock specimens, the mean σ_c and tangential elastic modulus (at 50% of peak stress), E_{50}, were found to be 4.47 MPa and 0.67 GPa with the

standard deviations of 0.15 MPa and 0.02 GPa, respectively. From the axial and radial strain measurements, the Poisson's ratio v, was determined as 0.13. The important physical and mechanical properties of the synthetic mudstone are summarized in Table 4-2.

Table 4-2 Physical and mechanical properties of synthetic mudstone after 28 days of curing

Property		**Value**
Saturated unit weight, γ_{sat} (kN/m^3)		18.12
Dry unit weight, γ_{dry} (kN/m^3)		12.93
Void ratio, e		1.2
Water content, w_w (%)		45
At strain rate = 10^{-5} s^{-1}	σ_c (MPa)	4.47 ± 0.15
	Elastic modulus, E_{50} (GPa)	0.65 ± 0.02
	Poisson's ratio, ν	0.13

For each plot shown in Figure 4-2a, using the peak deviatoric stress (σ_1 - σ_3), achieved at each σ_3, the Mohr-circles were plotted to determine the failure envelope (refer to Figure 4-2c). The Mohr-Coulomb failure criterion was found to provide a fair estimate of the failure envelope in a confining pressure range from 0 to 4 MPa. As shown in Figure 4-2c, using the Mohr-Coulomb linear fit, the undrained cohesion c, and friction angle ϕ were found to be 2.06 MPa and 10°, respectively.

4.5.2 Strain Rate Sensitivity

To characterize the strain-rate sensitivity of the synthetic mudstone, 15 triaxial compression tests were conducted with a constant confining stress of 1 MPa and with three tests at each of the following axial strain rates, $\dot{\varepsilon}_1$ of 5 x 10^{-6} s^{-1}, 1.3 x 10^{-5} s^{-1}, 1.7 x 10^{-5} s^{-1}, 2.3 x 10^{-5} s^{-1} and 1.5 x 10^{-4} s^{-1}.

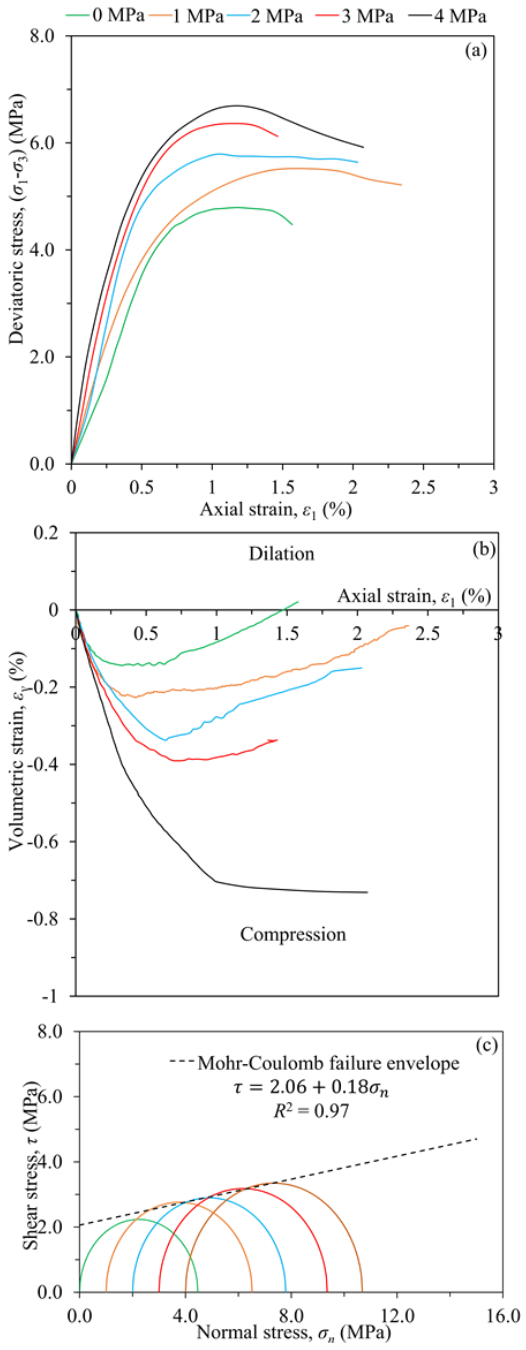

Figure 4-2 (a) Axial stress-strain plot for UCT and triaxial tests, (b) change in volumetric strain with increase in axial strain for UCT and triaxial tests, and (c) Mohr circle for UCT and triaxial tests with best fitting for Mohr-Coulomb failure envelope.

It can be seen from Figure 4-3a and 4-3b that the maximum value of the deviatoric stress and the elastic tangential modulus, given by the tangential slope of the linear portion of the stress-strain curve, increased with increases in the strain rate, respectively. The strain rate dependency of a material's strength can be represented by the power-law relationship in Eq. 4-2 (Katsuki and Gutierrez 2011)

$$\sigma_d = \sigma_{dS} + \sigma_{dVR}\dot{\varepsilon}_1^m \quad (4\text{-}2)$$

where σ_{dS} is the static component of the material strength, σ_{dVR} is a material parameter for the strain rate sensitive material strength, and m represents the strain rate sensitivity parameter for material strength at σ_3 = 1 MPa. Based on the experimental observations of Katsuki and Gutierrez (2011), it is assumed that the material does not show significant rate sensitivity for $\dot{\varepsilon}_1 \leq 1 \times 10^{-5}$ s^{-1}. Hence from the triaxial test data ($\dot{\varepsilon}_1 = 1 \times 10^{-5}$ s^{-1}), the value of σ_{dS} could be taken as 4.51 MPa at σ_3 = 1 MPa. The best fit for Eq. 4-2 is shown in Figure 4-3a as a dotted line, which was obtained by taking σ_{dVR} = 187.39 MPa and m = 0.65. The value of strain rate sensitivity m = 0.65 suggests that at the 1 MPa of confining stress, the response could be intensified approximately 4, 20, and 89 times higher with the 10^1, 10^2, and 10^3 times increase in the strain rate, respectively.

4.5.3 Creep Behavior

Uniaxial compression tests were performed to determine the creep behavior of the 28 day-cured synthetic mudstones. The cylindrical specimens 51 mm in diameter 102 mm long were subjected to a constant axial stress and unconfined state for a period of seven days in a servo-controlled creep test setup. The axial and lateral deformations were continuously monitored using the linear variable differential transformer (LVDT) and the chain extensometer. Figure 4-4 shows the creep test setup with its key component.

The creep behavior of synthetic mudstone specimen is described by using the Burger's viscoelastic model. According to this model, the behavior of material under constant stress can be explained by the springs and dashpots arrangement shown in Figure 4-5. This model also considers the Maxwell and Kelvin model connected in series and the total strain accumulated in creep recovery (constant stress) is the sum of Maxwell and Kelvin strains. The model is characterized by the following four parameters: Maxwell dynamic viscosity η^M and elastic modulus E^M, Kelvin dynamic viscosity η^K and elastic modulus E^K.

In the creep tests, the stress level was lower than the yield strength; and for a cylindrical specimen subjected to axial stress σ_1, the induced axial strain ε_1 with time t can be expressed by Eq. 4-3 (Bonini et al., 2009)

$$\varepsilon_1 = \frac{\sigma_1}{E^M} + \frac{\sigma_1}{\eta^M}t + \frac{\sigma_1}{E^K}\left[1 - \exp\left(-\frac{E^K}{\eta^K}t\right)\right] \quad (4\text{-}3)$$

The right-hand side of the above equation is the sum of three terms: the first term is the constant component of the elastic strain, the second term is linear with time, and the third term approaches exponentially to zero. Parameter E^M is the elastic modulus of the material and can be determined during the loading of the rock specimen from zero to σ_1. The creep strain can be given by Eq. 4-4 as follows

$$\varepsilon_1^{creep} = \frac{\sigma_1}{E^K} + \frac{\sigma_1}{\eta^M}t - \frac{\sigma_1}{E^K}\left[\exp\left(-\frac{E^K}{\eta^K}t\right)\right] \quad (4\text{-}4)$$

The creep parameters can be calculated by fitting the model in Eq. 4-4 to the experimental data. The experimental data were interpolated to up to a level where the fourth term of the Eq. 4-4

became almost negligible and the trend was a straight line. The slope of that straight line is $\frac{\sigma_1}{\eta^M}$ and its intercept is $\frac{\sigma_1}{E^K}$ and the parameter η^M and E^K were derived.

Parameter η^K was computed from the gap Δ between the experimental data and the linear part of Eq. 4-4, given by Eq. 4-5

$$\Delta = \frac{\sigma_1}{E^K}\left[\exp\left(-\frac{E^K}{\eta^K}t\right)\right] \quad (4\text{-}5)$$

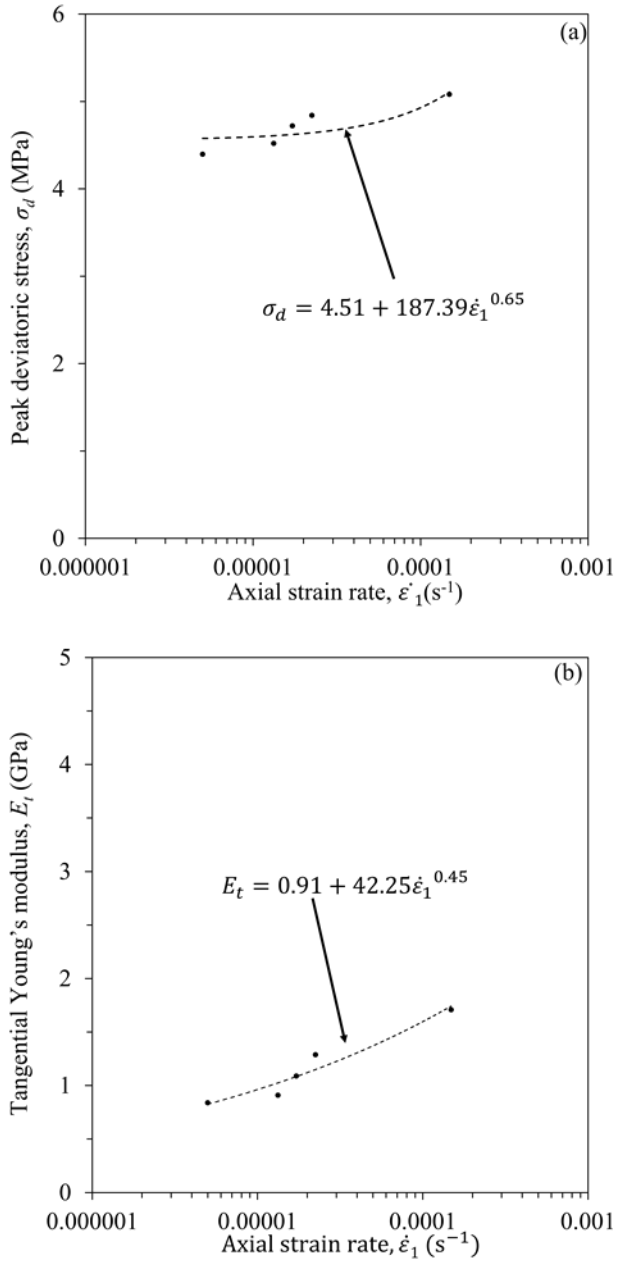

Figure 4-3 Change in peak deviatoric with axial strain rate ($\dot{\varepsilon}_1$) with σ_3 = 1MPa, and (b) change in tangential elastic modulus (E_t) with axial strain rate ($\dot{\varepsilon}_1$) at σ3 = 1MPa

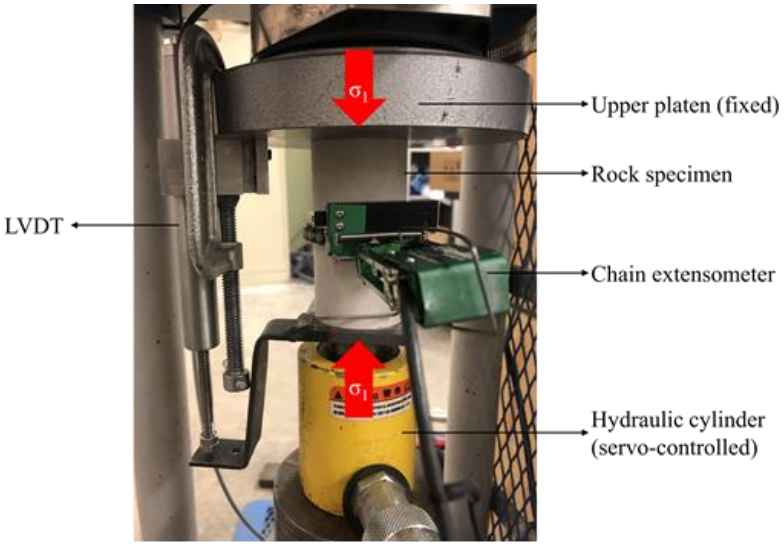

Figure 4-4 Creep test setup with a loaded cylindrical mudstone specimen.

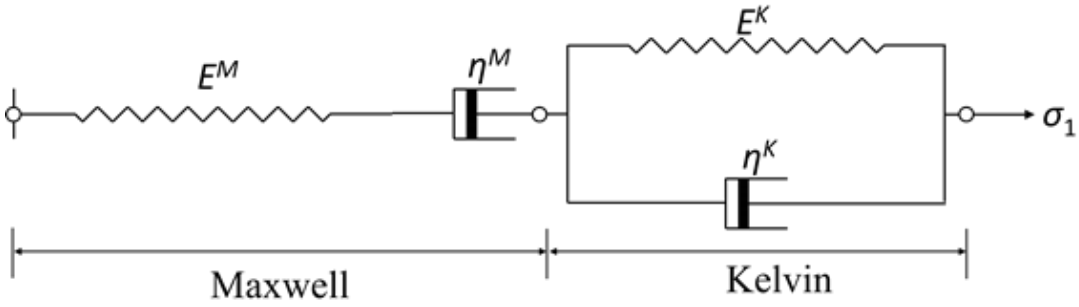

Figure 4-5 Sketch of the Burger's model considering viscoelastic behavior (modified from Bonini et al., 2009).

Taking the natural log of both sides of Eq. 4-5 resulted in

$$\ln_e(\Delta) = \ln_e\left(\frac{\sigma_1}{E^K}\right) - \frac{E^K}{\eta^K}t \qquad (4\text{-}6)$$

From the best linear fit of $\ln_e(\Delta)$ and time plot, the value of η^K can be determined.

In this work, three creep tests were carried out at axial stress levels equal to $0.40\sigma_c$, $0.50\sigma_c$ and $0.75\sigma_c$. Figure 4-6a, 4-6b and 4-6c show the increases in the axial creep strain with time (with σ_1 constant) for the three creep tests, respectively. It can be seen that the axial strain rate decreased with time and became constant after a certain time. The first part of the declining strain rate is known as the primary creep and the second part is known as the secondary or steady state creep. There is a third type of creep known as tertiary creep, but the onset of tertiary creep takes several weeks and was beyond the scope of this study.

Burger's model parameters (E^K, η^K, E^M and η^M) were determined using the described methodology and through Eqs. (4-3) through (4-6) for each of the three creep tests. Figures. 4-6a through 4-6c

also show the best linear fit in the steady state region for the creep tests. Figures 4-7a to 4-7c show the linear fit for each creep test as per the Eq. 4-6. Best fitting values for the Burger's model parameters are summarized in Table 4-3.

It can be observed from Table 4-3 that the values of the Burger's model parameter obtained from tests fell in a very narrow range, indicating that the parameters are not dependent on the stress level. Hence, to develop a viscoelastic constitutive model for the synthetic mudstone specimen, the average values of the Burger's model parameters were considered.

Table 4-3 Burger's model parameters for the creep behavior of synthetic mudstone

Stress level	**Burger's model parameters**			
	E^M **(MPa)**	E^K **(MPa)**	η^M **(MPa.hour)**	η^K **(MPa.hour)**
$0.40\sigma_c$	680	93	1.93×10^5	3.81×10^3
$0.50\sigma_c$	701	91	1.38×10^5	3.86×10^3
$0.75\sigma_c$	695	95	1.50×10^5	3.51×10^3
Average value	692	93	1.60×10^5	3.73×10^3

4.6 Discussions

In nature, mudstones are present in different compositions and conditions and possess different strengths (Meng and Xian, 2013). Due to this high scatter, quantitatively comparing the properties of synthetic mudstone with the naturally occurring mudstone is not an appropriate way to justify "similitude." Therefore, a qualitative comparison of synthetic mudstone with the naturally occurring clay-rich squeezing rock was conducted in the study presented in this chapter. Mudstone, in general, has low strength and low elastic modulus compared to other rocks (Meng and Xian, 2013). As shown in Table 4-2, the σ_c and elastic modulus E of the synthetic mudstone were 4.47 MPa and 0.69 GPa, respectively which are very low in comparison to other rocks. Squeezing clay-rich rocks (mudstones) tend to show very small or negligible strain softening effects and dilatancy (Bonini et al., 2009). It can be observed from UCT and triaxial tests in Figure 4-2a and 4-2b, the material does not show significant post-peak drop in the stresses for σ_3 between 0 MPa to 4 MPa and doesn't show high dilatancy.

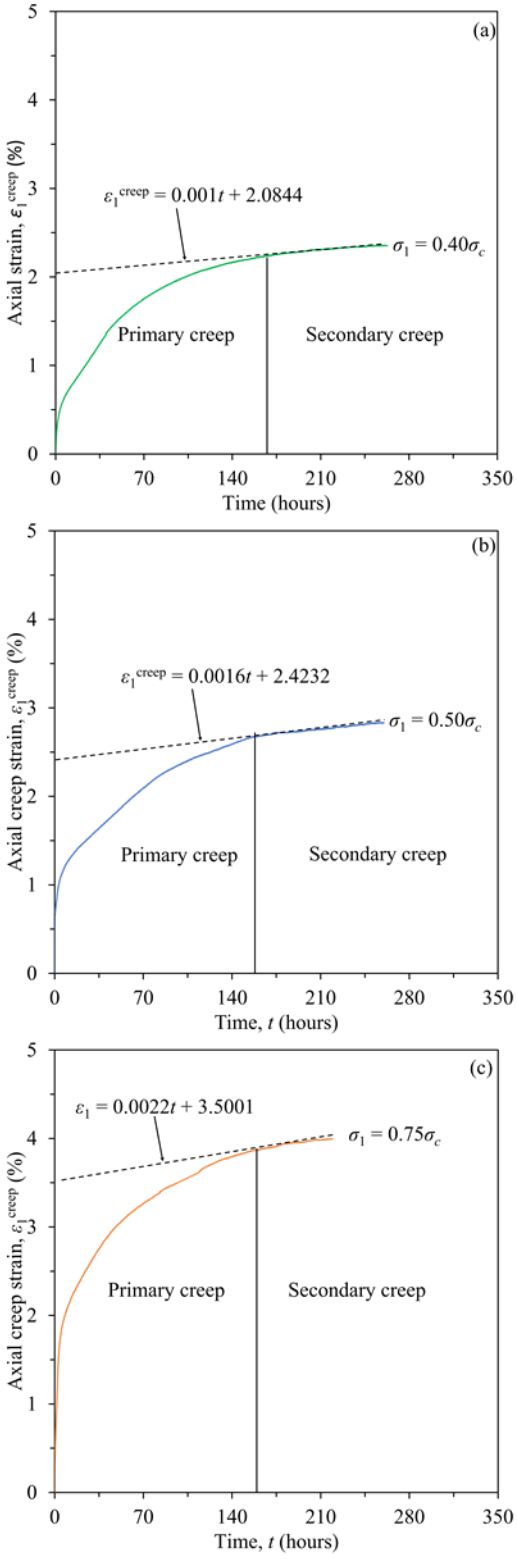

Figure 4-6 Creep strain with time along with best linear fit for steady state creep (a) $0.40\sigma_c$, (b) $0.50\sigma_c$ and (c) $0.75\sigma_c$.

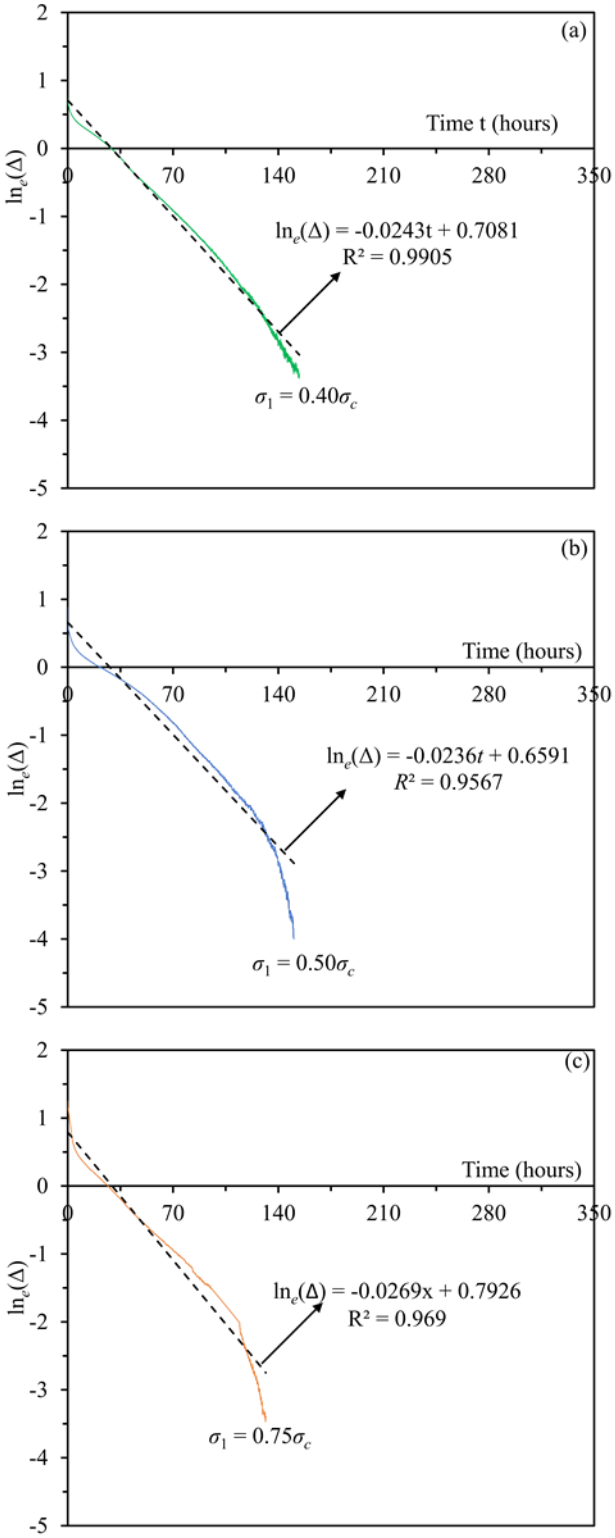

Figure 4-7 $\ln_e(\Delta)$ with time plot along with the best linear fit for steady state creep (a) $0.40\sigma_c$, (b) $0.50\sigma_c$ and (c) $0.75\sigma_c$.

In undrained conditions, squeezing clay-rich rocks have a very low angle of internal friction ϕ (Bonini, et al., 2009). For synthetic mudstone, the value of ϕ for a given σ_3 was 10°, which was very low. The squeezing clay-rich rocks also showed significant strain-rate sensitivity to mechanical behavior and creep properties (Barla, 2001; Bonini et al., 2009; Debernardi and Barla, 2009). The mechanical behavior of the synthetic mudstone specimen discussed in this chapter was highly sensitive to the strain rate (refer to Figure 4-3) and significant creep strain (refer to Figure 4-6).

Based on the above-mentioned observations, the condition of "similitude," in terms of mechanical behavior, was satisfied by comparing the strength, modulus, ductility, plastic parameters, strain-rate sensitivity, and creep behavior of the model rock and prototype.

4.7 Conclusions

To study the problem of squeezing in clay-rich rocks, a need exists for representative mudstone specimens for laboratory use. In this study, a systematic procedure for preparation and testing of specimen is presented. The material is prepared by mixing clay, cement, water, and admixtures in a definite proportion. The material was easy to produce, homogeneous, and isotropic and can be produced in different shapes and sizes. Unconfined compressive tests and undrained triaxial tests were carried out on the cylindrical specimen of the material to determine its mechanical properties.

From the creep tests, it was observed that the material showed significant deformation with time, which can be explained by Burger's constitutive model for viscoelastic materials. Based on a qualitative comparison with actual squeezing clay-rich rocks, it was concluded that the proposed material can be used for laboratory model studies concerned with the squeezing in clay-rich rocks.

CHAPTER 5 - TIME-DEPENDENT BEHAVIOR OF THE TUNNELS IN SQUEEZING GROUND: AN EXPERIMENTAL STUDY

5.1 Abstract

The presence of squeezing ground conditions often poses significant challenges in predicting tunnel response over time and to the design of an adequate support system to stabilize the tunnel. Many analytical, empirical, observational and numerical models have been proposed over the years for the design of tunnels in squeezing ground conditions, but they all have some limitations. The study presented in this chapter focused on improving the understanding of tunnel squeezing via a unique physical model test that simulated tunnel boring machine (TBM) excavation in squeezing clay-rich rocks. The physical model included a large true-triaxial cell, a miniature TBM, a laboratory-prepared synthetic test specimen having properties similar to natural mudstone, and instrumentations to monitor deformations around the tunnel boundary during and after the excavation. Experiments were conducted at realistic in-situ stress levels to study time-dependent tunnel convergence in three-dimensions. A tunnel was excavated using the miniature TBM in a cubical rock specimen loaded in the true-triaxial cell, then the confining stress was increased in stages to values above the rock unconfined compressive strength. Strain gauges embedded in the rock specimen and a digital borehole caliper monitored tunnel wall deformations with time. The degree of tunnel squeezing was characterized using a classification system based on tunnel radial strain. A model for time-dependent tunnel longitudinal displacement profile (LDP) was proposed using measurements of the tunnel convergence at different times and different stress levels.

5.2 Introduction

Squeezing ground conditions in tunnels can lead to excessive movement of the ground surrounding tunnel openings. This problem is generally encountered in tunnel excavations at great depths when high deviatoric stresses approach or exceed the shear strength of the rock mass (Barla, 1995). Due to yielding, excessive plastic deformations occur along and close to the tunnel boundary. Squeezing ground conditions also involve time-dependent ground response in the tunnel boundary, which can continue for a long time after the original excavation (Barla et al., 2012). Squeezing behavior is often associated with highly-weathered and weak clay-rich rocks which exhibit very ductile behavior, with very little strain softening, less pronounced peak shear strength, small dilation, bulging at failure, and strong time-dependent and creep response (Terzaghi, 1946; Dusseault & Fordham 1993; Cristescu & Hunsche, 1998; Fabre & Pellet, 2006). The potential for squeezing ground conditions is a major challenge for engineers in their selection of excavation and support methods for tunnels (Steiner, 1996; Hoek, 2001). For example, a tunnel excavated using a tunnel boring machine (TBM) in squeezing ground conditions may lead to shield entrapment (Dalgiç, 2002; Shang et al., 2004; Sterpi, 2007).

Squeezing ground conditions can cause many difficulties in tunnel construction, including extreme deformation, support system failure or even complete collapse, and not only can delay a project but also can significantly impact tunnel construction from an economic perspective. Some examples of such tunnels are the Yacambu-Quibor water supply tunnel in Venezuela (Hoek & Guevara, 2009); the John street pumping station tunnel in Canada (Czurda et al., 1973; Lo et al., 1987); the Laodongshan railway tunnel in China (Cao et al., 2018); the Uluabat project tunnel in

Turkey (Bilgin & Algan, 2012); the Stillwater tunnel in the United States (Phienwej & Cording, 1991); and the Kaligandaki tunnel in Nepal (Shreshtha & Panthi, 2015).

Due to the extreme loads in comparison to the shear strength of the ground surrounding the tunnel boundary, designing tunnels in squeezing conditions is a challenging task (Dalgic, 2002, Tiwari et al., 2018). Many researchers have proposed different methodologies using experimental approach (Semple et al., 1973; Mesri et al., 1981); analytical approach (Kallhawy, 1974; Ghaboussi & Gioda, 1977, Ghaboussi et al., 1981; Gioda 1981 and 1982; Sulem et al., 1987; Pan & Dong, 1991; Gioda & Cividini, 1996); and empirical approach (Terzaghi, 1946; Deere et al., 1970; Barton et al., 1974; Singh et al., 1992; Goel et al., 1995).

Previous studies have proposed various approaches for predicting tunnel response under squeezing conditions that were aimed at predicting long-term tunnel convergence within a range of ±1% of the actual tunnel convergence (Barla, 2001). A constitutive model for the time-dependent behavior of geomaterials along with their elastic and plastic response was found to be indispensable for the design of tunnels in squeezing ground conditions (Barla et al., 2012). Several other such models are discussed in the literature, but only a few of them were specifically conceived for the design and analysis of tunnels (Ladanyi, 1993; Cristescu & Gioda, 1994; Malan, 2002; Pellet et al., 2005; Phienwej et al., 2007). Other models allow for the degradation of the ground shear strength and modulus over time (Ladanyi, 1974; Tran-Manh et al., 2016). However, such models have limited applications in the design of tunnels in severe squeezing ground conditions as they have found to underestimate the tunnel convergence and the only advantage associated is a simpler identification of design parameters for preliminary design (Barla et al., 2012). Empirical and numerical methods are generally considered the most effective way to design tunnels in squeezing ground conditions, but they also have shortcomings (Wang et al., 2019). The extensive review of the methodology is discussed in detail by Arora et al. (2020a).

Despite the challenges that squeezing ground conditions can bring to tunneling, understanding of the tunnel squeezing phenomenon, particularly at the field level, remains limited. This is because field monitoring of tunnel response under squeezing conditions remain not only difficult but can also be perilous. Due to the high loads and extreme deformations, field sensors, just like the tunnel support system themselves, are under extreme environments and often fail before meaningful data can be obtained once the squeezing has started. Without reliable field data, it is difficult to validate methods to predict response and design tunnel in squeezing ground. Since in-situ monitoring is often limited in squeezing environment, in addition to the time and cost required, physical model tests are now considered a viable option to better understand the stability and failure of geotechnical structures (Lin et al., 2015).

One of the methods for consideration of the interaction between the tunnel and its support system is the convergence-confinement method. This method consists of three components of longitudinal deformation profile (LDP), ground reaction curve (GRC), and support characteristic curve (SCC). The LDP provides the variations in the radial displacement of the unsupported tunnel as a function of the distance from the tunnel face. Various analytical and empirical solutions exist to determine the LDP of a tunnel excavated in the elastic and elasto-plastic ground (e.g., Vlachopoulos & Diederichs, 2009; Panet, 1995; Prassetyo & Gutierrez, 2018). However, in squeezing ground conditions, the time-dependent behavior of the ground material around the tunnel boundary

changes the LDP of the excavated tunnel and these changes with time in the presence of squeezing ground conditions are largely unexplored.

The objective of this chapter is to present the test setup and the results of a carefully conducted laboratory test that simulated tunnel squeezing in a physical model test. The test involved TBM excavation in a synthetic test sample, with squeezing and time-dependent behavior like a mudstone, under increasing confining stresses. The physical model test investigated the crucial features of tunnel excavation, such as tunnel advance, three-dimensional effects, and highly plastic and ductile time-dependent behavior of the ground. The experimental observations and results are synthesized in terms of squeezing potential, and tunnel convergence at different times and levels of loading through the formulation of a new time-dependent LDP model. It is envisioned that the results can be used in more quantitative prediction, analysis and design of tunnels in squeezing ground.

5.3 Experimental Setup

The experimental setup physically simulated TBM excavation in a cubical rock specimen loaded at field stress levels (up to 550 meters overburden for mudstones) in a true-triaxial cell (for more details of the experimental setup, please see Arora et al., 2019 a, b). The spatial and temporal changes and deformation during, and even after, the tunnel excavation stage were monitored and analyzed. Figure 5-1a illustrates the overall experimental setup, and Figure 5-1b is a photo of the actual experimental setup at the Colorado School of Mines, where this study took place. The critical components of the experimental arrangement included a true-triaxial cell, a miniature TBM, cubical clay-rich rock specimen, and the monitoring unit. The essential aspects of the test setup, along with excavation and loading, are discussed in the following sections.

5.3.1 Cubical rock specimen

In this study, a synthetic mudstone that simulates clay-rich rock was used in the physical model test. Due to the soft nature of mudstone and the size needed, it is difficult to obtain natural homogenous and undisturbed specimens needed in the test from the field. Therefore, a synthetic mudstone was prepared in the laboratory with the objective of producing a test material that exhibits the characteristics of squeezing clay-rock rock namely ductility even at low confining stresses, large plastic deformation and pronounced time and loading rate dependency. The synthetic rock was obtained by mixing clay, cement and water in the proportions listed in Table 5-1 (Arora et al., 2020b). The mix had a cement ratio C (equal to the weight of cement to the total weight of the sample) of 30%, and the water to cement ratio by weight w/c_m was 1.50. The workability of the mix was improved by adding superplasticizer MasterGlenium 7920, in the proportion indicated in Table 5-1.

Arora et al. (2020b) carried out unconfined compressive tests (UCTs) and undrained triaxial compression tests on 28 day-cured cylindrical specimens of the synthetic mudstone used in the physical test. The specimens, 51 mm in diameter and 102 mm in height, were used to determine the physical and mechanical properties of the synthetic rock. As presented in Table 5-2, the mean unconfined compressive strength σ_c was 4.47 MPa with a standard deviation of 0.15 MPa, the mean Young's modulus E was 0.65 GPa with a standard deviation of 0.02 GPa, and the Poisson's ratio ν was 0.13. The triaxial compression tests were conducted under different levels of confining

stresses ranging from 1 to 6 MPa. Using Mohr-Coulomb linear fit, the effective cohesion *c* and friction angle ϕ were found to be 2.06 MPa and 10°, respectively. The laboratory test results demonstrated the similarity between the synthetic material and naturally occurring and squeezing-susceptible mudstone based on the obtained shear strength, modulus, ductility, strain-rate sensitivity and creep behavior of the model rock. For confining pressures in the range of 0 to 4 MPa, the synthetic mudstone showed very ductile behavior with minimal post-peak strain softening and low dilatancy. Also, during the creep tests, the mudstone was observed to develop a substantial amount of creep strain with time (Arora et al., 2020b).

Table 5-1 Mix proportion for the synthetic mudstone prepared in the laboratory (modified from Arora at al. 2020a).

Component (unit)	Cement ratio, *C*	Water to cement ratio by weight, w/c_m	Quantity required for 1 m^3 of the mix			
			Clay (kg)	Cement (kg)	Water (kg)	Superplasticizer, MasterGlenium 7920 (liters)
Quantity	0.3	1.5	859.79	368.48	552.72	45

Table 5-2 Physical and mechanical properties of synthetic mudstone after 28 days of curing.

Property	Saturated unit weight, γ_{sat} (kN/m^3)	Dry unit weight, γ_{dry} (kN/m^3)	Void ratio, *e*	Water content, w_w (%)	At strain rate = 10^{-5} s^{-1}		
					UCS, σ_c (MPa)	Elastic modulus, E_{50} (GPa)	Poisson's ratio, ν
Value	18.12	12.93	1.20	45	4.47 ± 0.15	0.65 ± 0.02	0.13

The 300x300x300 mm3 cubical synthetic mudstone specimen was prepared using the same composition as the unconfined compression and triaxial tests. A mixture of clay, cement and water was poured in a cubical mold and the specimen was removed from the mold after 24 hours and further cured in water for 28 days before the testing commenced.

5.3.2 Test instrumentation and monitoring

The experimental setup included continuous monitoring of the mini-TBM output (thrust, torque and advance), the deformation around the excavation using a miniature Multiple-Point Borehole Extensometer (MPBEx), the longitudinal displacement profile of the tunnel with time using a borehole caliper, and strain gauges placed on the specimen surface. The thrust of the TBM was controlled by a pair of servo-controlled pumps under continuous constant pressure (CCP) mode, which allowed the TBM to apply constant thrust at the excavation face. The change in the advance

rate of the TBM was back-calculated from the change in flow rate Q with time t of the servo-controlled pumps. The torque provided by the TBM was continuously monitored by a separate data acquisition unit (DAQ) that recorded the power output from the constant speed alternating current (AC) motor.

Strain gauges were embedded in the cubical specimen of the mudstone to monitor the strains at multiple points around the excavation. Due to the very high-water content of the synthetic mudstone, there was insufficient adhesion between the strain gages and mudstone. Hence, the strain gauges could not be directly embedded in the specimen. An MPBEx was prepared using a thin, flexible Teflon material and an array of strain gauges, as shown in Figures 5-2a and 5-2b.

This methodology ensured adequate adhesion of the strain gauges to the Teflon sheet, providing a way to measure the strain at multiple points in the rock specimen. The methodology was validated by embedding an axial strain gauge in a cylindrical specimen loaded in uniaxial compression and comparing the observations with the strain gauge observations on the surface. A total of four MPBExs were embedded along the length of the tunnel in the cubical rock specimen to monitor the radial strain at multiple points, as shown in Figure 5-2b.

The MPBExs monitored the strains at multiple points in the rock specimen around the tunnel. However, there was still a need to monitor the LDP of the tunnel wall with time to account for the squeezing experienced by the tunnel. In this study, the tunnel wall displacements at multiple locations were determined by monitoring the changes in diameter over time using the digital borehole caliper. The borehole caliper was placed at the tunnel portal after the excavation stage and was moved along the tunnel boundary with the help of a constant speed linear actuator (as shown in Figure 5-2c) and recorded the profile of the diameter of the tunnel. The piston of the actuator at 12 volts direct current (DC) moved the caliper at a constant speed of 10 mm/s. The maximum sampling rate of the digital borehole caliper was two samples per second, meaning the assembly was recording the diameter of the tunnel at every 5 mm.

5.3.3 The loading unit

The physical model test incorporated the use of a true-triaxial cell developed by Frash et al. (2014) at Colorado School of Mines as the loading unit. This true-triaxial cell can independently apply principal compressive stress up to 13 MPa in each direction through the use of dog-bone flat jacks. Figure 5-1 shows the major principal stress σ_1 and the minor principal stress σ_2 applied on the cubical rock specimen in a true-triaxial cell. The direction of the intermediate principal stress σ_2 was perpendicular to both σ_1 and σ_3 and into the plane in Figure 5-1.

The unique feature of this cell is that the drilling process can be carried out in the rock specimen while it is loaded in a true-triaxial stress state, which made it suitable for the realistic physical model test setup in this study. The true-triaxial cell was initially designed to carry out the thermo-mechanical simulation of enhanced geothermal systems in Frash et al. (2014) but later was modified to study TBM-excavated tunnels in squeezing ground conditions. The detailed design of this true-triaxial cell is provided in Frash et al. (2014), and the modifications for the tunneling experiments in this study are provided in Arora et al. (2019 a, b).

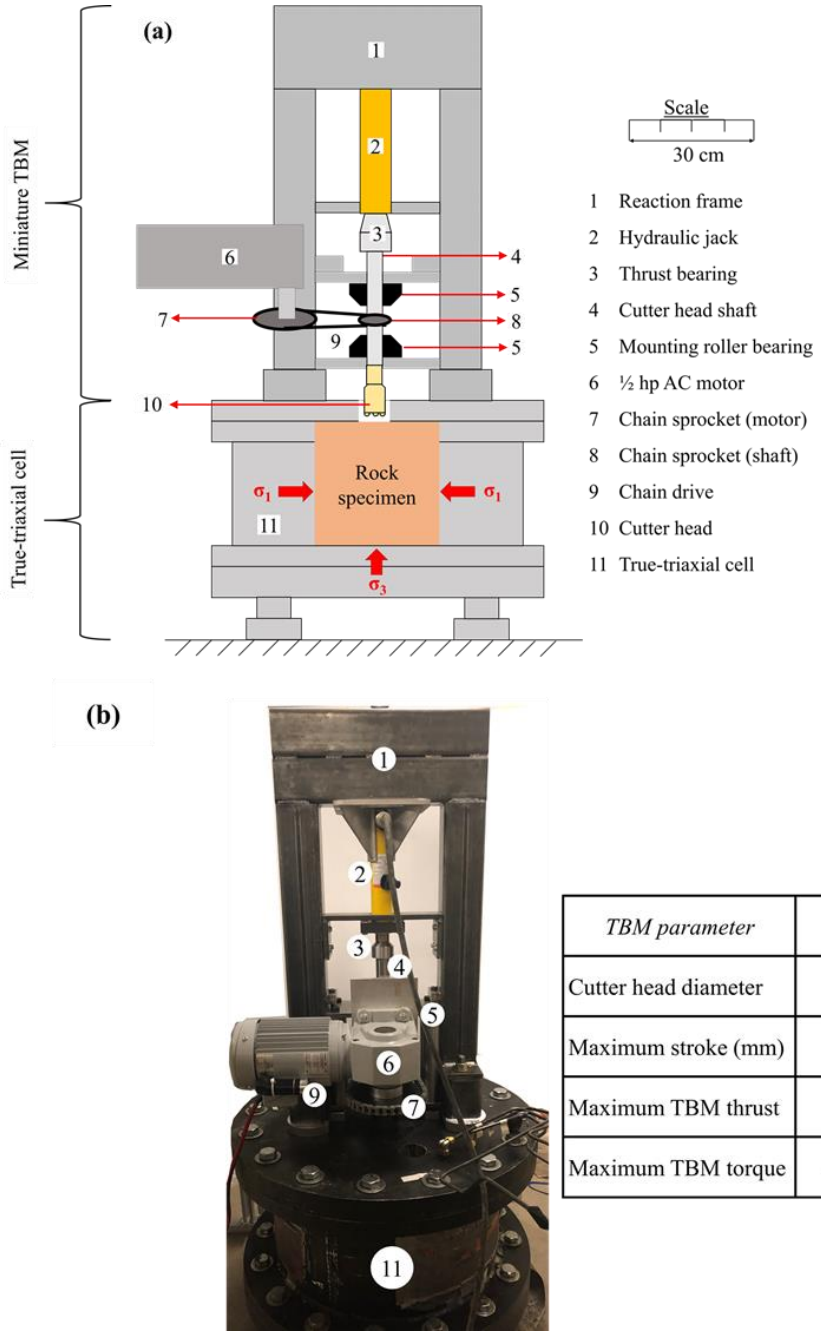

TBM parameter	*Value*
Cutter head diameter	50 mm
Maximum stroke (mm)	160 mm
Maximum TBM thrust	100 kN
Maximum TBM torque	400 N-m

Figure 5-1 Experimental arrangement to study tunnels in squeezing ground conditions: (a) schematic diagram, and (b) actual setup at Colorado School of Mines.

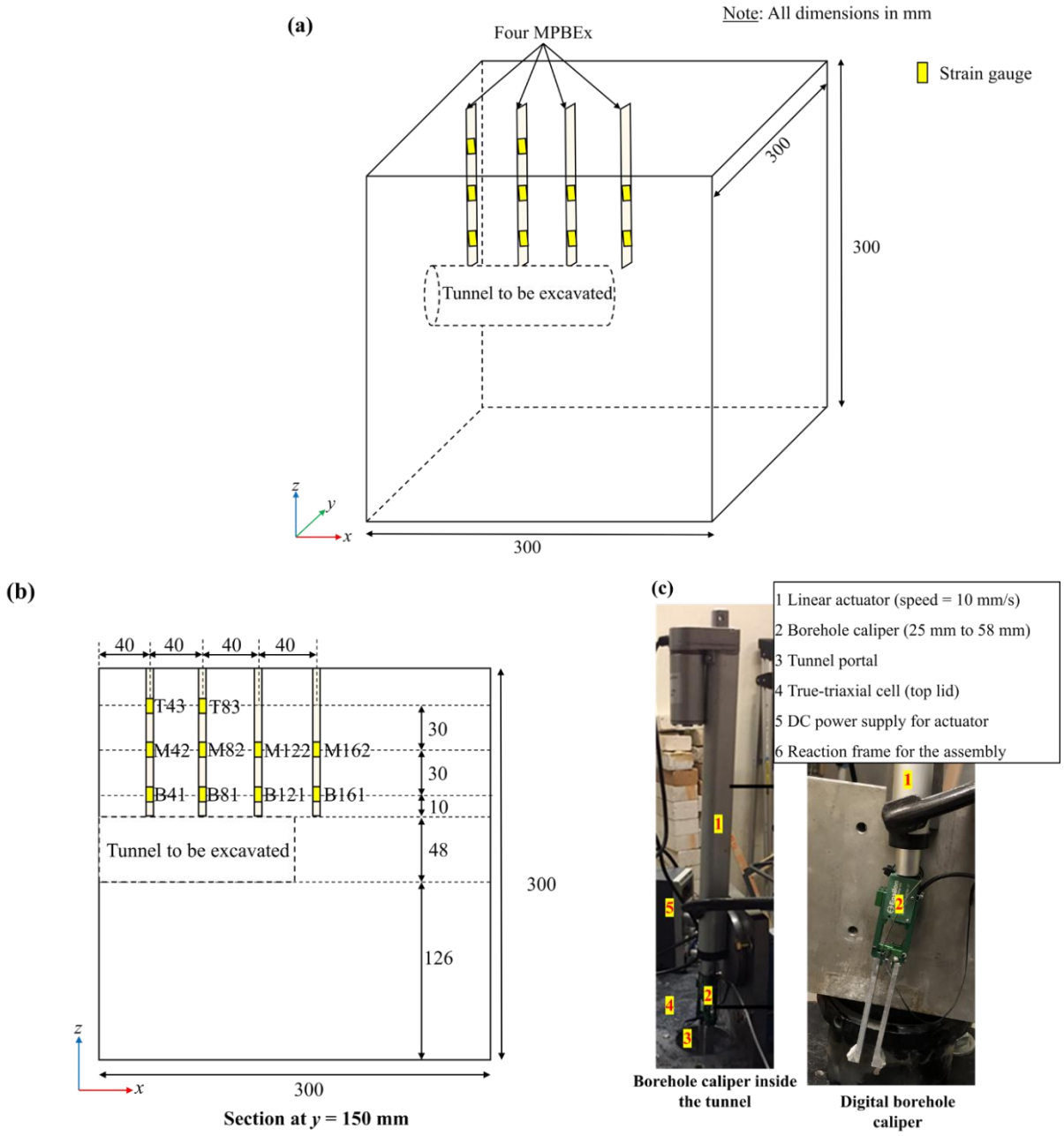

Figure 5-2 Schematic diagram representing: (a) location of MPBEx in the cubical rock specimen, (b) section showing the location of MPBEx and strain gauges concerning tunnel to be excavated, and (c) digital borehole caliper to monitor LDP with time after excavation stage.

5.3.4 Tunnel excavation unit

The experimental setup further incorporated a miniature soft ground open face TBM, which was mounted on the top of the existing true-triaxial cell. The miniature TBM used can excavate a tunnel with high cutter head thrust and torque that emulates in-situ conditions at laboratory scale. Figure 5-1 conceptually shows the miniature TBM mounted on the top of the true-triaxial cell.

The four main components of the miniature TBM include the thrust unit, torque unit, cutting unit, and supporting unit. The diameter of the cutter head disc is 48 mm, and the maximum possible length of tunnel that can be excavated is 150 mm. A pair of ISCO syringe pumps and a hydraulic cylinder provided the required face pressure (thrust) for the excavation to the cutter head. The apparatus can apply a maximum face pressure of 10 MPa. The torque is provided by a 0.5 hp, 115V, single-phase, constant speed, alternating current (AC) motor via a chain drive, as shown in Figure 5-1. The motor rotates at a constant speed of seven revolutions per minute and can provide a maximum torque of 400 N-m.

As shown in Figure 5-1, the cutting unit has a shaft with a cutter head connected at one end. The other end of the shaft is coupled with a hydraulic jack using a thrust bearing. The miniature TBM was designed for excavation in soft rock (e.g., mudstone) and the drill bit had a with a cutter head with nine button-type tungsten carbide bits.

5.4 Test Procedures

After sample preparation, curing, and embedding of strain gauges, the sample was placed in the cubical triaxial cell. The specimen was then subjected to an isotropic compressive stress $p_o = 0.5\sigma_c$, and a 48-mm diameter and 140-mm long tunnel was excavated in the rock specimen using the miniature TBM. The axis of the excavated tunnel was along the *x*-axis of the coordinate system shown in Figure 5-3.

After excavation, the isotropic stress p_o ($\sigma_1 = \sigma_2 = \sigma_3 = p_o$) was applied for 708 hours in four loading stages, as shown in Figure 5-3. The total time of loading (and monitoring) was based on the onset of the steady-state, i.e., the rock specimen was loaded until the tunnel wall deformation reached the steady-state. The four loading stages of the test were as follows:

Loading Stage I: After excavating the tunnel, the miniature TBM was retracted from the tunnel without changing the isotropic stress in the true-triaxial stress. From this loading stage onward, the LDP of the tunnel also was observed over time for 101 hours, while monitoring the ground response around the tunnel boundary using the MPBEx.

Loading Stage II: The isotropic stress on the rock specimen was increased rapidly from $0.5\cdot\sigma_c$ to $1.0\cdot\sigma_c$, as shown in Figure 5-3. This isotropic stress was kept constant for 168 hours before applying the next increment.

Loading Stage III: The isotropic stress on the cubical rock specimen was further increased by $0.5\cdot\sigma_c$, making $p_o = 1.5\cdot\sigma_c$. The total time of loading for this stage at $p_o = 1.5\cdot\sigma_c$ was 218 hours.

Loading Stage IV: In this final loading stage, p_o was further increased rapidly from $1.5\cdot\sigma_c$ to $2\cdot\sigma_c$. The rock specimen was loaded for 222 hours and finally unloaded, making $p_o = 0$ MPa.

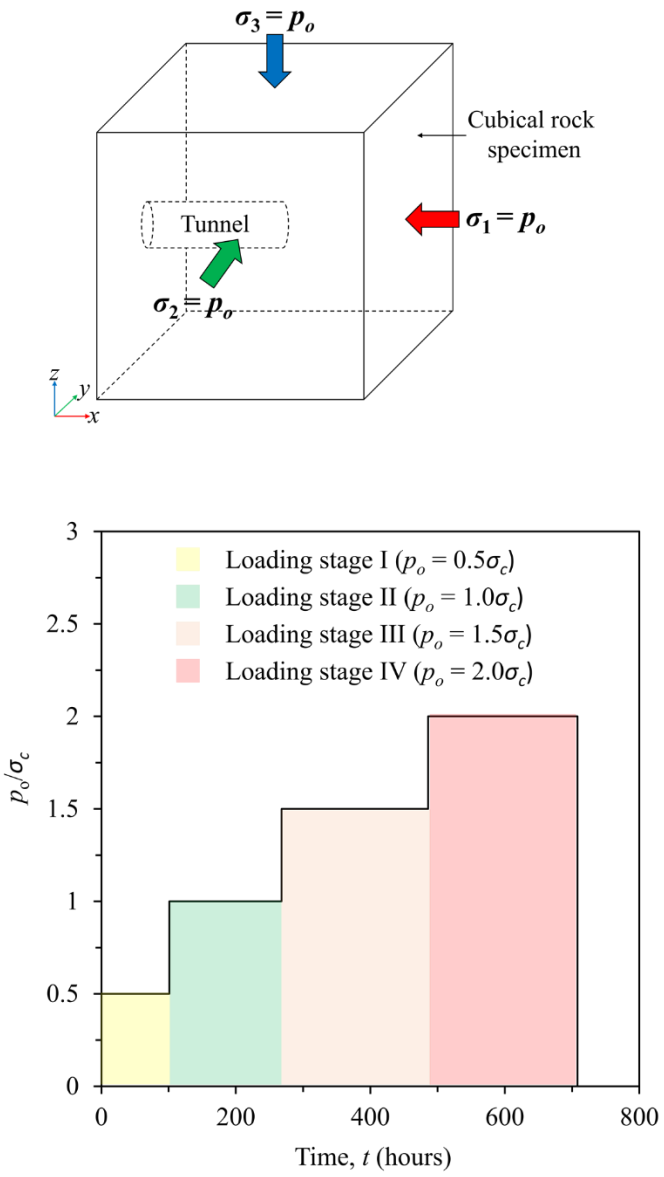

Figure 5-3 Isotropic stress applied on a cubical rock specimen during four loading stages.

5.5 Experimental Observations and Results

5.5.1 Tunnel excavation

Figure 5-4a shows the response of the 48-mm diameter tunnel after it was excavated in the specimen in 33 hours and in two phases. As shown, the mean TBM face pressure f_p applied to the tunnel face via the cutter head throughout the excavation stage was about 1.12 MPa with a standard deviation of 0.05 MPa. Isotropic stress p_o applied on the cubical rock specimen was $0.5 \cdot \sigma_c$, which was roughly two times that of f_p. The miniature TBM shaft rotated at a constant speed of 13 revolutions per minute, and the torque output was continuously monitored, as shown in Figure 5-4b.

During Phase I of the excavation, a 100-mm long tunnel was excavated in 28 hours, followed by removal of the cut material. It was observed that if the cut material was not removed efficiently, the tunnel became clogged and the excavation rate significantly slowed down, as can be seen in Figure 5-4d. Phase II of the tunnel excavation began after the cut material was removed. In this phase, a 40-mm long tunnel was excavated in five hours, making the total length of the tunnel 140 mm. As shown in Figures 5-4c and 5-4d, the tunnel advance rate significantly increased in Phase II of the excavation compared to the last seven hours of Phase I of the excavation.

During the excavation of the tunnel, four MPBExs were used for continuous monitoring of the rock around the tunnel boundary over time. As shown in Figure 5-5a, the MPBExs were placed 40 mm from each other along the *x*-direction, starting at 40 mm from the tunnel portal. During the excavation phase, the TBM reached the tunnel section having the first, second, and third MPBExs in 6.25, 15.70 and 30.50 hours, respectively (Figure 5-4). The total tunnel advance was 140 mm, and the fourth MPBEx was at 160 mm from the tunnel portal. Hence, there was no excavation below the fourth MPBEx. Figures 5-5b through 5-5e show the strain ε_M recorded by ten strain gauges on the four MPBExs with excavation time t_e.

Two important observations were made from Figure 5-5 regarding the importance of the MPBEx in monitoring the three-dimensional effects of the tunnel excavation. First, as the TBM was approaching a tunnel section, that section influenced the excavation even before the TBM reached it. For example, as shown in Figure 5-5b, strain gauge B41 on the first MPBEx recorded the strain 3.25 hours before the TBM reached this section, and from this point on, the strain increased with the tunnel advance. Second, after the excavation was completed, the section at the farthest point from the face of the excavated tunnel, monitored by the strain gauge B41, experienced the maximum deformation influence of the excavation. For example, strain gauges B41, B81 and B121 were at the same radial distance of 10 mm from the tunnel boundary but at different longitudinal distances of 100, 60 and 20 mm from the tunnel face, respectively, and the strains recorded in these three strain gauges were 0.18, 0.09 and 0.05 %, respectively. The point to be highlighted here is that the MPBEx strain did not necessarily represent the strain of the rock material as the strain gauges of the MPBEx were glued with the Teflon strip and not with the rock. Hence, we considered the MPBEx monitoring as qualitative rather than quantitative.

5.5.2 Loading stage

The observations made from the MPBExs and the digital borehole caliper during the four loading stages of the tunnel excavation are discussed in detail in the following section.

MPBEx observations

In terms of the MPBEx measurement for each loading stage and each strain gauge observations, these are presented as the change in the ratio of the strain accumulated in the strain gauge over time ε_{Mt} to the strain recorded by the strain gauge at the starting point of that loading stage ε_{Mt} over time in that loading stage *t*. It was quite clear that the higher this ratio for the strain gauge was, the more the squeezing ground condition's influence was at that strain gauge's location.

For Loading Stage I, the isotropic stress on the cubical rock specimen was $0.5 \cdot \sigma_{c,}$ which was identical to the excavation phase. Therefore, the ε_{Mi} for any strain gauge in Loading Stage I was

equal to the strain recorded by that strain gauge at the end of the excavation phase. During Loading Stage I, there was negligible change in the amount ratio $\varepsilon_{Mt}/\varepsilon_{Mi}$ for 101 hours of loading. Hence, it was concluded that there was negligible influence of the time-dependent behavior of the material around the excavated tunnel at the MPBEx locations, and the excavated tunnel still was not in the squeezing ground conditions.

At the end of Loading Stage I, the isotropic stress p_o on the rock specimen immediately increased from $0.5{\cdot}\sigma_c$ to $1.0{\cdot}\sigma_c$, which marked the beginning of Loading Stage II. During Loading Stage II, p_o was kept constant for 168 hours. The strain recorded by the strain gauges at the beginning of Loading Stage II was ε_{Mi}. Figure 5-6a shows the increase in the ratio $\varepsilon_{Mt}/\varepsilon_{Mi}$ over time t during Loading Stage II. The maximum and minimum magnitude of $\varepsilon_{Mt}/\varepsilon_{Mi}$ at the end of this loading stage were 2.90 and 1.05, which were obtained for strain gauges B41 and M162, respectively. Strain gauge B41 was at a longitudinal distance x_f = 100 mm from the tunnel face and at a radial distance r = 34 mm from the tunnel center. In comparison, the MPBEx at strain gauge M162 was on the other side of the tunnel face (x_f = -20 mm) compared to strain gauge B41.

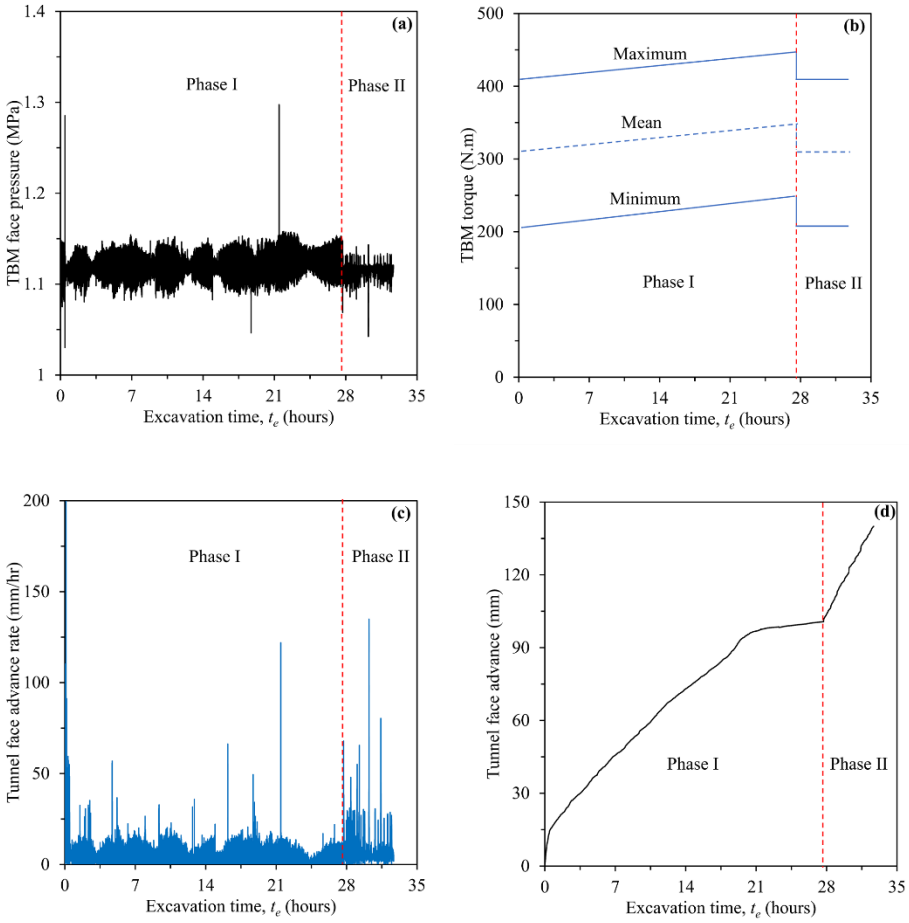

Figure 5-4 Monitoring of miniature TBM parameters during the excavation stage: (a) face pressure (thrust), (b) advance rate, (c) cutter head torque and (d) TBM advance.

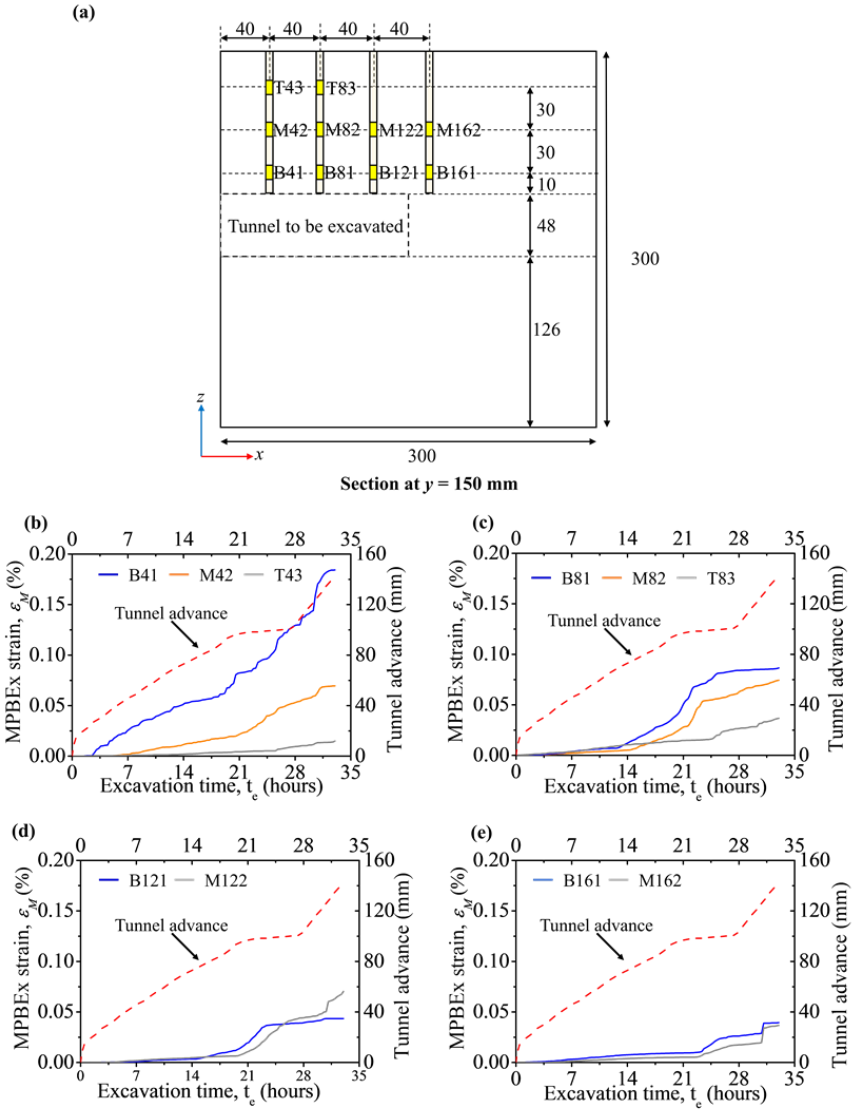

Figure 5-5 (a) Location of MPBEx in the cubical rock specimen (top), and strain recorded by strain gauges on MPBEx with time during the excavation phase for MPBEx at a distance from tunnel portal: (b) 40 mm, (c) 80 mm, (d) 120 mm and (e) 160 mm.

After Loading Stage II, the isotropic stress p_o on the rock specimen increased from $1.0 \cdot \sigma_c$ to $1.5 \cdot \sigma_c$, and the test entered Loading Stage III. The time duration for Loading Stage III with $p_o = 1.5 \cdot \sigma_c$ was 222 hours. Strain ε_{Mi} was obtained for each strain gauge based on the MPBEx reading at the beginning of this loading stage. Figure 5-6b shows the increase in the ratio $\varepsilon_{Mt}/\varepsilon_{Mi}$ with loading stage time t during Loading Stage III. The maximum and minimum magnitudes of $\varepsilon_{Mt}/\varepsilon_{Mi}$ at the end of Loading Stage III were 3.05 and 1.13, which were obtained for strain gauges B41 and M162, respectively (see Figure 5-6b). The MPBEx having strain gauge M162 was on the other side of the tunnel face (x_f = -20 mm) compared to strain gauge B41.

The isotropic stress p_o on the rock specimen increased from $1.5 \cdot \sigma_c$ to $2.0 \cdot \sigma_c$ to take the specimen from Loading Stage III to Loading Stage IV. During Loading Stage IV, p_o was $2.0 \cdot \sigma_c$ for 218

hours, and the strain was ε_{Mi}, which was similar to the strain in Loading Stages II and III. Figure 5-6c shows the increase in the ratio $\varepsilon_{Mt}/\varepsilon_{Mi}$ with loading stage time *t* during Loading Stage IV. The maximum and minimum magnitude of $\varepsilon_{Mt}/\varepsilon_{Mi}$ at the end of this loading stage were 5.15 and 1.29, which were obtained for strain gauges B41 and M162, respectively.

Longitudinal displacement profile (LDP)

The convergence-confinement method CCM (e.g., Duncan-Fama 1993; Panet, 1993, 1995; Carranza-Torres and Fairhurst 2000) is an approach in tunnel design that considers the ground response to the advancing tunnel face and its interaction with the installed support. This method has been widely used for the preliminary design of tunnel support systems. CCM uses an LDP of a tunnel to determine the optimal design and appropriate timing for the installation of the tunnel support system (Vlachopoulos and Diederichs 2009).

This section discusses the change in the LDP of the model tunnel over time during the four loading stages shown in Figure 5-3. Tunnel wall displacement *u* at any time *t* is the difference between the excavated radius of tunnel *R* and the tunnel radius R_t at time *t*. Displacement *u* and the longitudinal distance from the tunnel face x_f were normalized with the radius of the tunnel *R* to normalize the results with respect to tunnel size. The ratio *u*/*R* (in %) is effectively the tunnel wall radial strain, and parameter $X = x_f/R$ is the normalized longitudinal distance from the face.

The LDP of the excavated tunnel as function of time for different loading stages determined using the borehole caliper is shown in Figure 5-7. The LDP of the tunnel was determined by monitoring the change in the radius of the tunnel at seven cross-sections equally spaced along the longitudinal axis of the tunnel with parameter *X* varying from 0 to 4.8. Since the borehole caliper could not monitor the LDP of the tunnel during the excavation phase with the existing test setup, the LDP of the tunnel was observed during each of the four loading stages. After the excavation phase (at the beginning of Loading Stage I), the longitudinal diameter profile of the tunnel was measured continuously during the four loading stages, and the LDP of the tunnel was determined by considering *R* = 24 mm as a constant value.

Figure 5-7a shows some of the LDP readings (*u*/*r* versus *X* plot) of the tunnel over time for Loading Stage I ($p_o = 0.5 \cdot \sigma_c$). It can be clearly seen that at any time *t*, *u*/*r* increased with increases in *X*, and for constant *X*, *u*/*R* first increased with loading stage time *t* and then became constant. The maximum change in *u*/*r* with the loading stage time was observed at *X* = 4.8, and *u*/*r* increased by 10% in the first hour to its initial value. In Figure 5-7a, at 11.5 hours and 50 hours, the increase in *u*/*r* was around 16% and 17%, respectively. However, after 50 hours of the loading stage time, there was no significant change in *u*/*R*, and the excavated tunnel did not squeeze further.

The change in the LDP of the tunnel for Loading Stage II with time is shown in Figure 5-7b. As expected, tunnel strain *u*/*R* was found to increase with *X* at any loading stage time. Also, for a given *X*, the rate of increase in *u*/*R* was found to decrease as the loading stage time increased. Similar to Loading Stage I, the maximum change in *u*/*R* was at *X* = 4.8 for which the *u*/*R* increased by 10, 21, 42 and 48% in one, 24, 46 and 75 hours of loading time, respectively. After 75 hours of the loading stage time, there was no significant change in *u*/*R*, and hence, the effect of squeezing ground conditions diminished.

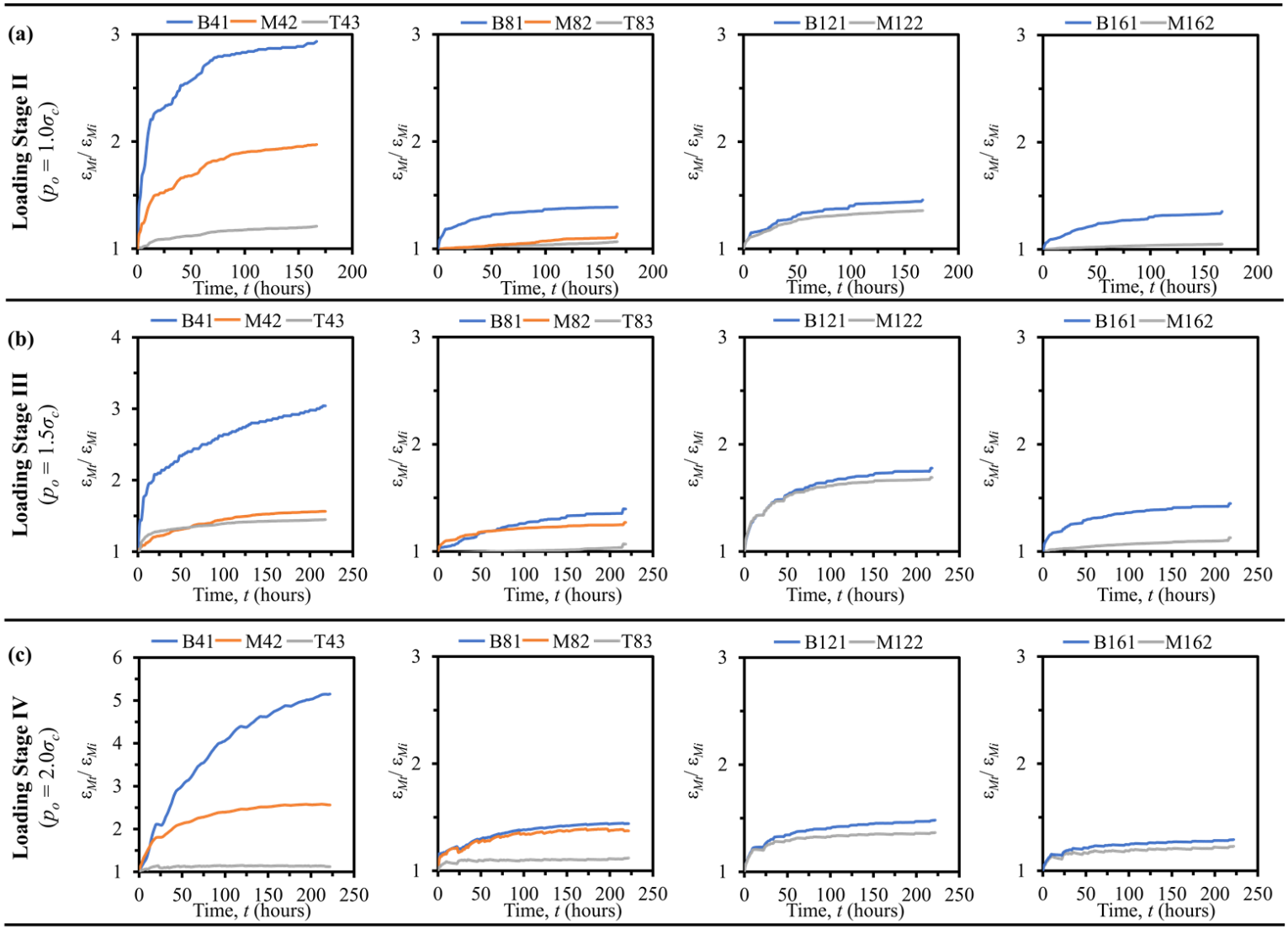

Figure 5-6 Increase in the relative strain of strain gauge on MPBEx $\varepsilon_{Mt}/\varepsilon_{Mi}$ with loading stage time t during the loading stage: (a) II, (b) III and (c) IV.

The change in the LDP of the tunnel over time for Loading Stage III is shown in Figure 5-7c. It was observed that for X = 4.8, the u/R increased by 12, 25, 31, 40, 51 and 68% in one, 11, 23, 52, 103 and 218 hours of loading time, respectively. Like the case of Loading Stages I and II, during Loading Stage III, the rate of increase in u/R decreased with the loading stage time. However, the tunnel was found to be squeezing throughout Loading Stage III, which was not the case in Loading Stages I and II.

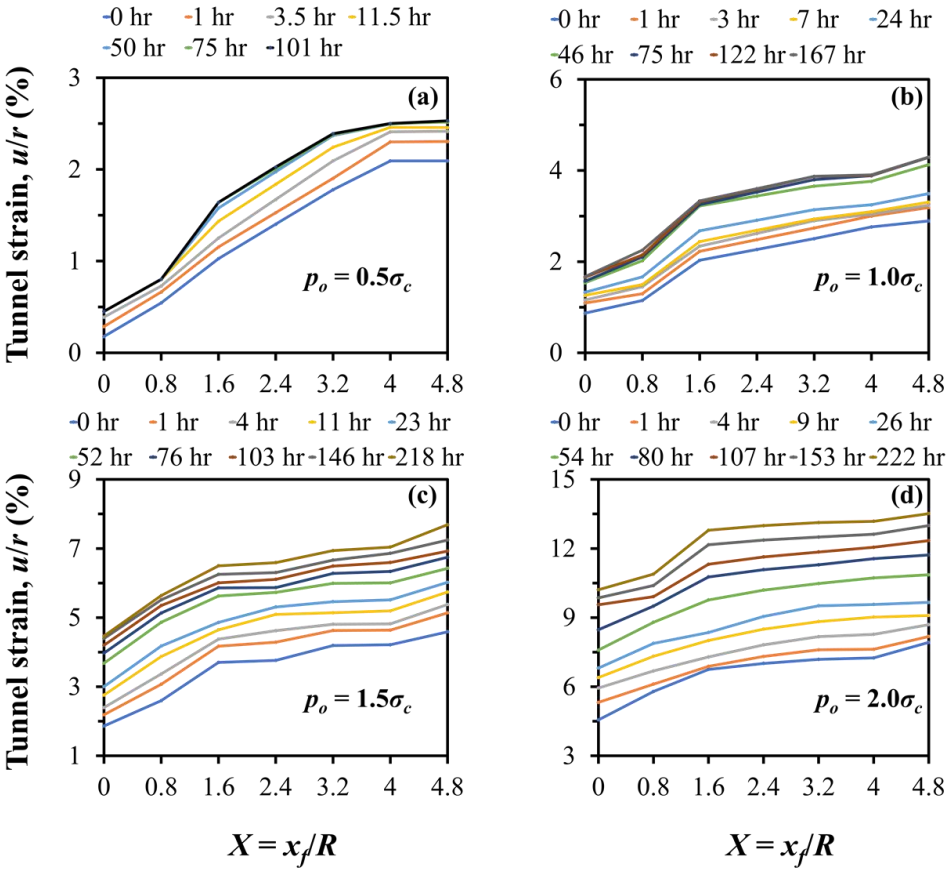

Figure 5-7 Longitudinal displacement profiles (LDP) of the tunnel at the different times for the loading stage: (a) I, (b) II, (c) III and (d) IV.

The change in the LDP of the tunnel over time for Loading Stage IV is presented in Figure 5-7d. For X = 4.8, the u/R increased by 4, 15, 22, 38, 56 and 71% in one, 11, 23, 52, 103 and 218 hours of loading time, respectively. Like the case of Loading Stages I, II, and III, during Loading Stage IV, the rate of increase in u/R decreased with the loading stage time. The tunnel was found to be squeezing throughout Loading Stage IV.

Hoek and Marinos (2000) developed a classification method for tunnel squeezing in terms of the tunnel radial strain. The findings of Hoek and Marinos (2000) and our experimental observations were combined to classify the level of squeezing. During Loading Stage I, the total tunnel strain was 2.53% in 101 hours and, in accordance with Hoek and Marinos (2000), this was classified as the light squeezing stage in the tunnel. The total tunnel strain after 167 hours during Loading Stage II was 4.30%, which was classified as fair to moderate squeezing. During Loading Stage III, the

total tunnel strain developed in 218 hours was 7.69%, which was classified as high to very high squeezing. In Loading Stage IV, the tunnel total strain developed in 222 hours was 13.51%, which was classified as extreme squeezing. These observations are summarized in Table 5-3.

Comparison of MPBEx and borehole caliper data

The normalized longitudinal distances x_f/R from the tunnel face for the three MPBExs installed above the excavated tunnel were 0.8, 2.4 and 4.0. Hence, it was possible to compare the tunnel convergence data obtained using the borehole caliper with the MPBEx data at these tunnel sections, as presented in Table 5-3. For the borehole caliper data, the results are presented in the form of the increase in tunnel strain (u/R) from the beginning to the end of the loading stage while the MPBEx data are presented in the form of ratio $\varepsilon_{Mt}/\varepsilon_{Mi}$ at the end of the loading stage at different radial distances r from the center of the excavated tunnel.

It can be seen in Table 5-3 that the higher the $\Delta(u/R)$ for all the loading stages and value of X were, the higher $\varepsilon_{Mt}/\varepsilon_{Mi}$ was. For example, in Loading Stage IV at $X = 4.8$, the total change in the tunnel strain $\Delta(u/R)$ was 5.93% and the corresponding $\varepsilon_{Mt}/\varepsilon_{Mi}$ ratios were 5.15, 2.57 and 1.24 for the value of r equal to $1.4R$, $2.6R$ and $3.8R$, respectively. From the MPBEx observations, it also was concluded that the time-dependent deformation around the tunnel boundary decreased with increases in r. Also, in Loading Stages I, II, III, and IV, the maximum tunnel strains were 2.53, 4.30 7.69 and 13.51%, respectively. Based on the observations presented in Table 5-3, it was concluded that the combination of MPBEx analysis and digital borehole caliper analysis in this physical model confirms that it is a suitable tool for three-dimensional study of tunnels in squeezing ground conditions.

After Loading Stage IV, the excavated tunnel collapsed as shown in Figure 5-8a. At this point, all the stresses on the cubical rock specimen were released, and the LDP of the tunnel was immediately obtained. Figure 5-8b shows the LDP of the tunnel at the beginning of Loading Stage I, after 222 hours of loading stage IV and immediately after Loading Stage IV ($p_o = 0$). It can be seen in Figure 5-8b that as soon as the stress was released, some of the tunnel strain was recovered instantaneously. The recovered tunnel strains were 0.59, 0.65, 0.70, 0.86, 0.95, 1.01 and 1.49% for X equal to 0, 0.8, 1.6, 2.4, 3.2, 4.0 and 4.8, respectively.

5.6 A time-dependent LDP

The most widely used models to determine the LDP of tunnels were provided by Panet (1995), and Vlachopoulos and Diederichs (2009). Both models simulated the support to any tunnel section by applying a pseudo-support pressure p_f in the radial direction as a function of X. The solution by Panet (1995) is valid for the elastic behavior of the ground material around the tunnel boundary. In contrast, the solution by Vlachopoulos and Diederichs (2009) applies to both the elastic and elasto-plastic behavior of the ground. However, neither solution considers the time-dependent convergence of the tunnel boundary. In this section, a new model to determine the LDP of an excavated tunnel in squeezing clay-rich rocks is proposed.

Table 5-3 Comparison of the quantitative borehole caliper data with the qualitative MPBEx data.

Loading stage	Loading time t (hours)	*Normalized radial distance from the tunnel face* $X = x_f/R$	$\Delta(u/r)$ in % at the end of loading stage (at $r = R$)	MPBEx strain $\varepsilon_{Mt}/\varepsilon_{Mi}$ at the end of the loading stage with r			Classification according to Hoek and Marinos (2000)
				1.4R	2.6R	3.8R	
I ($p_o = 0.5\sigma_c$)	101	0.8	0.26	1.00	1.00	--	Light squeezing
		2.4	0.41	1.00	1.00	1.00	
		4.0	0.48	1.00	1.00	1.00	
II ($p_o = 1.0\sigma_c$)	167	0.8	1.10	1.45	1.35	--	Fair to moderate squeezing
		2.4	1.36	1.39	1.14	1.07	
		4.0	1.38	2.92	1.98	1.21	
III ($p_o = 1.5\sigma_c$)	218	0.8	2.54	1.77	1.69	--	High to very high squeezing
		2.4	2.84	1.27	1.39	1.06	
		4.0	2.85	3.04	1.57	1.44	
IV ($p_o = 2.0\sigma_c$)	222	0.8	5.09	1.49	1.37	--	Extremely high squeezing
		2.4	5.92	1.45	1.38	1.12	
		4.0	5.93	5.15	2.57	1.24	

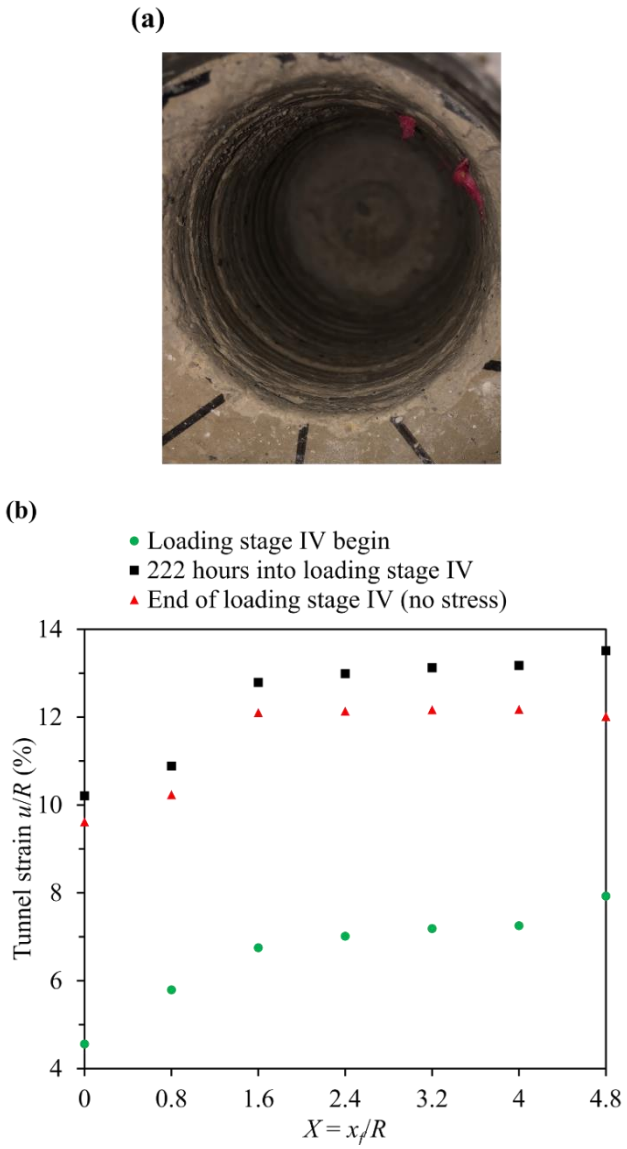

Figure 5-8 (a) Excavated tunnel after loading stage IV, and (b) LDPs of the tunnel at the beginning, 222 hours and immediately after loading stage IV.

Figures 5-9 through 5-12 depict the change in the tunnel strain with the loading stage time *t* for the four loading stages in seven equally spaced longitudinal tunnel sections from $X = 0$ to 4.8. Based on the experimental data in Figures 5-9 through 5-12, it can be seen that for any tunnel section and during any loading stage, the correlation between tunnel strain u/R in % and time *t* in hours could be expressed as an asymptotic model given by the following equation:

$$\frac{u}{R}(t) = a - b(d)^t \qquad (5\text{-}1)$$

where *a*, *b* and *d* are the model parameters, and the values are determined from the best fitting curve having the maximum coefficient of determination with the experimental data. The best fit values of the model parameters *a*, *b* and *d* for all the plots in Figures 5-9 through 5-12, along with

the coefficient of determination between the fitting curve and experimental data are given in Table 5-4. According to Eq. (5-1), the parameter *a* (for $d < 1$) also can be defined for any tunnel section as the tunnel strain at infinite time,

$$\frac{u}{R}(t = \infty) = a \tag{5-2}$$

Also, according to Eq. (5-1), the difference between parameters *a* and *b* is the tunnel strain at the beginning of any loading stage ($t = 0$),

$$\frac{u}{R}(t = 0) = a - b \tag{5-3}$$

It can be seen that parameter *a* increased with the increase in p_o as well as with the increase in *X*. Figure 5-13a shows the change in *a* with *X* for Loading Stage I ($p_o = 0.5 \cdot \sigma_c$), Loading Stage II ($p_o = 1.0\sigma_c$), Loading Stage III ($p_o = 1.5\sigma_c$), and Loading Stage IV ($p_o = 2.0 \cdot \sigma_c$). For any loading stage, *a* had a linear relationship with *X*, and the value of *a* when *X* was zero solely depended on p_o. Hence, *a* can be expressed by the following equation,

$$a = f\left(X, \frac{p_o}{\sigma_c}\right) \tag{5-4}$$

which depends on the normalized distance *X* and the ratio of the confining stress to the unconfined compressive strength p_o/σ_c . Parameter *b* was found to be independent of *X* but to increase with an increase in p_o (Table 5-4). The average value of parameter *b* for the seven tunnel sections was calculated for each loading stage and plotted with the ratio (p_o/σ_c) in Figure 5-13b. The relationship between *b* and (p_o/σ_c) can be expressed as a power relation, as shown in Figure 5-13b. However, this relationship between *b* and (p_o/σ_c) was established based on four data points and needs to be explored further. Hence, parameter *b* can be defined by the following equation,

$$b = h\left(\frac{p_o}{\sigma_c}\right) = 1.22\left(\frac{p_o}{\sigma_c}\right)^{1.913} \tag{5-5}$$

where $h(p_o/\sigma_c)$ is a function of (p_o/σ_c). As presented in Table 5-4, parameter *d* was found to be dependent on (p_o/σ_c) and independent of parameter *X*. For Loading Stage I, the average value from the seven tunnel sections for parameter *d* was 0.65. However, for Loading Stages II, III, and IV the value of parameter *d* was found to be constant ($d = 0.98$) and did not change with(p_o/σ_c), as given in Table 5-4. As already discussed, during Loading Stage I, the tunnel experienced light squeezing, but during Loading Stages II, III, and IV, the tunnel experienced a significant amount of squeezing. Hence, for squeezing ground conditions, the parameter *d* was 0.98. By substituting Eq. (5-4), Eq. (5-5), and $d = 0.98$ in Eq. (5-1), it can be rewritten as,

$$\frac{u}{R}(t) = f\left(X, \frac{p_o}{\sigma_c}\right) - h\left(\frac{p_o}{\sigma_c}\right)(0.98)^t \tag{5-6}$$

The LDP of a tunnel at any time and for a given p_o can be determined using Eq. (5-6). Differentiating Eq. (5-6) with time gives,

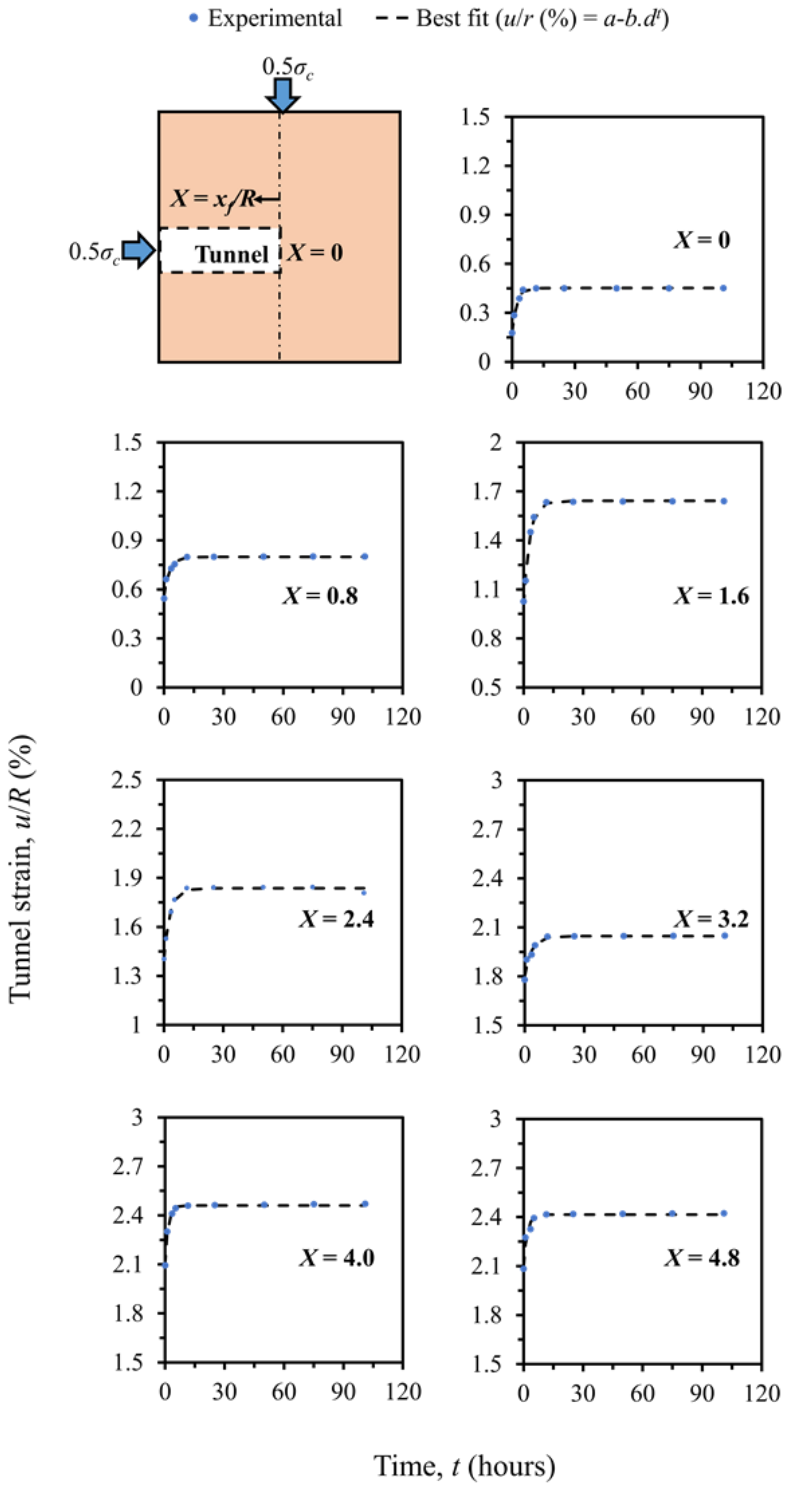

Figure 5-9 Tunnel strain u/R (in %) with loading stage time t for X varying from 0 to 4.8 for loading stage I.

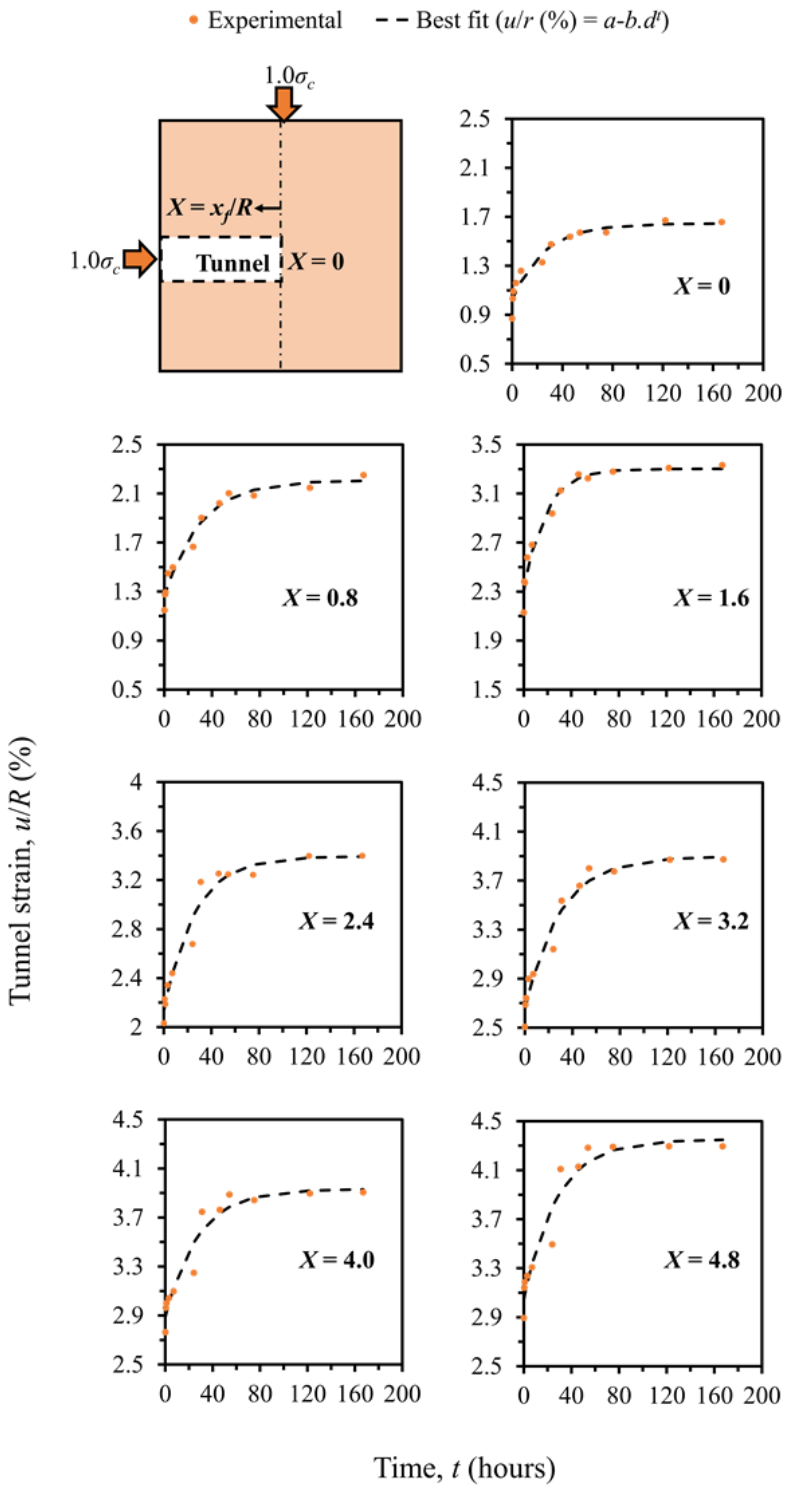

Figure 5-10 Tunnel strain u/R (in %) with loading stage time t for X varying from 0 to 4.8 for loading stage II.

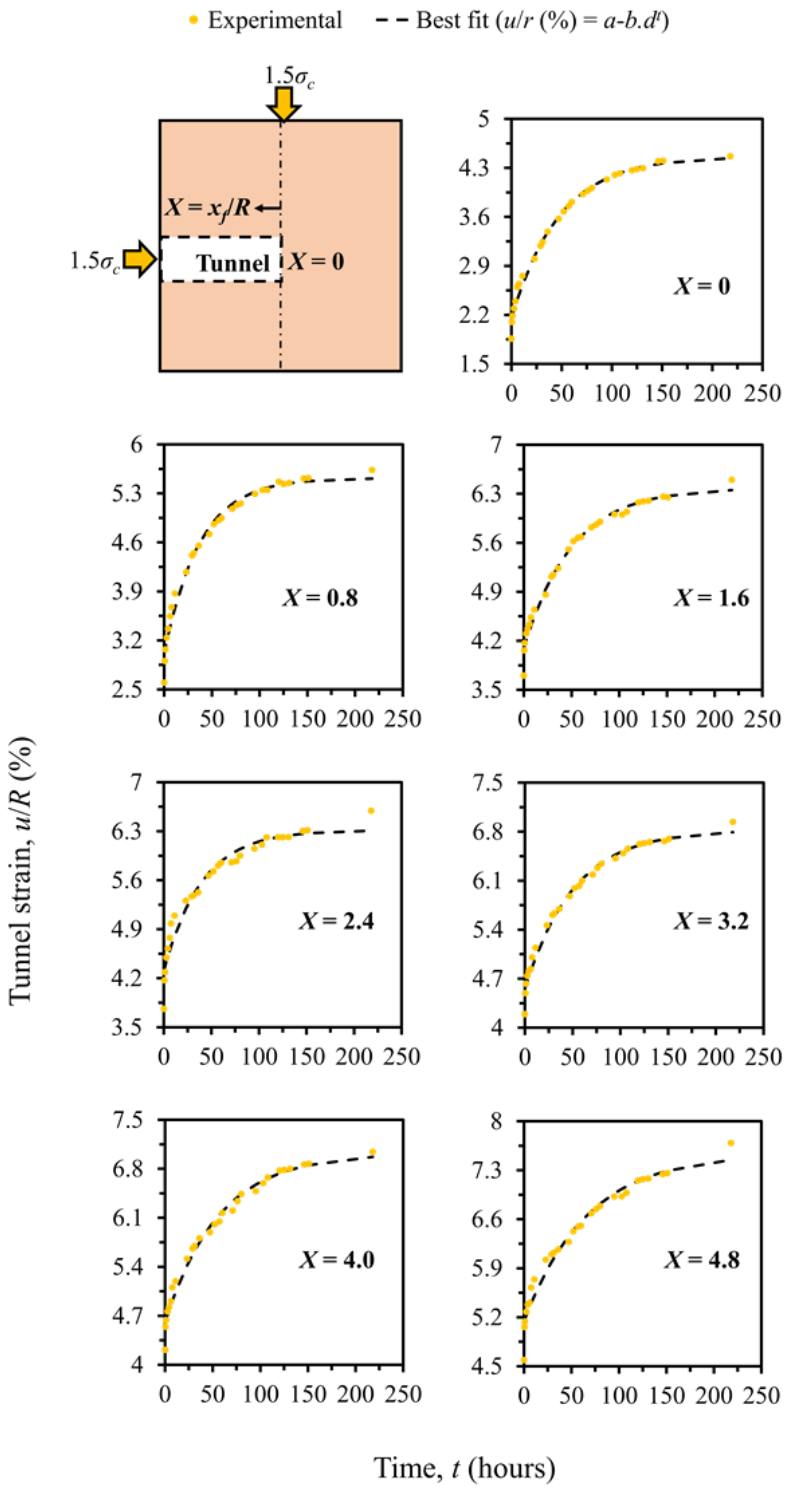

Figure 5-11 Tunnel strain u/R (in %) with loading stage time t for X varying from 0 to 4.8 for loading stage III.

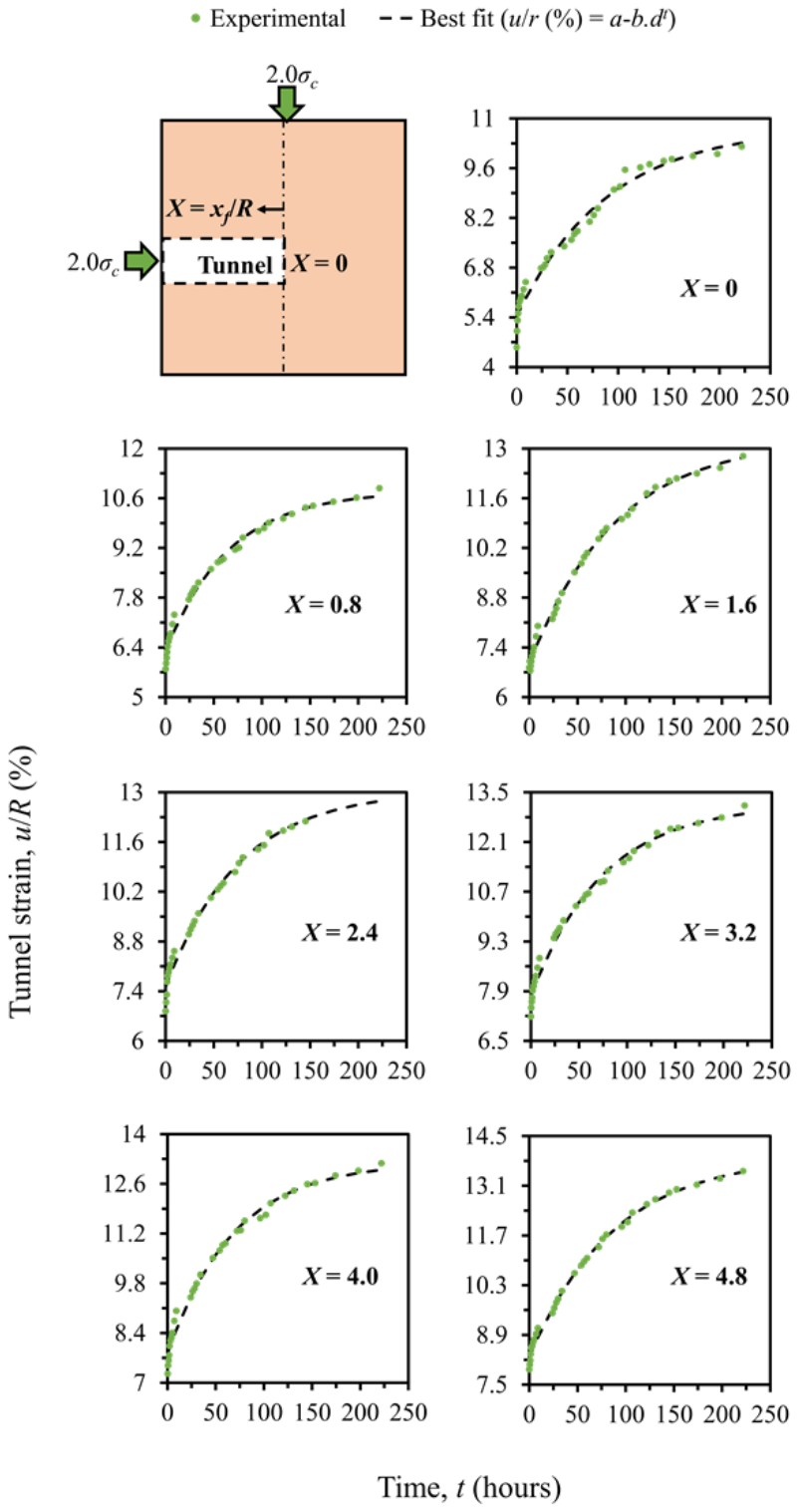

Figure 5-12 Tunnel strain u/R (in %) with loading stage time t for X varying from 0 to 4.8 for loading stage IV.

Table 5-4 Curve fitting parameters for the four-loading stage and different X.

p_o/σ_c	$X = x_f/R$	Proposed model parameters $(u/R = a - b(d)^t)$			Coefficient of determination R^2
		a	b	d	
0.5	0	0.45	0.27	0.62	0.99
	0.8	0.80	0.24	0.67	0.98
	1.6	1.64	0.63	0.72	0.99
	2.4	1.84	0.43	0.72	0.99
	3.2	2.05	0.25	0.75	0.95
	4.0	2.46	0.36	0.48	0.99
	4.8	2.42	0.31	0.57	0.95
1.0	0	1.64	0.62	0.96	0.93
	0.8	2.21	0.95	0.97	0.97
	1.6	3.30	1.00	0.95	0.96
	2.4	3.39	1.26	0.96	0.96
	3.2	3.90	1.25	0.97	0.96
	4.0	3.93	1.05	0.96	0.93
	4.8	4.35	1.31	0.96	0.93
1.5	0	4.46	2.31	0.98	0.99
	0.8	5.52	2.51	0.97	0.98
	1.6	6.38	2.29	0.98	0.98
	2.4	6.32	2.01	0.98	0.95
	3.2	6.82	2.27	0.98	0.98
	4.0	7.02	2.41	0.98	0.98
	4.8	7.54	2.40	0.99	0.96
2.0	0	10.76	5.33	0.99	0.97
	0.8	10.81	4.53	0.98	0.99
	1.6	13.29	6.35	0.99	0.99
	2.4	13.06	5.53	0.99	0.99
	3.2	13.18	5.42	0.99	0.99
	4.0	13.21	5.39	0.99	0.99
	4.8	13.95	5.66	0.99	0.99

$$\frac{1}{R}\frac{du}{dt} = 0.0202h\left(\frac{p_o}{\sigma_c}\right)(0.98)^t \qquad (5\text{-}7)$$

Eq. (5-7) states that the rate of increase in tunnel strain decreased with an increase in loading stage time *t*, and as *t* approached infinity, the change in *u/R* approached zero. In other words, in squeezing ground conditions as the time approaches infinity, the tunnel strain at any location will approach a constant value and will be equal to parameter *a*.

Although the parameters derived were determined only for a synthetic mudstone specimen, the LDP given in Eq. (5-6) exhibited a very high correlation from experimental data with a very high

coefficient of determination. In future work, the dependency of parameters *a*, *b* and *c* on the material properties will be calibrated by carrying out more tests on different rocks and from field monitoring data from tunnels excavated in squeezing ground conditions.

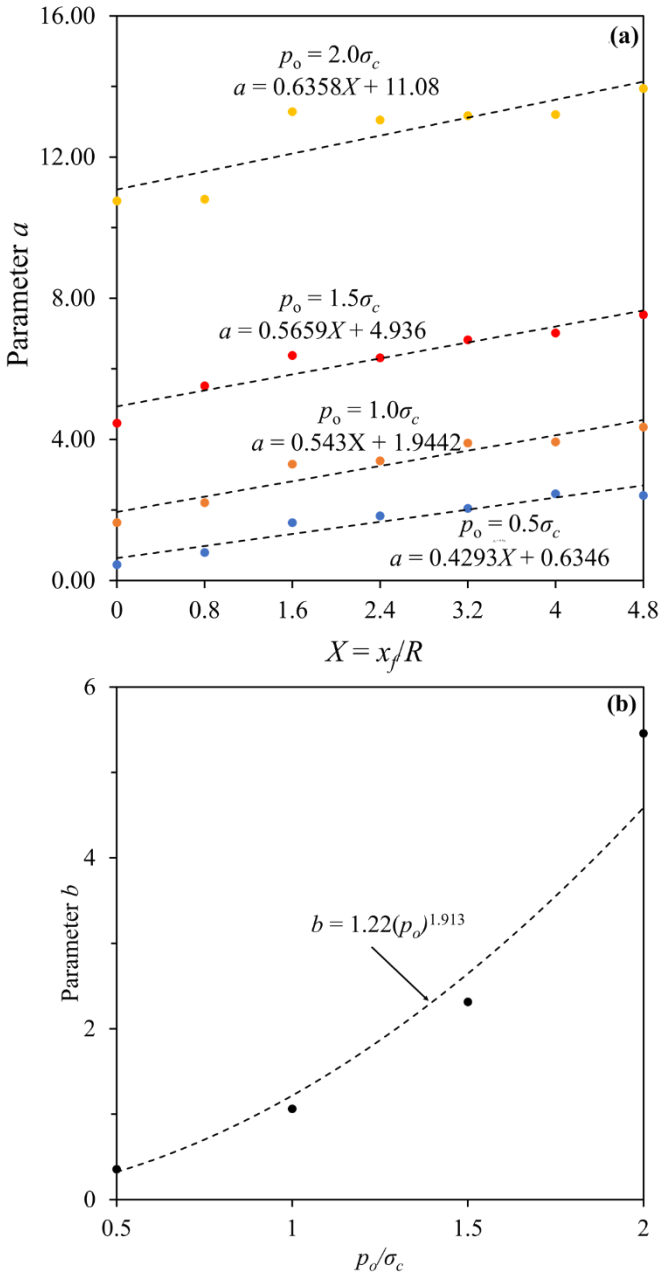

Figure 5-13 Plots showing the dependency of the LDP model parameters: (a) *a* on p_o and *X*, and (b) *b* on p_o.

5.7 Conclusions

This chapter presented a study involving a physical model and test to observe tunnel closure over time in the presence of squeezing ground conditions. The physical model simulated TBM

excavation in a tunnel as it advanced and time-dependent strains developed at and around the tunnel boundary under squeezing ground conditions were monitored. Analysis of the data using embedded strain gauges provided an estimate of the amount of squeezing at different radial and longitudinal distances with time around the excavated tunnel boundary, and a digital borehole caliper provided a quantitative assessment of the LDP of the tunnel at different times and stress levels.

Based on the experimental observations, a model was proposed to express the LDP of the tunnel as function of tunnel stand time. The parameters of the LDP were found to be a function of the ratio of the isotropic stress applied and unconfined compressive strength of the rock specimen and normalized distance from the tunnel face. The LDP was found to be in good agreement with the experimental observations with excellent coefficients of determination. Future work will calibrate the proposed LDP against different rock properties and the long-term behavior of the squeezing tunnels particularly using field case histories.

CHAPTER 6 - AN EXPERIMENTAL STUDY OF THE ROCK-SUPPORT INTERACTION FOR A TUNNEL IN SQUEEZING GROUND

6.1 Abstract

The presence of squeezing ground conditions poses significant challenges in the design of an adequate support system for tunnels. Numerous empirical, observational and analytical methods have been proposed over the years for the design of support systems in squeezing ground conditions, but they all have some limitations. In this study, a unique physical model for simulating the tunnel boring machine (TBM) excavation and support installation in squeezing clay-rich rocks is developed and the observations are made to better understand the interaction between the support and the squeezing ground. The physical model included a large true-triaxial cell, miniature TBM, laboratory-prepared synthetic test specimen with properties similar to natural mudstone, and an instrumented cylindrical aluminum support system. Experiments were conducted at realistic in-situ stress levels to study the time-dependent three-dimensional tunnel support convergence. The tunnel was excavated using the miniature TBM in the cubical rock specimen loaded in the true-triaxial cell, followed by the installation of the support. The confining stress was then increased in stages to values greater than the rock's unconfined compressive strength and using the tunnel convergence measurements at different times and stress levels, a model for time-dependent longitudinal displacement profile (LDP) for the supported tunnel was proposed. The LDP model was then compared with the model for the unsupported model, presented in Chapter 5, to calculate the amount of squeezing resisted by the support. The increase in thrust in the support was also back-calculated from an analytical solution with the assumption of a linear elastic support. Based on the observations, a recommendation for the future analysis to optimize the support requirement for the tunnels in squeezing ground is proposed.

6.2 Introduction

The tunnel wall convergence after the tunnel excavation is a function of the in-situ stresses and the rock mass behavior at the tunnel location. In squeezing ground conditions, the tunnel converges significantly and continuously with time during or even after the tunnel excavation. As the tunnel converges with time, the loads applied to the tunnel support system increase, resulting in severe stability issues in some cases. Hence, the beforehand estimation of the interaction between the rock mass and the tunnel support system (or rock-support interaction) with time is essential to counter the squeezing.

In tunneling, rock-support interaction is used as a preliminary tool for assessing the behavior of the tunnel support system during both the design and construction process (Panet, 1995; Carranza-Torres & Fairhurst, 2000; Gschwandtner & Galler, 2012). There are several practices reported in the literature to carry out rock-support interaction study (Fenner, 1938; Parcher, 1964; Lombardi, 1975; Brown et al., 1983; Corbetta et al. 1991; Duncan-Fam, 1993; Panet, 1993, 1995; Peila & Oreste, 1995; Carranza-Torres & Fairhurst, 2000; Alejano et al., 2009; Vrakas & Anagnostou, 2014; Cai et al., 2015; Cui et al., 2015). Most of the proposed solutions are based on simplifying the three- dimensional (3D) into a two-dimensional (2D) plain-strain problem. A common example of such approach is the Convergence-Confinement Method (CCM). The CCM has three basic components of: (a) the ground reaction curve (GRC), (b) the longitudinal displacement profile

(LDP) of tunnel and (c) the support characteristic curve (SCC). The GRC defines the relationship between the decreasing internal pressure in the tunnel and the increase in tunnel convergence. The LDP is the plot of the tunnel convergence that occurs along the axis of the tunnel as a function of the distance from the tunnel face. The SCC expresses the relationship between the increasing stresses on the tunnel support and the increasing support displacement.

The conventional CCM considers the tunnel deformation only due to the advancement of the tunnel and the change in the internal pressure. However, in squeezing ground conditions, the tunnel also converges with time even after the excavation is complete. This time-dependent convergence can generate additional stresses in the tunnel support system and can ultimately cause unpredictable support failure, construction hazards, cost overruns and project delays (Paraskevopoulou & Benardos, 2013).

The only approach reported in the literature to develop the CCM for squeezing ground conditions incorporates a time dependent rock mass model for the tunnel (Paraskevopoulou & Diederichs, 2018). The time-dependent behavior can be explicitly studied for the rock mass (Paraskevopoulou & Diederichs, 2018) or indirectly by monitoring the change in stresses on the tunnel support (Gschwandtner & Galler, 2012). The former approach modifies the LDP with time using a time-dependent constitutive model while assuming visco-elastic behavior of the rock mass. On the other hand, the latter approach predicts the increase in stresses applied to the support system in the excavated tunnel based on the field monitoring data. This approach, given that the change in stresses applied to the tunnel support system is monitored for a real project, can be more accurate that the first approach. However, due to high levels of applied loads and deformations, field sensors, just like the tunnel support system themselves, are under extreme environments and often fail before meaningful data can be measured once the squeezing has started. Without reliable field data, it is challenging to develop the CCM to calculate stresses on the tunnel support. This is the primary reason that tunnel designers mostly rely on the empirical equations derived from the limited field observations for tunnels in squeezing ground conditions, as reviewed in Arora at al. (2020). Since in-situ monitoring is often limited in squeezing environments, realistic physical model tests can provide valuable information to better evaluate the interaction between the support and the squeezing ground (Lin et al., 2015).

The objective of this Chapter is to provide a comparison between the LDP of supported and unsupported tunnels, using carefully conducted laboratory-scale physical model tests in squeezing ground. The experiment involved TBM excavation and support installation in a synthetic mudstone specimen, with squeezing and time-dependent behavior, under increasing in-situ stresses. The physical model test explored the critical aspects of tunnel excavation such as the tunnel advancement, 3D effects, support installation, and highly plastic and ductile time-dependent behavior of the ground. The experimental observations and results are synthesized in terms of convergence and support stresses at different times and levels of loading. It is envisioned that the results of this study can help with a more quantitative prediction, analysis and design of tunnel support in squeezing ground.

6.3 Experimental Setup

The setup physically simulates TBM excavation and support installation in a cubical rock specimen loaded at field stress levels (up to 550 meters overburden for mudstones) in a true-triaxial

cell (for more details of the experimental setup, please see Arora et al. 2019 a, b). The temporal changes in the liner deformation were monitored and analyzed throughout the test.

The experimental setup is illustrated in Figure 6-1a using a schematic diagram, and the actual experimental setup at the Colorado School of Mines, where this study took place, is shown in Figure 6-1b. The critical components of the experimental arrangement included a true-triaxial cell, a miniature TBM, a cubical clay-rich rock specimen as mudstone like material, the tunnel support system and the monitoring unit. The essential aspects of the test setup, along with loading, excavation and support installation, are discussed in the following sections.

6.3.1 Cubical rock specimen

It is difficult to obtain natural, homogenous and undisturbed specimens of mudstone from the field. Therefore, this study incorporated synthetic mudstone prepared in the laboratory by mixing cement, clay and water as described in Arora et al. (2020a). The synthetic mudstone exhibits the characteristics of squeezing clay-rock rock, namely ductility even at low confining stresses, extensive plastic deformation, and pronounced time and loading rate dependency.

Based on the laboratory tests, Arora et al. (2020a) reported that the mean unconfined compressive strength σ_c was 4.47 MPa with a standard deviation of 0.15 MPa, the mean Young's modulus E was 0.65 GPa with a standard deviation of 0.02 GPa with a constant Poisson's ratio v of 0.13. For the confining stresses varying from 1 to 6 MPa and using the Mohr-Coulomb linear fit, the effective cohesion c and friction angle ϕ were found to be 2.06 MPa and 10°, respectively. Also, during the creep tests, the synthetic mudstone was observed to develop a considerable amount of creep strain with time (Arora et al. 2020b). The laboratory test results showed that both the synthetic mudstone as tested and the naturally occurring and squeezing- mudstone have similar shear strength, elastic modulus, ductility, strain-rate sensitivity and creep behavior.

The 300x300x300 mm^3 cubical synthetic mudstone specimen was prepared using the same material, composition and procedure as given in Arora et al. (2020a). The specimen made of the mixture of clay, cement and water was removed from the mold after 24 hours and further cured in distilled water for 28 days before the testing commenced.

6.3.2 The loading unit

The physical model test incorporated the use of a true-triaxial cell developed by Frash et al. (2014) at Colorado School of Mines as the loading unit. This cell can apply principal compressive stress as high as 13 MPa on a cubical rock specimen independently in all the three directions. The unique feature of this cell is that the drilling process can be carried out in the rock specimen while it is loaded in a true-triaxial stress state, which made it suitable to simulate in-situ stress conditions. The true-triaxial cell was designed to carry out the thermo-mechanical simulation of enhanced geothermal systems by Frash et al. (2014) and later modified to study TBM-excavated tunnels in squeezing ground conditions by Arora et al. (2019a). The detailed design of this true-triaxial cell is provided in Frash et al. (2014), and the modifications for the tunneling experiments in this study are presented in Arora et al. (2019 a, b).

6.3.3 Tunnel excavation unit

A miniature soft ground open face TBM was mounted on the top of the existing true-triaxial cell to excavate a tunnel. At the same time, the cubical rock specimen was loaded in a true-triaxial cell. As the tunnel excavation needed to occur while the rock was subjected to the in-situ stress levels, the miniature TBM was designed to provide the sufficient amount of cutter head thrust and torque. Figure 6-1 conceptually shows the miniature TBM mounted on the top of the true-triaxial cell.

The four main components of the miniature TBM include the thrust unit, torque unit, cutting unit, and supporting unit. The diameter of the cutter head disc is 48 mm, and the maximum possible length of tunnel that can be excavated is 150 mm. The detailed design and working of this miniature TBM can be found in Arora at al. (2019b).

6.3.4 Tunnel support system

A thin cylinder made of 6061 aluminum alloy, 44.5-mm in outer diameter (OD) and 1.65-mm in thickness t_s was used as the tunnel support system. The ultimate tensile strength, Young's modulus E_s and Poisson's ratio v_s of the 6061 aluminum are 276 MPa, 68.9 GPa and 0.35, respectively (Zwilsky & Langer, 2001). The annular gap between the support system and the tunnel boundary measured 1.5 mm and was filled with non-shrinking grout and cured for three days. The 3-days compressive strength of this grout was 1.12 MPa, which is the same as σ_c. Considering the strength difference between the grout and the aluminum material, it is reasonable to assume that the grout, similar to the real backfill grout in tunnels, played the role of transferring the ground loads to the support system.

Figure 6-2a is the schematic diagram of the cubical rock specimen with the tunnel loaded in the true-triaxial cell and Figure 6-2b shows the support system with strain gauges in the tangential direction. The position of the strain gauges on tunnel support in longitudinal view is shown in Figure 6-2c and in the cross-sectional view in Figure 6-2d.

6.4 Test Procedures

After 28 days of curing in water, the cubical synthetic mudstone specimen was placed in the true-triaxial cell. The specimen was then subjected to an isotropic compressive stress $p_o = 0.5\sigma_c$, and a 48-mm in diameter and 140 mm in length tunnel was excavated in the rock specimen using the miniature TBM along the x-axis of the coordinate system shown in Figure 6-2a.

After ground cured for three days, the isotropic stress p_o was applied in five stages over a period of 605 hours, as shown in Figure 6-3. The total time of loading and monitoring was based on the onset of the steady-state, i.e., the rock specimen was loaded until the tunnel support reached the steady-state. The five loading stages of the test were as follows:

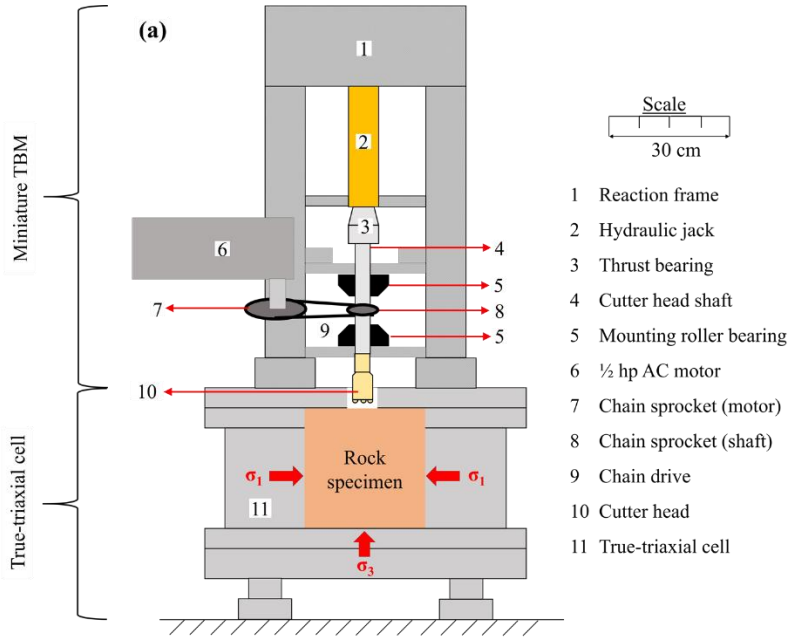

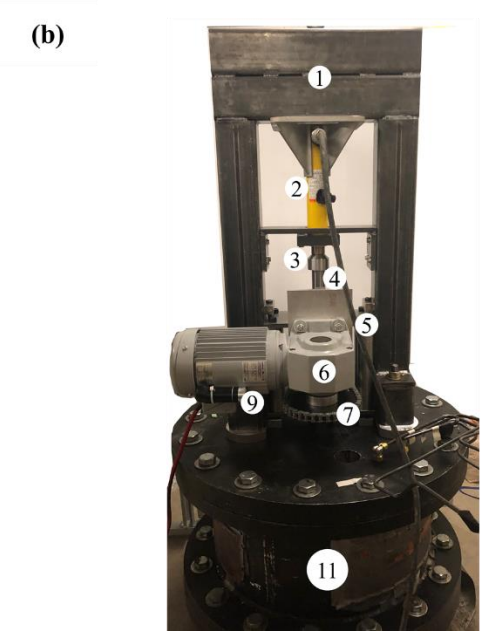

TBM parameter	*Value*
Cutter head diameter	48 mm
Maximum stroke (mm)	150 mm
Maximum TBM thrust	100 kN
Maximum TBM torque	400 N.m

Figure 6-1 Experimental arrangement to study tunnels in squeezing ground conditions: (a) schematic diagram, and (b) actual setup at Colorado School of Mines.

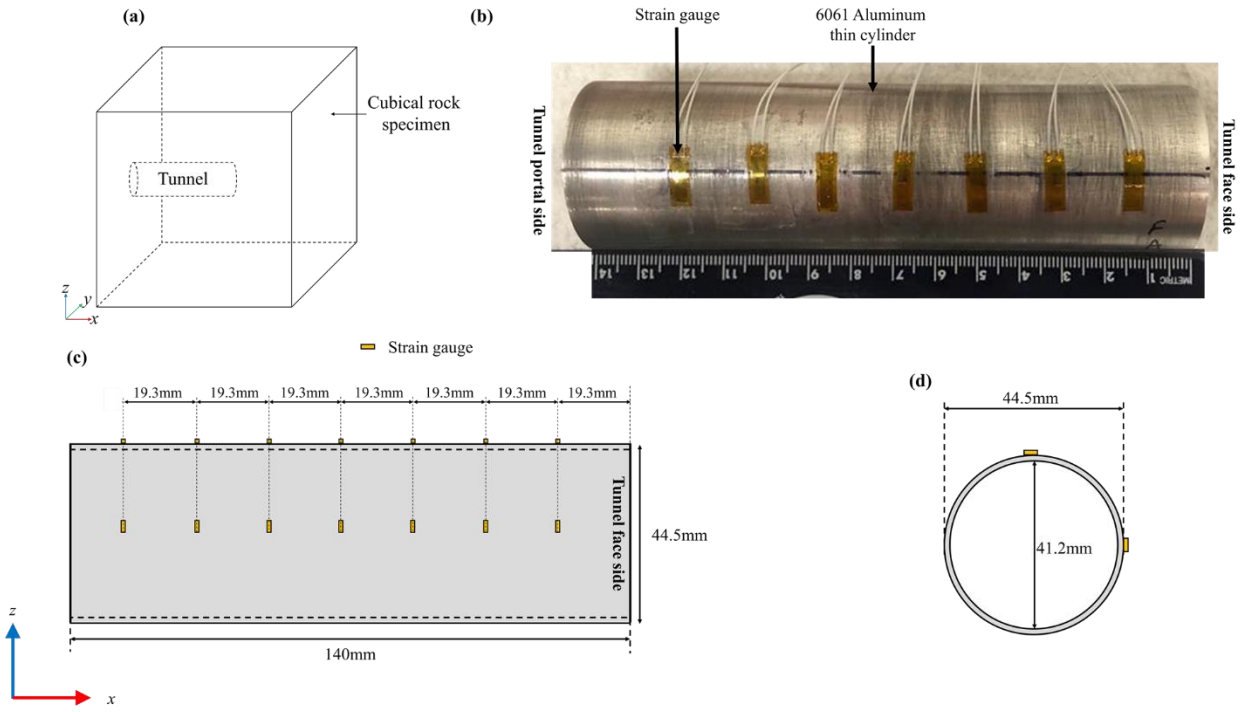

Figure 6-2 (a) Schematic diagram of cubical rock specimen in true-triaxial stress state with tunnel, (b) aluminum tunnel support with strain gauges in tangential direction, (c) longitudinal view of the tunnel support system along with position of strain gauges and (d) cross-section of the tunnel support system.

Loading stage I: After excavating the tunnel and installation of the tunnel support, p_o was increased from $0.5\sigma_c$ to $1.0\sigma_c$. As shown in Figure 6-3, points A and B are the beginning and end of the loading stage I, respectively. The total loading stage time was 125 hours and p_o was equal to σ_c.

Loading stage II: At the end of the loading stage I, p_o was increased rapidly from $1.0\sigma_c$ (point B) to $1.5\sigma_c$ (point C), as shown in Figure 6-3. Point C is the beginning and after 120 hours point D is the end of loading stage II in Figure 6-3.

Loading stage III: The isotropic stress on the cubical rock specimen was further increased by $0.5\sigma_c$, making $p_o = 2.0\sigma_c$. The total time of loading for this stage was 120 hours. The beginning and the endpoint of this loading stage are point E and F in Figure 6-3.

Loading stage IV: In this loading stage, $p_o = 2.5\sigma_c$ was kept constant for another 120 hours while monitoring tunnel support behavior.

Loading stage V: In this final loading stage, p_o was further increased from $2.5\sigma_c$ to $3\sigma_c$. The rock specimen was loaded for 120 hours and finally unloaded to reach $p_o = 0$ MPa.

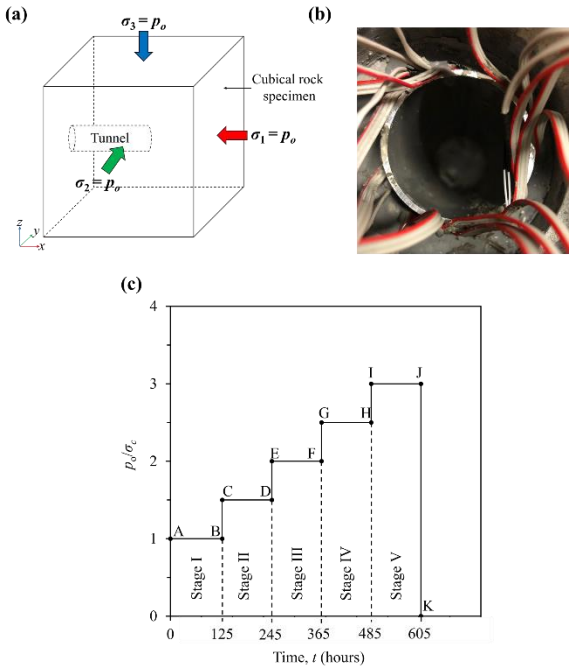

Figure 6-3 (a) Conceptual diagram of the cubical rock specimen with tunnel loaded in true-triaxial stress, (b) support placed inside the tunnel and (c) isotropic stress ratio applied on a cubical rock specimen during the five loading stages.

6.5 Experimental Observations and Results

6.5.1 Tunnel excavations in three phases

Figure 6-4 shows the response of the 48-mm diameter tunnel after it was excavated in three phases, lasting 19.5 hours. As shown in Figure 6-4a, the mean TBM face pressure p_f applied to the tunnel face via the cutter head throughout the excavation stage was about 1.12 MPa with a standard deviation of 0.05 MPa. Isotropic stress p_o applied on the cubical rock specimen was $0.5\sigma_c$, which was roughly two times that of p_f. The miniature TBM shaft rotated at a constant speed of 13 revolutions per minute, and the torque output was continuously monitored, as shown in Figure 6-4b.

During Phase I of the excavation, a 42-mm long tunnel was excavated in 5 hours, followed by removal of the cut material. It was observed that when the cut material was not removed efficiently, the tunnel became clogged and the excavation rate significantly slowed down, as can be seen in Figure 6-4c. Phase II of the tunnel excavation began after the cut material of Phase I was removed. In this phase, a 38-mm long tunnel was excavated in 5.3 hours, making the total length of the tunnel 80 mm. In the last phase of the excavation, the tunnel further advanced by 60-mm in 9.2 hours, making the total length of the tunnel 140 mm. As shown in Figures 6-4c, the tunnel advance rate significantly increased at the beginning of Phase II and III of the excavation compared to the end of Phase I and II, respectively.

6.5.2 Support deformations

In this study, the tunnel support behavior throughout the experiment was monitored by the tangential strain gauges on the support system, as shown in Figure 6-2c. The strain gauges were installed on the outer surface of the cylinder in contact with the grout. Considering the continuity in the tangential strain at this interface, it can be assumed that at the point of contact, the strains in the rock and support are the same. The tangential strain at the tunnel boundary is the ratio of tunnel convergence u to its radius R. Hence, the strain gauges on the support provide the LDP of the supported tunnel at any given p_o and time.

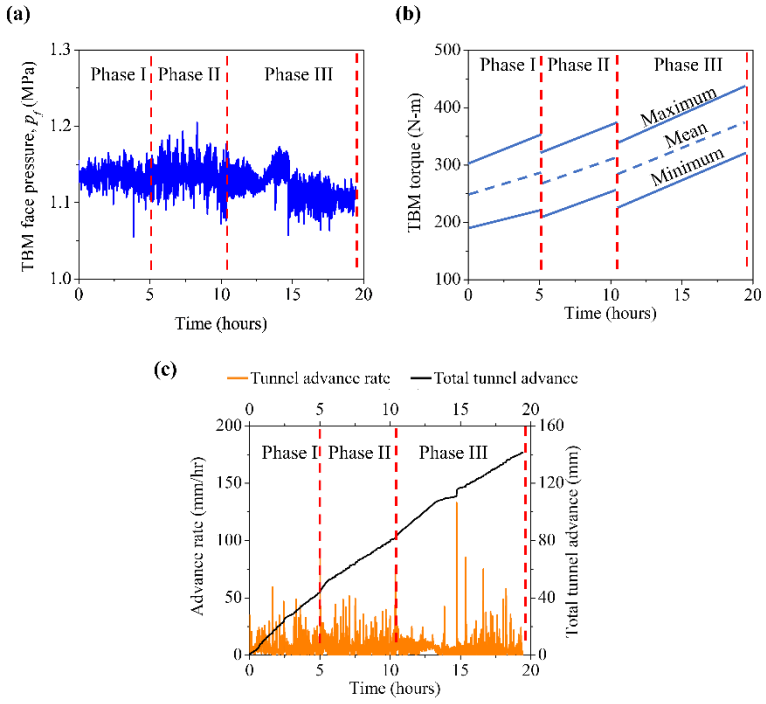

Figure 6-4 Monitoring of miniature TBM parameters during the excavation stage: (a) face pressure (thrust), (b) TBM torque and (c) TBM advancement and the advance rate.

This section discusses the change in the LDP of the supported tunnel over the time during the five loading stages shown in Figure 6-3. Displacement u and the longitudinal distance from the tunnel face x_f were normalized with the radius of the tunnel R to present the results in the most common form. The ratio u/R (in %) is effectively the tunnel wall radial strain, and parameter $X = x_f/R$ is the normalized longitudinal distance from the tunnel face.

Figure 6-5 shows selected but representative LDP readings (u/R versus X plot) of the tunnel over the time for all five loading stages. Due to squeezing, the LDP of the tunnel was observed to shift upwards with time. Out of the five tunnel sections studied, the maximum and minimum upward shift of LDP with time were recorded at X = 4.5 and 0.9, respectively, throughout the test. The corresponding increases in u/R at X = 4.5 for loading stage I to V due to squeezing were 0.005%, 0.125%, 0.132%, 0.166% and 0.452%, respectively. However, the increases in u/R at X = 0.9 were relatively low and recorded as 0.001%, 0.038%, 0.055%, 0.074% and 0.091% during loading stage I to V, respectively.

6.6 A Time-Dependent LDP

The most widely used LDPs for unsupported tunnels were proposed by Panet (1995), and Vlachopoulos and Diederichs (2009). In squeezing ground conditions, due to the time-dependent behavior of the rock, the stresses on the tunnel support increase with time. The complications reported in the literature regarding the application of CCM in squeezing ground were discussed earlier in this Chapter. However, the study presented here deals with the direct monitoring of the tunnel support response in squeezing ground condition subjected to different in-situ stress levels. Hence, a time-dependent LDP of the supported tunnel can simplify the study of the behavior of tunnel support in squeezing ground conditions.

Figures 6-6 (a-e) depict the changes in the tangential strain as a function of the loading stage time t for the five loading stages for five equally spaced longitudinal tunnel sections ranging from X = 0.9 to 4.5. As can be seen, for any tunnel section and during any loading stage, the correlation between the tunnel strain u/R in % and time t in hours could be expressed as an asymptotic model, given by the following equation:

$$\frac{u}{R}(t) = a_s - b_s(d_s)^t \qquad (6\text{-}1)$$

where a_s, b_s and d_s are the model parameters, determined from the best fitting curve having the maximum coefficient of determination with the experimental data. The best fit values of the model parameters a_s, b_s and d_s for all the plots along with the coefficient of determination are given in Table 6-1. According to Eq. (6-1), the parameter a (for $d_s < 1$) also can be defined for any tunnel section as the tunnel strain at infinite time,

$$\frac{u}{R}(t = \infty) = a_s \qquad (6\text{-}2)$$

Also, according to Eq. (6-1), the difference between parameters a_s and b_s is the tunnel strain at the beginning of any loading stage (t = 0),

$$\frac{u}{R}(t = 0) = a_s - b_s \qquad (6\text{-}3)$$

Parameter d_s governs the time-dependent response of the supported tunnel and from the test observations, it was found constant (d_s=0.98). As given in Table 6-1, the parameters a_s increased with an increase in X as well as p_o/σ_c. It can also be observed in Table 6-1 that parameter b_s increased with an increase in p_o/σ_c but shows weak correlation with X.

6.6.1 Effect of support system on the LDP

In addition to the influence of p_o/σ_c and X, the LDP is also influenced by the presence of the support system. This influence can be explored by comparing the LDP of supported tunnel, presented in this chapter, and the unsupported tunnels, presented in Chapter 5. The support system influences the instantaneous as well as long-term convergence of the tunnel.

The change in u/R in percentage at t = 0 due to support installation, calculated using Eq. 6-3, is given in the following equation

$$\Delta\left(\frac{u}{R}\right)_{instant} = \left(\frac{(a-b)-(a_s-b_s)}{(a-b)}\right) \text{x}100\% \qquad (6\text{-}4)$$

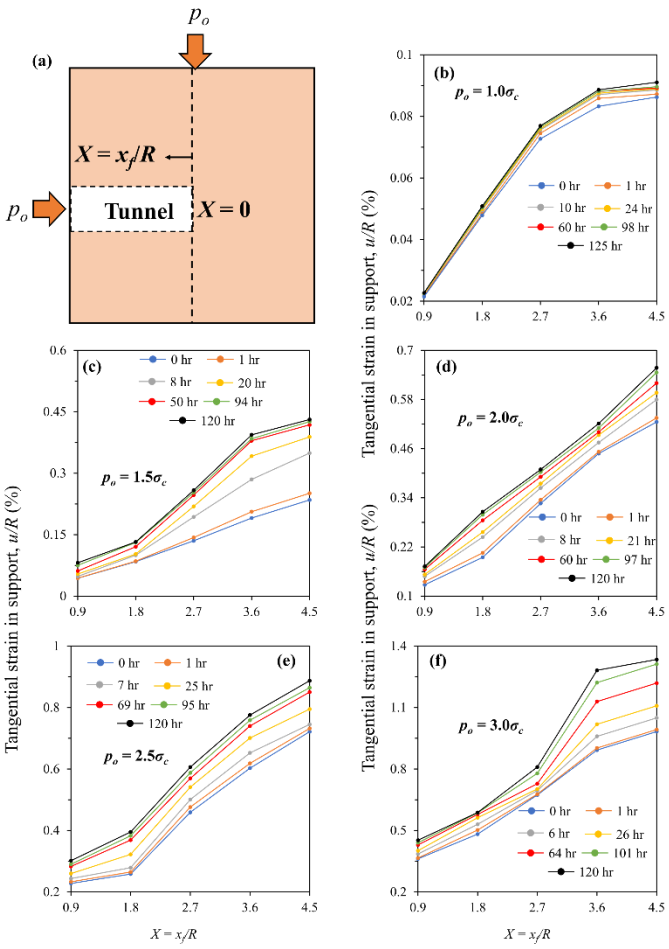

Figure 6-5 (a) Longitudinal tunnel excavated in isotropic stress state, and longitudinal displacement profiles (LDP) of the tunnel at the different times for the loading stage: (b) I, (c) II, (d) III, (e) IV and (f) V.

Similarly, the percentage change in u/R at infinite time due to support installation, calculated using Eq. 6-2, is given in the following equation

$$\Delta\left(\frac{u}{R}\right)_{ultimate} = \left(\frac{a-a_s}{a}\right) \text{x}100 \qquad (6\text{-}5)$$

The parameters a, b and d for the unsupported tunnel for different loading stages are provided in Table 6-1 and discussed in Chapter 5. Parameters in Table 6-1 were used to calculate $\Delta(u/R)_{\text{instant}}$ and $\Delta(u/R)_{\text{ultimate}}$. It was observed the installed tunnel support reduced both the instantaneous and ultimate tunnel convergence by 96-98% for all the cross-sections and loading conditions.

Table 6-1 LDP model parameters for supported and unsupported tunnel.

p_o/σ_c	$X = x_f/R$	Supported tunnel $(u/R = a_s - b_s(d_s)^t)$				Unsupported tunnel*		
		a_s	b_s (x 10^{-3})	d_s	Coefficient of determination	a	b	d
1.0	0.90	0.02	0.85	0.76	0.87	2.43	1.22	0.98
	1.80	0.05	2.21	0.87	0.96	2.92		
	2.70	0.08	3.02	0.66	0.89	3.41		
	3.60	0.09	4.10	0.50	0.88	3.90		
	4.50	0.09	2.68	0.85	0.88	4.39		
1.5	0.90	0.13	82.96	0.99	0.99	5.45	2.65	
	1.80	0.13	49.49	0.98	0.99	5.95		
	2.70	0.25	112.78	0.94	0.98	6.46		
	3.60	0.39	86.37	0.94	0.99	6.97		
	4.50	0.42	180.89	0.92	0.98	7.48		
2.0	0.90	0.17	34.51	0.96	0.95	11.65	4.59	
	1.80	0.30	86.70	0.95	0.94	12.22		
	2.70	0.40	64.07	0.95	0.94	12.80		
	3.60	0.51	56.85	0.93	0.94	13.37		
	4.50	0.64	102.31	0.95	0.93	13.94		
2.5	0.90	0.31	76.97	0.98	0.99	20.65	7.04	
	1.80	0.41	149.99	0.98	0.99	21.30		
	2.70	0.61	131.83	0.98	0.97	21.94		
	3.60	0.77	156.29	0.97	0.98	22.59		
	4.50	0.92	187.74	0.99	0.99	23.24		
3.0	0.90	0.46	92.09	0.98	0.99	32.76	9.98	
	1.80	0.58	84.65	0.94	0.96	33.51		
	2.70	0.93	251.48	0.98	0.92	34.27		
	3.60	1.31	401.45	0.99	0.95	35.02		
	4.50	1.36	366.36	0.98	0.96	35.78		

* The value presented in the Table are extracted from the LDP model for the unsupported tunnel proposed in Chapter 5

6.6.2 Load applied to the support system

It was observed throughout the experiment that the tunnel support strains increased with time due to squeezing ground. The support system given its modulus and dimensions did not reach the yielding stage and remained linear elastic throughout the test. Hence, it can be stated that the stresses on the tunnel support also increased linearly with the increase in measured strains. These stresses can be calculated from the analytical solution of the tunnel support system given by Schwartz & Einstein (1980), which considers that the tunnel boundary transfers bending and thrust forces to the tunnel support. The convergence of the tunnel support is a combined effect of the bending and thrust given by the following equations for the full slip condition (no shear stress) between the rock and support, and tunnel excavated in an isotropic stress state:

$$\frac{T}{PR} = (1 - a_o^*) \tag{6-6}$$

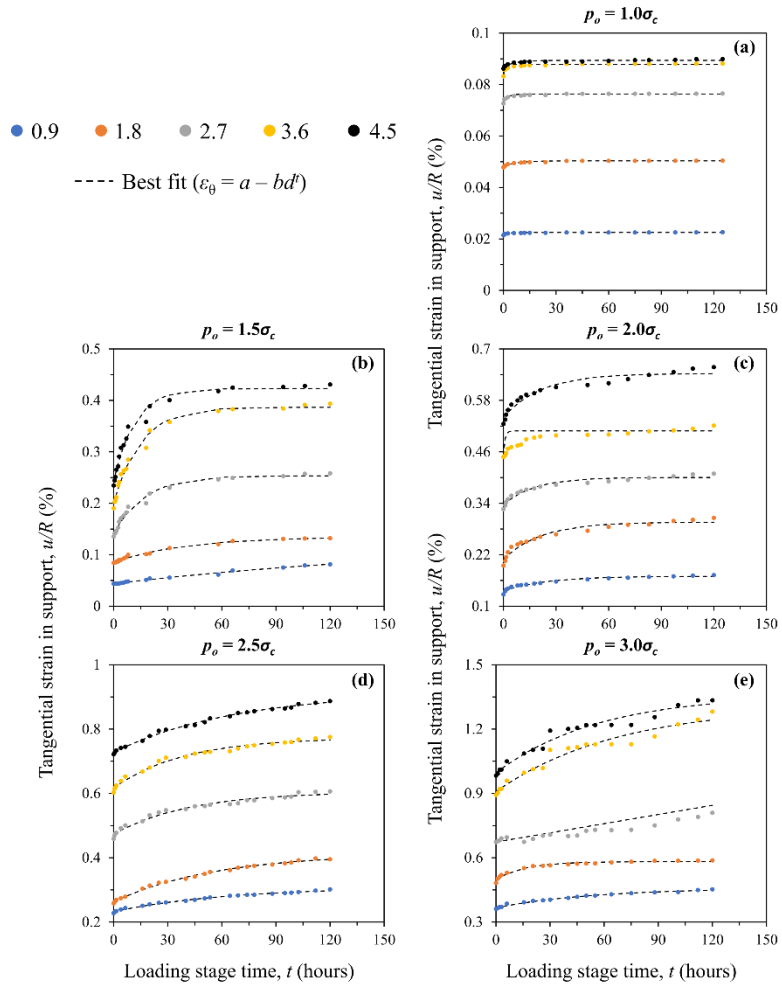

Figure 6-6 Tunnel strain u/R (in %) with loading stage time t for X varying from 0.9 to 4.5 for Loading Stage: (a) I, (b) II, (c) III, (d) IV and (e) V.

$$\frac{M}{PR^2} = 0 \tag{6-7}$$

$$\frac{u}{R} = P\left(\frac{1+\nu_g}{E_g}\right) a_o^* \tag{6-8}$$

where P is the ground stress that is acting on the support, T is the thrust force on the support, and M is the bending moment on the support and is zero in isotropic stress conditions (Schwartz & Einstein, 1980). Eg and ν_g are Young's modulus and Poisson's ratio of the rock. The parameter a_o^* is the function of compressibility ratio C^* and flexibility ratio F^* of the rock and support given by the following equations

$$a_o^* = \frac{C^* F^* (1-\nu_g)}{C^* + F^* + C^* F^* (1-\nu_g)} \tag{6-9}$$

$$C^* = \frac{E_g R(1-\nu_s^2)}{E_s A_s(1-\nu_g^2)} \quad (6\text{-}10)$$

$$F^* = \frac{E_g R^2(1-\nu_s^2)}{E_s I_s(1-\nu_g^2)} \quad (6\text{-}11)$$

$$I_s = \frac{t_s^3}{12} \quad (6\text{-}12)$$

$$A_s = t_s \quad (6\text{-}13)$$

where E_s and ν_s are Young's modulus and Poisson's ratio of the support. I_s and A_s are the moment of inertia per unit length of the support cross-section about its centerline, and area of the support per unit length experiencing the thrust and moment, respectively.

Combing Eq. 6-6 and 6-8 to calculate T for a given u in the following equation

$$T = \frac{uE_g}{(1+\nu_g)a_o^*}(1 - a_o^*) \quad (6\text{-}14)$$

Using Eq. 6-14, thrust forces T at the start and end of each loading cycle are presented in Table 6-2. As seen, except during the Loading Stage I, the thrust on the support increased significantly during Loading Stage II to V. This additional increase in T with time is the result of the additional squeezing of the rock.

Table 6-2 Thrust in the tunnel support at the beginning and end of different loading stages

$X = x_f/R$	Thrust on support, T (kN/m)									
	Stage I ($p_o = 1.0\sigma_c$)		Stage II ($p_o = 1.5\sigma_c$)		Stage III ($p_o = 2.0\sigma_c$)		Stage IV ($p_o = 2.5\sigma_c$)		Stage V ($p_o = 3.0\sigma_c$)	
	Begin	End	Begin	End	Begin	End	Begin	End	Begin	End
0.9	28	29	57	106	166	224	296	391	469	587
1.8	62	66	109	172	253	397	335	513	626	762
2.7	94	100	175	335	424	531	596	787	874	1051
3.6	108	115	247	511	581	676	782	1006	1158	1663
4.5	112	118	305	559	682	853	936	1151	1275	1732

6.7 Discussions

The parameters (a_s, b_s and d_s) of the LDP determined from this model study depend on the rock elastic properties, support elastic properties and its geometry. However, exploring the individual effect of involved parameters requires numerous tests which may not be feasible. One feasible approach to account for the rock and support system variations is to utilize the compressibility ratio C^* and flexibility ratio F^* concept, given in Eq. 6-10 and 6-11, respectively.

The support system used in this model study reduced the time-dependent convergence of the tunnel by 96% compared to the unsupported tunnel. The C^* and F^* for the conducted test determined from Eq. 6-10 and 6-11 are 1.18×10^{-4} and 0.24, respectively. For unsupported tunnels, C^* and F^* both approach infinity. To optimize the support requirements, additional tests should be conducted on supported tunnels with different C^* and F^*. The tests will provide a correlation between C^* and F^*, and reduction in the convergence of the tunnel.

6.8 Conclusions

The work presented in this chapter involved a physical model test to observe supported tunnel closure over time in squeezing ground conditions. The physical model simulated TBM excavation in a tunnel as it advanced and time-dependent strains developed due to rock-support interaction after the excavation were monitored. Analysis of the data from the strain gauges on the liner provided a quantitative assessment of the LDP of the supported tunnel at different times and stress levels.

Based on the experimental observations, a model was proposed to express the LDP of the tunnel as a function of time. The LDP parameters were found to be a function of the ratio of the isotropic stress applied to the unconfined compressive strength of the rock specimen as well as the normalized distance from the tunnel face. The LDP parameters of supported and unsupported tunnel were compared to account for the influence of the support system. The back-calculation of thrust forces on the support system provided an estimate of the additional thrust forces in the support due to squeezing. Additional work is needed to explore the effects of different rock properties, compressibility ratio, flexibility ratios and the long-term behavior of the squeezing tunnels.

CHAPTER 7 - CONCLUSIONS, CONTRIBUTIONS AND FUTURE WORK

The focus of this report was improving the understanding of tunnels constructed in squeezing clay-rich rocks through laboratory-scaled physical model tests. All the practices in the current literature for tunnels in squeezing ground conditions were critically studied to determine the known critical factors that contribute to squeezing. An experimental setup was designed to conduct physical model tests at field stress levels for tunnels in squeezing ground.

The motivation to develop a laboratory-scale physical model was the inconsistent information and results in past practices and studies. Most of the methodologies in the literature are empirical and case-specific due to limited field monitoring. As there is no widely applicable criterion, geotechnical engineers often have to design the support systems for tunnels constructed under squeezing conditions while making assumptions for the ground behavior. Like non-squeezing tunnels, a rational design approach for squeezing tunnels would be to correlate the prior knowledge with the current observations. However, due to high ground deformations and excessive squeezing pressure, squeezing ground poses hazardous conditions for the installation of monitoring systems; and, if a system is installed, it could fail before providing quality data. Hence, in this report, a physical model test was considered a viable option for the analysis of these tunnels. The physical model test simulated TBM excavation in squeezing ground and monitored 3-D deformations during and after the excavations stage. The approach to meet the objectives, tasks carried out and the corresponding significant outcomes are summarized in Table 7-1.

7.1 Major Conclusions

Based on the results obtained from the case studies and experiments, the major conclusions of this report are presented in the following subsections.

7.1.1 Squeezing number

- A methodology based on the SHANSEP model, Peck's stability number, and Hoek–Brown's GSI to calculate a critical effective stress $\sigma'_{\text{critical}}$ profile for tunnels constructed in clay-rich rocks is proposed. If $\sigma'_{\text{critical}}$ is less than major effective principal stress σ' at the tunnel location, the tunneling is in squeezing ground conditions. Based on the ratio of σ' and $\sigma'_{\text{critical}}$, a squeezing number S is proposed to predict the level of squeezing for tunnels in clays and cemented clays.
- It was observed that if *S* was less than 1, the tunnel experienced no to very light squeezing and the tunnel strain was less than 1%. If *S* was between 1 and 2, then the tunnel experienced light squeezing, and the ultimate tunnel strain was between 1.5% and 2%. If *S* was between 2 and 7, then the tunnel experienced fair to moderate squeezing and the tunnel strain was 2.5% to 5%. Any value of *S* between 7 and 17 corresponded to high to very high squeezing conditions, and the tunnel strain was 5% to 10%. Values of S higher than 17 indicated very high squeezing, and the tunnel strain was expected to be more than 10%.
- The proposed methodology demonstrated very good agreement with the existing field data and proved efficient in the quick assessment of squeezing ground conditions with 82% accuracy.

Table 7-1 Summary of the approach, tasks and outcomes to meet the report objectives.

Report objectives	Approach	Tasks	Outcome
Objective 1	Carry out case studies to identify the major causes of squeezing in tunnels excavated in clay-rich rocks.		
	Literature review	Case study of tunnels and methodologies	Squeezing number *S*
Objective 2	Design and fabricate an experimental setup that is capable of simulating tunnel squeezing in cubical rock specimens subjected to true-triaxial stress state at a laboratory scale.		
	Machine design	Design and fabrication of miniature TBM and monitoring system	A physical model test setup to simulate tunneling
Objective 3	Develop a synthetic rock material for laboratory model study with mechanical behavior comparable to naturally occurring squeezing mudstone and characterize the behavior of the material.		
	Experimental	Preparation of mudstone from clay, cement and water	Synthetic mudstone specimen
Objective 4	Perform a series of laboratory-scale physical simulation of tunnel squeezing under different conditions based on data from the tunnels experienced squeezing.		
	Experimental	Model test of the lined and unlined tunnel at different confining stresses	Tunnel wall and support convergence with time
Objective 5	Analyze and synthesize model test results to develop an improved and reliable procedure to predict tunnel squeezing.		
	Data analysis	Critical analysis of the test observations	A time-dependent LDP for tunnels in squeezing ground

7.1.2 Experimental setup

- The physical model that was designed and fabricated to simulate the effects of full-scale TBM excavation in squeezing ground conditions was shown to simulate well the excavation of tunnels in squeezing ground conditions.

- The monitoring method proved to be adequate for providing an estimate of the damage and deformation that occurs around a tunnel along with important TBM parameters, such as thrust, rotational speed, and torque with tunnel advance. The torque required to drive the TBM cutter head at constant rotational speed was found to increase as the tunnel wall convergence increased, providing a qualitative estimate of squeezing.
- The AE sensors and embedded strain gauges (MPBEx) were used to monitor damages and deformations, respectively around the excavation. The methodology adopted to embed the strain gauge was validated in an unconfined compression test and the strain obtained showed good agreement with the expected strain.
- The damage monitoring conducted using AE sensors indicated that the damages around the tunnel boundary increased with time. The high magnitude of non-recoverable tunnel convergence (u/R = 1.45 %) further quantified the amount of squeezing the tunnel experienced over the studied period.
- The physical model proved to be quite capable of capturing the time-dependent behavior of rocks around a tunnel boundary during the excavation stage and for a long time thereafter.

7.1.3 Synthetic mudstone

- The stress-strain behavior, dilatancy, ductility and shear strength parameters of the synthetic mudstone were determined from the unconfined compressive tests and undrained triaxial tests.
- The results of the creep tests determined that the material showed significant deformation with time, which was explained by Burger's constitutive model for viscoelastic materials.
- Based on a qualitative comparison of the engineering behavior with actual squeezing clay-rich rocks, it was concluded that the proposed material could be used for laboratory model studies pertaining to squeezing in clay-rich rocks.

7.1.4 Time-dependent tunnel convergence

Unsupported tunnels

- The tunnel closure over time in the presence of squeezing ground conditions was monitored during the tests. Analysis of the data using embedded strain gauges provided an estimate of the amount of squeezing at different radial and longitudinal distances with time around the excavated tunnel boundary. The digital borehole caliper provided a quantitative assessment of the LDP of the tunnel at different times and stress levels.
- Based on the experimental observations, a model based on regression analysis was proposed to express the LDP of the tunnel as a function of time. The parameters of the LDP were found to be a function of the ratio of the isotropic stress applied and the unconfined compressive strength of the rock specimen and normalized distance from the tunnel face.

Supported tunnels

- A physical model and test to observe supported tunnel closure over time in squeezing ground conditions was conducted. The physical model simulated the TBM excavation in a tunnel as it advanced and the time-dependent strains that developed due to rock-support interaction after the excavation. Analysis of the data from the strain gauges on the liner

provided a quantitative assessment of the LDP of the supported tunnel at different times and stress levels.

- Based on the experimental observations, a model was proposed to express the LDP of the tunnel as a function of time. The LDP parameters of the supported and unsupported tunnel were then compared to account for the convergence due to squeezing countered by the support system. The back-calculation of thrust forces on the support system provided an estimate of the additional stresses due to squeezing.
- An approach based on compressibility and the flexibility ratio of the rock and support system was proposed for the support design consideration in squeezing ground conditions.

7.2 Major Contributions

The specific scientific contributions of this report to advance the state of knowledge associated with the tunnels in squeezing ground can be summarized in detail as follows:

- The detailed review of the existing methodologies established that two common contributing factors to the large convergence of the tunnel due to squeezing are clay minerals and ground's incompetency in response to excavation.
- It was determined that the Squeezing number *S* could be employed for preliminary estimation of the squeezing zones along the tunnel alignment. Further, the value of *S* provides a fair estimate of the magnitude of convergence tunnel will experience.
- A physical model setup was proposed that simulates tunneling features such as TBM excavation, tunnel advance, 3-D effects, and time-dependent behavior at field stress level. In addition to squeezing, the setup can be easily modified to study other tunnel problems such as rockburst, spalling, etc.
- The laboratory study of the synthetic mudstone confirmed the similarity in engineering behavior with its prototype. It is quite clear that the natural mudstone specimen, which is difficult to obtain, can be replaced by synthetic mudstone for any laboratory study concerned with engineering behavior.
- Tunnel construction in squeezing ground generally rely on the empirical methods. The proposed time-dependent longitudinal displacement profile (LDP) will provide a rational approach to the designer and engineers for the tunnel construction in squeezing ground.
- It was established the rock-support interaction with time aids the tunnel designers in the selection of the efficient and economic support system for tunnels constructed in squeezing ground conditions.

7.3 Recommendations for Future Research

The aim of this report was to advance the knowledge related to tunnels in squeezing ground conditions using a novel physical model test. As additional queries always accompany new findings, there are various ways to advance the research pursued in this report, which could include the following.

- Determine the critical stress and squeezing number profile for a tunnel to be constructed in clay-rich rocks and then correlate these values with the field observations during the excavation. This will expand the database used for the development of the criteria while testing its performance.

- The contribution to squeezing by different clay minerals (smectite, kaolin, etc.) should be studied experimentally to identify the most critical mineral for better prediction of squeezing ground conditions.
- Introduce additional advanced monitoring methods in the physical model test for the better quantification of the damages and deformations in the test specimen such as embedded fiber optics, ultrasonic methods, improved multi-channel AE system etc. This will improve the capabilities for detection of excavation induced damage with time around the tunnel boundary and in front of the tunnel face.
- Conduct the same physical model tests on actual clay-rich rock specimens from the field and compare those observations with that of the synthetic rock.
- Study the effect of anisotropic loading on tunnels constructed in squeezing ground conditions using the physical model tests.
- Calibrate the proposed LDP against different rock properties and the long-term behavior of the squeezing tunnels, particularly using field case histories. The proposed physical model test involves similar rock and the stresses corresponding to field. The only scale difference between the model tunnel and prototype is in terms of geometry of the excavation. This can be nullified by normalizing the model and prototype deformations with their respective radius of excavation.
- Expand the knowledge of rock-support interaction by studying the change in long-term behavior of the tunnel support with any alteration in compressibility and flexibility ratios. The study will facilitate in safe and economical support design for the tunnel constructed in squeezing ground conditions.
- The time dependent behavior of tunnel is a multi-physics phenomenon, influenced by several factors such as creep, damage and consolidation. The influence of individual factors will need to be systematically explored to determine their contributions to the time dependent behavior of the tunnel.

REFERENCES

Adachi, T., Tamura, T., Kimura, K. & Nishimura, T. (1995). Axial symmetric trap door tests on sand and cohesion soil. *In Proceedings of the 30th Japan National Conference on Geotechnical Engineering*, 1973-1976.

Alejano, L.R., Rodríguez-Dono, A., Alonso, E. & Fdez-Manín, G. (2009). Ground reaction curves for tunnels excavated in different quality rock masses showing several types of post-failure behavior. *Tunneling and Underground Space Technology 24(6)*, 689–705.

Arora, K., Gutierrez, M. & Hedayat, A. (2019a). Experimental setup for studying tunnels in squeezing ground conditions. *In Tunnels and Underground Cities. Engineering and Innovation Meet Archaeology, Architecture and Art: Naples, Italy, CRC Press*, 3515-3524.

Arora, K., Gutierrez, M. & Hedayat, A. (2019b). Miniature Tunnel Boring Machine for Simulating Tunnel Excavation in Squeezing Ground Conditions. *In 4th International Conference on Tunnel Boring Machine in Difficult Ground: Denver, Colorado*, 183-192.

Arora, K., Gutierrez, M. & Hedayat, A. (2020a). Physical Modeling of Lined Tunnel in Squeezing Ground Conditions. *In Geo-Congress 2020: Engineering, Monitoring, and Management of Geotechnical Infrastructure Reston, VA: American Society of Civil Engineers*, 335-344.

Arora, K., Gutierrez, M. & Hedayat, A. (2020b). *Characterization of Synthetic Mudstone for Physical Model Studies*. In 54th US Rock Mechanics/Geomechanics Symposium. American Rock Mechanics Association, Accepted.

Arora, K., Gutierrez, M., Hedayat, A. & Xia, C. (2020c). Tunnels in Squeezing Clay-Rich Rocks. *Underground space*, Accepted.

Atkinson, J.H., Brown, E.T. & Potts, M. (1975). Collapse of shallow unlined tunnels in dense sand. *Tunnels and Tunneling, 7(3)*, 81-87.

Attwell, P.B. (1978). Ground movements caused by tunneling in soil. *Proceedings of the Large Ground Movements and Structures Conference*: 812–948. Cardiff, Pentish Press, London.

Aydan, Ö., Akagi, T. & Kawamoto, T. (1996). The squeezing potential of rock around tunnels: theory and prediction with examples taken from Japan. *Rock Mechanics and Rock Engineering, 29(3)*, 125-143.

Barla, G. (1995). Squeezing rocks in tunnels. *International Society of Rock Mechanics News Journal, 2(3)*, 44-49.

Barla, G. (1995). Squeezing rocks in tunnels. *ISRM News Journal, 2(3)*, 44-49.

Barla, G. (2000). Tunnelling under squeezing rock conditions. *Department of structural and geotechnical engineering*, Politecnico.

Barla, G. (2001). Tunnelling under squeezing rock conditions, Chap 3. *In: Kolymbas D (ed). Tunnelling mechanics-advances in geotechnical engineering and tunnelling. Euro-summer-School in Tunnel Mechanics, Innsbruck. Logos Verlag Berlin*, 169–268.

Barla, G. (2001). Tunnelling under squeezing rock conditions. *Eurosummer-school in tunnel mechanics: Innsbruck*, 169-268.

Barla, G., Debernardi, D. & Sterpi, D. (2012) Time-dependent modeling of tunnels in squeezing conditions. *International Journal of Geomechanics, 12(6)*, 697-710.

Barla, G., Debernardi, D., & Sterpi, D. (2011). Time-dependent modeling of tunnels in squeezing conditions. *International Journal of Geomechanics, 12(6)*, 697–710.

Barton, N. & Grimstad, E. (1995). The Q-system following twenty years of application in NMT support selection. *International Journal of Rock Mechanics and Mining Sciences and Geomechanics Abstracts*, 5(32), 232-239.

Barton, N., Lien, R. & Lunde, J. (1974). Engineering classification of rock masses for the design of tunnel support. *Rock mechanics*, *6(4)*: 189-236.

Barton, N., Lien, R. & Lunde, J. (1974). Engineering classification of rock masses for the design of tunnel support. *Rock Mechanics*, 6(4), 189–236.

Bhasin, R. (1991). Evaluation of soft rock conditions in tunnels through the Lower Himalayan regions; A Contribution for updating of the Q-system. *MSc Thesis*, University of Oslo, 45-64.

Bieniawski, Z.T. (1989). Engineering rock mass classifications: a complete manual for engineers and geologists in mining, civil, and petroleum engineering. *John Wiley & Sons*, 48–66.

Bilgin, N. & Algan, M. (2012). The performance of a TBM in a squeezing ground at Uluabat, Turkey. *Tunnelling and Underground Space Technology, 32*, 58-65.

Bo, M.W., Choa, V. & Hong, K.H. (2003). Material characterization of Singapore Marine Clayat Changi. *Quarterly Journal of Engineering Geology and Hydrogeology*, 36(4), 305–319.

Bonini, M., & Barla, G. (2012). The Saint Martin La Porte access adit (Lyon–Turin Base Tunnel) revisited. *Tunnelling and Underground Space Technology*, *30*, 38-54.

Bonini, M., Debernardi, D., Barla, M. & Barla, G. (2009). The mechanical behaviour of clay shales and implications on the design of tunnels. *Rock Mechanics and Rock Engineering, 42(2),* 361-388.

Broms, B.B. Bennermark, H. (1967). Stability of clay at vertical openings. *Journal of Soil Mechanics & Foundations Division, 93*, 71–94.

Brown, E.T., Bray, J.W., Ladanyi, B. & Hoek, E. (1983). Ground response curves for rock tunnels. *ASCE Journal of Geotechnical Engineering 109 (1)*, 15–39.

Cai, Y., Jiang, Y., Djamaluddin, I., Iura, T. & Esaki, T. (2015). An analytical model considering interaction behavior of grouted rock bolts for convergence–confinement method in tunneling design. International Journal of Rock Mechanics and Minning Sciences 76, 112–126.

Cao, C., Shi, C., Lei, M., Yang, W. & Liu, J. (2018). Squeezing failure of tunnels: A case study. *Tunnelling and Underground Space Technology*, *77*, 188-203.

Carranza-Torres, C., Fairhurst, C. (2000) Application of the convergence–confinement method of tunnel design to rock masses that satisfy the Hoek–Brown failure criterion. *Tunneling and Underground Space Technology*, *15(2)*, 187–213.

Carter, B.J. (1992). Size and stress gradient effects on fracture around cavities. *Rock Mechanics and Rock Engineering*, *25(3)*, 167-186.

Chambon, P., Corte, J.F. & Garnier, J., (1991). Face stability of shallow tunnels in granular soils. *Proceedings of an International Conference on Centrifuge*, 99–105.

Chandler, R.J. (1969). The effect of weathering on the shear strength properties of Keuper Marl. *Geotechnique*, *19(3)*, 321-334.

Chian, S.C., Nguyen, S.T. & Phoon, K.K. (2015). Extended strength development model of cement-treated clay. *Journal of Geotechnical and Geoenvironmental Engineering*, 142(2) 060150141-7.

Corbetta, F., Bernaud, D. & Nguyen-Minh, D. (1991). Contribution a la methode convergence–confinement par le principle de la similitude. *Rev. Fr. Geotech. 54*, 5–11.

Cristescu N.D. & Hunsche, U. (1998). Time effects in rock mechanics. *Wiley, Chichester, U.K*, 45-67.

Cristescu, N.D. & Gioda, G. (1994). Visco-plastic behaviour of geomaterials. *Springer, Vienna, Austria*, 1-25.

Crossland, B., & Bones, J. A. (1955). The ultimate strength of thick-walled cylinders subjected to internal pressure. *Engineering*, 80–83 and 114–117.

Cui, L., Zheng, J.J., Zhang, R.J. & Lai, H.-Jiang. (2015). A numerical procedure for the fictitious support pressure in the application of the convergence–confinement method for circular tunnel design. *International Journal Rock Mechanics and Mining Sciences 78*, 336–349.

Czurda, K., Winder, C.G. & Quigley, R.M. (1973) Sedimentology, mineral facies, and petrofabric of the Meaford–Dundas Formation (Upper Ordovician) in southern Ontario. *Canadian Journal of Earth Sciences, 10(12)*, 1790-1804.

Dalgıç, S. (2002). Tunneling in squeezing rock, the Bolu tunnel, Anatolian Motorway, Turkey. *Engineering Geology*, 67(1-2): 73-96.

De Pater, C.J., Cleary, M.P., Quinn, T.S., Barr, D.T., Johnson, D.E. & Weijers, L. (1994). Experimental verification of dimensional analysis for hydraulic fracturing. *SPE Production & Facilities, 9(4),* 230-238.

Debernardi, D., & Barla, G. (2009). New viscoplastic model for design analysis of tunnels in squeezing conditions. *Rock mechanics and Rock Engineering*, *42(2)*, 259.

Deere, D.U., Peck, R.B., Parker, H.W., Monsees, J.E. & Schmidt B. (1970). Design of tunnel support systems. *In Highway Research Record, 339*, 26-33.

Dube, A.K. (1993). Squeezing under high stress conditions, assessment and prevention of failure phenomena in rock engineering. *In: Pasamehmetoglu AK et al (eds) Mine*, 751-757.

Duncan-Fama, M.E. (1993). Numerical modelling of yield zones in weak rocks. *Comprehensive Rock Engineering*, *2*, 49-75.

Dusseault, M.B. & Fordham, C.J. (1993). Time-dependent behavior of rocks. Comprehensive Rock Engineering Principles, Practice and Project. *In Rock Testing and Site Characterization*, *3*, 119-149.

Dwivedi R.D., Singh M., Viladkar M.N. & Goel R.K. (2013). Prediction of tunnel deformation in squeezing grounds. *Engineering Geology*, *161*:55–64.

Ebrahim, F. & Rostami, J. (2009). Effect of adverse geological condition on TBM operation in Ghomroud tunnel conveyance project. *Tunnelling and Underground Space Technology 24*, 436-446.

Ehrbar, H. (2008). Gotthard base tunnel, Switzerland. Experiences with different tunnelling methods. *In Proc. 2º Congresso Brasileiro de Túneis e Estruturas Subterrâneas, Sao Paulo*, 1-14.

Emori, R. I., Saito, K. & Sekimoto, K. (2008). Scale Models in Engineering (Mokei Jikken no Riron to Ohyou), (ISBN 4-7655-3252-6 C3053). *Tokyo, Japan: Gihodo. Second print in*.

Fabre, G. & Pellet, F. (2006). Creep and time-dependent damage in argillaceous rocks. *International Journal of Rock Mechanics and Mining Sciences, 43(6),* 950-960.

Farrokh, E. & Jamal, R. (2009). Effect of adverse geological condition on TBM operation in Ghomroud tunnel conveyance project. *Tunnelling and Underground Space Technology*, *24*, 436-446.

Fenner, R. (1938). Untersuchungen zur Erkenntis des Gebirgsdruckes bluckauf. *74*, 671–695 and 705-715.

Franklin, J.A. & Hoeck, E. (1970). Developments in triaxial testing techniques. *Rock Mechanics & Engineering Geology*, *4*, 223-228.

Frash, L.P., Gutierrez, M. & Hampton, J. (2014). True-triaxial apparatus for simulation of hydraulically fractured multi-borehole hot dry rock reservoirs. *International Journal of Rock Mechanics and Mining Sciences, 100(70)*, 496-506.

Frash, L.P., Gutierrez, M., Hampton, J. & Hood, J. (2015). Laboratory simulation of binary and triple well EGS in large granite blocks using AE events for drilling guidance. *Geothermics*, *55*:1-15.

Gallavresi, F. (1992). Grouting improvement of foundation soils. *In Grouting, soil improvement and geosynthetics ASCE*, *1*, 1-38.

Ghaboussi, J. & Gioda, G. (1977). On the time-dependent effects in advancing tunnels. *International Journal for Numerical and Analytical Methods in Geomechanics, 1(3)*, 249-269.

Ghaboussi, J., Ranken, R.E. & Hendron Jr., A.J. (1981). Time-dependent behavior of solution caverns in salt. *Journal of Geotechnical and Geoenvironmental Engineering, ASCE 16597 Proceeding, 107*: 43-69.

Gioda, G. & Cividini, A. (1996). Numerical methods for the analysis of tunnel performance in squeezing rocks. *Rock mechanics and rock engineering, 29(4)*, 171-193.

Gioda, G. & Cividini, A. (1996). Numerical methods for the analysis of tunnel performance in squeezing rocks. *Rock Mechanics and Rock Engineering, 29(4)*, 171–193.

Gioda, G. (1981). A finite element solution of non-linear creep problems in rocks. *International Journal of Rock Mechanics and Mining Sciences & Geomechanics Abstracts, Pergamon, 18(1)*: 35-46.

Gioda, G. (1982). On the non-linear 'squeezing'effects around circular tunnels. *International Journal for Numerical and Analytical Methods in Geomechanics, 6(1)*, 21-46.

Gioda, G. (1982). On the non-linear 'squeezing'effects around circular tunnels. International *Journal for Numerical and Analytical Methods in Geomechanics, 6(1)*, 21–46.

Goel R.K., Jethwa J.L. & Paithakan A.G. (1995). Tunneling through the young Himalayas a case history of the Maneri–Uttarkashi power tunnel. *Engineering Geology, 39(1–2)*,31–44.

Goodman, R.E. (1972). Geological investigations to evaluate stability, In: Geotechnical Practice for Stability in Open Pit Mining. *Proceedings of the Second International Conference on Stability in Open Pit Mining, Vancouver, Canada* 125-132.

Gschwandtner, G.G. & Galler, R. (2012). Input to the application of the convergence confinement method with time-dependent material behaviour of the support. *Tunnelling and Underground Space Technology*, *27*(1), 13-22.

Gutierrez, M. & Xia, C.C. (2009). Squeezing potential of tunnels in clays and clay shales from normalized undrained shear strength, unconfined compressive strength and seismic velocity. *Proc.*

6th Intl. Symp. Geotechnical Aspects of Underground Construction in Soft Ground (IS Shanghai 2008), Shanghai, China, April 10–12, 2008, Electronic Proceedings, 553-560.

Gutierrez, M., Vik, G. & Berre, T. (1996). Shale strength as function of stress history and diagenesis. *In ISRM International Symposium-EUROCK 96. International Society for Rock Mechanics, 96*, 69–76.

Hobbs, D.W. (1966). Scale model studies of strata movement around mine roadways. Apparatus, technique and some preliminary results. *International Journal of Rock Mechanics and Mining Sciences & Geomechanics Abstracts, 3 (2)*, 101-112.

Hoek, E. & Brown, E.T. (1997). Practical estimates of rock mass strength. *International Journal of Rock Mechanics and Mining Sciences, 34(8)*, 1165–1186.

Hoek, E. & Guevara, R. (2009). Overcoming squeezing in the Yacambú-Quibor tunnel, Venezuela. *Rock Mechanics and Rock Engineering, 42(2)*, 389-418.

Hoek, E. & Marinos, P. (2000). Predicting tunnel squeezing problems in weak heterogeneous rock masses. *Tunnels and Tunnelling International, 32(11)*, 45-51.

Hoek, E. (1971). Rock Engineering: Inaugural Lecture. *Imperial College of Science and Technology*, 1-56.

Hoek, E. (1998). Tunnel support in weak rock. *In Proc. Reg. Keynote address, Symposium of Sedimentary Rock Engineering, Taipei, Taiwan,* 20–22.

Hoek, E. (2001). Big tunnels in bad rock. *Journal of Geotechnical and Geoenvironmental Engineering, 127(9),* 726-740.

Hoek, E., Carranza-Torres, C. & Corkum, B. (2002). Hoek-Brown failure criterion-2002 edition. *Proceedings of NARMS-Tac, 1*, 267–273.

Horpibulsuk, S., Miura, N. & Nagaraj, T.S. (2005). Clay–water⁄ cement ratio identity for cement admixed soft clays. *Journal of Geotechnical and Geoenvironmental Engineering, 131(2),* 187-192.

Horpibulsuk, S., Rachan, R., Chinkulkijniwat, A., Raksachon, Y. & Suddeepong, A. (2010). Analysis of strength development in cement-stabilized silty clay from microstructural considerations. *Construction and building materials, 24(10)*, 2011-2021.

Indraratna, B., Jayanathan, M. & Brown, E.T. (2008). Shear strength model for overconsolidated clay-infilled idealised rock joints. *Géotechnique, 58(1)*, 55–65.

International Society for Rock Mechanics (ISRM) (1994). Comments and recommendations on design and analysis procedures for structures in argillaceous swelling rock. *International Journal of Rock Mechanics and Mining Sciences, 31(5)*,535–546.

Itasca Consulting Group (2013). FLAC3D: Fast Lagrangian Analysis of Continua in 3 Dimensions. *User's Guide. Minneapolis, MN: Itasca Consulting Group Inc*, 59-75.

Jaeger, J.C. & Cook, N.G. (1976). Fundamentals of Rock Mechanics. *Barnes and Noble: New York, Methuen, London,* 252-279.

Jeon, S., Kim, J., Seo, Y. & Hong, C. (2004). Effect of a fault and weak plane on the stability of a tunnel in rock—a scaled model test and numerical analysis. *International Journal of Rock Mechanics and Mining Sciences, 41*, 658-663.

Jethwa, J.L., Singh, B. & Singh, B. (1984). 28 Estimation of ultimate rock pressure for tunnel linings under squeezing rock conditions—a new approach. *In Design and Performance of Underground Excavations: ISRM Symposium—Cambridge, UK, Thomas Telford Publishing*, 231-238.

Johnston, I.W. & Choi, S. K. (1986). A synthetic soft rock for laboratory model studies. *Geotechnique*, *36(2)*, 251-263.

Kallhawy, F.H. (1974). Finite element modeling criteria for underground opening in rock. *International Journal of Rock Mechanics and Mining Sciences: Geomechanics Abstracts, 11*, 465-472.

Kamata, H., & Mashimo, H. (2003). Centrifuge model test of tunnel face reinforcement by bolting. *Tunnelling and Underground Space Technology, 18(2-3),* 205-212.

Katsuki, D. & Gutierrez, M. (2011). Viscoelastic damage model for asphalt concrete. *Acta Geotechnica, 6(4),* 231-241.

Khanlari, G., Meybodi R.G. & Mokhtari E. (2012). Engineering geological study of the second part of water supply Karaj to Tehran tunnel with emphasis on squeezing problems. *Engineering Geology, 145*, 9-17.

Kovári, K. & Staus, J. (1996). Basic considerations on tunnelling in squeezing ground. *Rock Mechanics and Rock Engineering, 29(4),* 203-210.

Kovari, K. (1998). Tunnelling in squeezing rock (Tunnelbau in druckhaftem Gebirge). *Tunnel*, *5*, 12–31.

Kwasniewski, M., Li, X. & Takahashi, M. (2012). True-triaxial testing of rocks. *CRC Press, 4*, 35-49.

Labasse, H. (1949). *Les pressions de terrains dans les mines de huiles*. *Revue Universelle des Mines, 5(3),* 78-88.

Ladanyi, B. (1974). Use of the long-term strength concept in the determination of ground pressure on tunnel linings. *In Proceedings, 3rd Congress of ISRM, National Academy of Sciences, 2*, 1150-1156.

Ladanyi, B. (1993). Time-dependent response of rock around tunnels. *In Analysis and Design Methods, Pergamon*, 77-112.

Ladd, C.C. & Foott, R. (1974). New design procedure for stability of soft clays. *Journal of Geotechnical Engineering Division, American Society of Civil Engineering, 100(4)*, 763–779.

Lajtai, E.Z. (1972). Effect of tensile stress gradient on brittle fracture initiation. *International Journal of Rock Mechanics and Mining Sciences & Geomechanics Abstracts*, 9(5), 569-578.

Lee, F. H., Lee, Y., Chew, S. H. & Yong, K. Y. (2005). Strength and modulus of marine clay-cement mixes. *Journal of geotechnical and geoenvironmental engineering, 131(2)*, 178-186.

Lee, Y.J. & Yoo, C.S. (2006). Behaviour of a bored tunnel adjacent to a line of loaded piles. *Tunnelling and Underground Space Technology, 21(3-4)*, 370-377.

Lin, P., Liu, H. & Zhou, W. (2015). Experimental study on failure behaviour of deep tunnels under high in-situ stresses. *Tunnelling and Underground Space Technology, 46*, 28-45.

Lin, P., Liu, H. & Zhou, W. (2015). Experimental study on failure behaviour of deep tunnels under high in-situ stresses. *Tunnelling and Underground Space Technology, 46*, 28-45.

Lo, K.Y., Cooke, B.H. & Dunbar, D.D. (1987). Design of buried structures in squeezing rock in Toronto, Canada. *Canadian Geotechnical Journal, 24(2)*, 232-241.

Lombardi, G. (1975). Qualche aspetto particolare della statica delle cavita sotterranee. *Rivista Italiana di Geotecnica 2*, 187–206.

Love, J.P. (1984). Model testing of geogrids in unpaved roads. *Doctoral dissertation, University of Oxford*, 45-53.

Lu, Y.T., Tan, T.S. & Phoon, K.K. (2012). Accelerated testing of cement treated Singapore marine clay cured under elevated temperature. *In GeoCongress 2012: State of the Art and Practice in Geotechnical Engineering*, 920-929.

Mair, R.J., Taylor, R.N. & Bracegirdle, A. (1993). Subsurface settlement profiIes above tunnels in clays. *Geotechnique, 43(2)*, 315–320.

Majumder, D., Viladkar, M.N. & Singh, M. (2017). A multiple-graph technique for preliminary assessment of ground conditions for tunneling. *International Journal of Rock Mechanics and Mining Sciences, 100*, 278-286.

Malan, D.F. (2002). Simulating the time-dependent behaviour of excavations in hard rock. *Rock Mechanics and Rock Engineering, 35(4)*, 225-254.

Manh, H.T., Sulem, J., Subrin, D. & Billaux, D. (2015). Anisotropic time-dependent modeling of tunnel excavation in squeezing ground. *Rock Mechanics and Rock Engineering, 48(6)*, 2301-2317.

Martin, C.D., Martino, J.B. & Dzik, E.J. (1994). Comparison of borehole breakouts from laboratory and field tests. *In Rock Mechanics in Petroleum Engineering*. Society of Petroleum Engineers, *1*, 183-190.

Meguid, M.A., Saada, O., Nunes, M.A. & Mattar, J. (2008). Physical modeling of tunnels in soft ground: a review. *Tunnelling and Underground Space Technology, 23(2),* 185-198.

Meng, Z.P. & Xian, X.M. (2013). Analysis of the mechanical property of mudstone/shale in paralic coal measures and its influence factors. *Journal of Coal Science and Engineering (China), 19(1),* 1-7.

Mercier-Langevin, F. & Hadjigeorgiou, J. (2011). Towards a better understanding of squeezing potential in hard rock mines. *Mining Technology, 120(1),* 36-44.

Mesri, G., Febres-Cordero, E., Shields, D. & Castro, A. (1981) Shear stress-strain-time behaviour of clays. *Geotechnique, 31(4),* 537-552.

Miura, N., Horpibulsuk, S. & Nagaraj, T.S. (2001). Engineering behavior of cement stabilized clay at high water content. *Soils and Foundations, 41(5),* 33-45.

Mogi, K. (2007). Experimental Rock Mechanics. *Tailor and Francis Group London, United Kingdom,* 361-364.

Moncarz, P.D. & Krawinkler, H. (1981). Theory and application of experimental model analysis in earthquake engineering. *California: Stanford University, 50,* 20-45.

Morton, J.D. & Provost, A.J. (1979). Stillwater Tunnel: A classroom in engineering geology. *In Proceedings Canadian Rock Mechanics Symposium Underground Rock Engineering, 22,* 80–89.

Naggar, H., Hinchberger, S.D. & Lo, K.Y. (2008). A closed-form solution for composite tunnel linings in a homogeneous infinite isotropic elastic medium. *Canadian Geotechnical Journal, 45(2),* 266-287.

Nomoto, T., Imamura, S., Hagiwara, T., Kusakabe, O. & Fujii, N. (1999). Shield tunnel construction in centrifuge. *Journal of geotechnical and geoenvironmental engineering, 125(4),* 289-300.

O'ReiIly, M.P. & New, B.M. (1982). Settlements above tunnels in the UK – their magnitude and prediction. *In Proceedings of Tunnelling'82, IMM, London,* 173-181.

O'Rourke T.D. (1984). Guidelines for tunnel lining design. American Society of Civil Engineering, *Cornell Univ., Ithaca, New York, NY, 10,* 1–98.

Ortlepp, W.D. & Stacey, T.R. (1994). Rockburst mechanisms in tunnels and shafts. *Tunnelling and Underground Space Technology, 9(1),* 59-65.

Pacher, F. (1964). Deformationsmessungen im Versuchsstollen als Mittel zur Erforschung des Gebirgsverhaltens und zur Bemessung des Ausbaues. *In Grundfragen auf dem Gebiete der Geomechanik/Principles in the Field of Geomechanics, Springer, Berlin, Heidelberg*, 149–161.

Pan, Y.W. & Dong, J.J. (1991). Time-dependent tunnel convergence-II. Advance rate and tunnel-support interaction. *International Journal of Rock Mechanics and Mining Sciences, 28(6)*, 477-488.

Panet, M. (1993). Understanding deformations in tunnels. *Comprehensive rock engineering, 1*, 663-690.

Panet, M. (1995). Calcul des Tunnels par la Me'thode de Convergence–Confinement. *Presses de l'Ecole Nationale des Ponts et Chausse'es, Paris, 178*, 11-19.

Panet, M. (1996). Two case histories of tunnels through squeezing rocks. *Rock mechanics and rock engineering*, *29(3)*, 155-164.

Paraskevopoulou, C. & Benardos, A. (2013). Assessing the construction cost of Greek transportation tunnel projects. *Tunnelling and underground space technology*, *38*, 497-505.

Paraskevopoulou, C. & Diederichs, M. (2018). Analysis of time-dependent deformation in tunnels using the Convergence-Confinement Method. *Tunnelling and Underground Space Technology*, *71*, 62-80.

Parcher, F. (1964). Deformationsmessung in Versuchstollen als Mittel zur Erforeschung des Gebirgsverhaltens und zur Bemmessung des Ausbaues. *Felsmechanik und Ingenieurgeologie Supplementun, 4*, 149–161.

Park, S.H., Adachi, T., Kimura, M. & Kishida, K. (1999). Trap door test using aluminum blocks. *In Proceedings of the 29th Symposium of Rock Mechanics, JSCE*, 106-111.

Park, S.H., Adachi, T., Kimura, M. & Kishida, K. (1999). Trap door test using aluminum blocks. *In Proceedings of the 29th Symposium of Rock Mechanics, J.S.C.E.*, 106-111.

Peck, R.B. (1969). Deep excavations and tunneling in soft ground. *In Proceedings 7th International Conference SMFE, State of the Art*, 225–290.

Peila, D. & Oreste, P.P. (1995). Axisymmetric analysis on ground reinforcing in tunnelling design. *Computer and Geotechnics, 17*, 253–274.

Pellet, F., Hajdu, A., Deleruyelle, F. & Besnus, F. (2005). A viscoplastic model including anisotropic damage for the time dependent behaviour of rock. *International journal for numerical and analytical methods in geomechanics, 29(9)*, 941-970.

Phien-wej, N. & Cording, E.J. (1991). Sheared shale response to deep TBM excavation. *Engineering geology*, *30(3-4*), 371-391.

Phien-wej, N., Thakur, P.K. & Cording, E.J. (2007). Time-dependent response of tunnels considering creep effect. *International Journal of Geomechanics, 7(4)*, 296-306.

Potter, P.E., Maynard, J.B. & Depetris, P.J. (2005). Mud and mudstones: Introduction and overview. *Springer Science & Business Media*, 1-4.

Prassetyo, S.H. & Gutierrez, M. (2018). Effect of transient coupled hydro-mechanical response on the longitudinal displacement profile of deep tunnels in saturated ground. *Tunnelling and Underground Space Technology, 75*, 11-20.

Rettighieri, M., Triclot, J., Mathieu, E., Barla, G. & Panet, M. (2008). Difficulties associated with high convergences during excavation of the Saint Martin La Porte access adit. *In Proc International Congress*, 395-404.

Robinsky, E.I. & Morton, J.D. (1973). Foundation investigation for CN Tower. *In Toronto: Preprints 26th Canadian Geotechnical Conference*, 237–245.

Rose, D. (1982). Revising Terzaghi's tunnel rock load coefficients. *In The 23rd US Symposium on Rock Mechanics (USRMS), American Rock Mechanics Association*, 953-960.

Saadeldin, R. & Siddiqua, S. (2013). Geotechnical characterization of a clay–cement mix. *Bulletin of Engineering Geology and the Environment, 72(3-4)*, 601-608.

Saari, K. (1982). Analysis of plastic deformation (squeezing) of layers intersecting tunnels and shafts in rock. *Doctoral dissertation, University of California, Berkeley*, 48-74.

Sakurai, S. (1997). Lessons learned from field measurements in tunnelling. *Tunnelling and Underground Space Technology, 12(4)*, 453-460.

Schmidt, B. (1974). Prediction of settlements due to tunneling in soil: three case histories. *In Proceedings of the Second Rapid Excavation and Tunneling Conference, San Francisco, USA, 2*, 1179-1199.

Schwartz, C.W. & Einstein, H.H. (1980). Improved Design of Tunnel Supports: Volume 1: Simplified Analysis for Ground-Structure Interaction in Tunneling (No. DOT-TSC-UMTA-80-27-I). *Urban Mass Transportation Administration, United States*, 9-326.

Semple, R.M., Hendron, A.J. & Mesri, G. (1973). Effect of time-dependent properties of altered rock on tunnel support requirements. *Dep of Transp, Fed Railroad Adm, Final Rep FRA-ORDD*, 74-30.

Seng, S. & Tanaka, H. (2011). Properties of cement-treated soils during initial curing stages. *Soils and foundations, 51(5)*, 775-784.

Shahriar, K., Mostafa S. & Jafar, K. H. (2008). Geotechnical risk assessment-based approach for rock TBM selection in difficult ground conditions. *Tunnelling and Underground Space Technology, 23*, 318-325.

Shamsoddin, S.M. & Maarefvand, P. (2014). Engineering geological study of NWCT Tunnel in Iran with emphasis on squeezing problems. *Indian Geotechnical Journal*, *44(3)*, 357–369.

Shang, Y., Xue, J., Wang, S., Yang, Z. & Yang, J. (2004). A case history of Tunnel Boring Machine jamming in an inter-layer shear zone at the Yellow River Diversion Project in China. *Engineering geology*, *71(3-4)*, 199-211.

Sharma, J.S., Bolton, M.D. & Boyle, R.E. (2001). A new technique for simulation of tunnel excavation in a centrifuge. *Geotechnical Testing Journal*, *24(4)*, 343-349.

Shrestha, P.K. & Panthi, K.K. (2015). Assessment of the effect of stress anisotropy on tunnel deformation in the Kaligandaki project in the Nepal Himalaya. *Bulletin of Engineering Geology and the Environment*, *74(3)*, 815-826.

Singh, B., Jethwa, J.L., Dube, A.K. & Singh, B. (1992). Correlation between observed support pressure and rock mass quality. *Tunnelling and Underground Space Technology, 7(1),* 59-74.

Singh, M., Singh, B., & Choudhari, J. (2007). Critical strain and squeezing of rock mass in tunnels. *Tunnelling and Underground Space Technology*, *22(3)*, 343-350.

Standard, ASTM (2001). ASTM C150: Standard specification for Portland cement. *Annual Book of ASTM Standards, American Society for Testing and Materials, West Conshohocken, PA*.

Standard, ASTM (2008). ASTM D4543: Standard Practices for Preparing Rock Core as Cylindrical Test Specimens and Verifying Conformance to Dimensional and Shape Tolerances. *Annual Book of ASTM Standards, American Society for Testing and Materials, West Conshohocken, PA.*

Standard, ASTM (2010). ASTM D7012-10: Standard test method for compressive strength and elastic moduli of intact rock core specimens under varying states of stress and temperature. *Annual Book of ASTM Standards, American Society for Testing and Materials, West Conshohocken, PA.*

Steiger, R.P. & Leung, P. (1991). Critical state shale mechanics. *In Proceedings of the 32nd U.S. Symposium on Rock Mechamics*, 293–302.

Steiner, W. (1996). Tunnelling in squeezing rocks: case histories. *Rock Mechanics and Rock Engineering*, *29(4)*, 211-246.

Sterpi, D. & Gioda, G. (2009). Visco-plastic behaviour around advancing tunnels in squeezing rock. *Rock Mechanics and Rock Engineering*, *42(2)*, 319-339.

Sterpi, D.V. (2007). Ground pressure and convergence for TBM driven tunnels in visco-plastic rocks. *In Proceedings of the ECCOMAS Thematic Conference on Computational Methods in Tunneling EURO: TUN, Vienna University of Technology*, 1-54.

Stimpson, B. (1970). Modelling materials for engineering rock mechanics. *International Journal of Rock Mechanics and Mining Sciences & Geomechanics Abstracts 7(1)*, 77-121.

Sulem, J., Panet, M. & Guenot, A. (1987). An analytical solution for time-dependent displacements in a circular tunnel. *International journal of rock mechanics and mining sciences & geomechanics abstracts, Pergamon, 24(3),* 155-164.

Tanimoto, C. (1984). NATM-1. *Morikita Shuppan*, 168–175.

Terzaghi, K. (1936). Stress distribution in dry and in saturated sand above a yielding trap-door. *International Conference on Soil Mechanics Proceedings*, *1*, 307-311.

Terzaghi, K. (1943). Theoretical Soil Mechanics. *Wiley, New York,* 44-48.

Terzaghi, K. (1946). Rock defects and loads on tunnel supports. Rock tunneling with steel supports. *In Proctor, R.V., White, T.L. (Eds.), Commercial Shearing and Stamping Company, Youngstown, OH*, 45-92.

Tiwari, G., Pandit, B., Gali, M.L. & Babu, G.L. (2018). Analysis of tunnel support requirements using deterministic and probabilistic approaches in average quality rock mass. *International Journal of Geomechanics, 18(4),* 1-20.

Tran-Manh, H., Sulem, J. & Subrin, D. (2016). Progressive degradation of rock properties and time-dependent behavior of deep tunnels. *Acta Geotechnica, 11(3),* 693-711.

Verman, M.K. (1993). Rock mass-tunnel support interaction analysis. *Ph. D. Thesis, Indian Institute of Technology, Roorkee, India,* 45-65.

Vlachopoulos, N. & Diederichs, M.S. (2009). Improved longitudinal displacement profiles for convergence confinement analysis of deep tunnels. *Rock mechanics and rock engineering, 42(2),* 131-146.

Vrakas, A. & Anagnostou, G. (2014). A finite strain closed-form solution for the elastoplastic ground response curve in tunnelling. *International Journal of Numerical and Analytical Methods in Geomechanics, 38(11),* 1131–1148.

Vrakas, A., Dong, W. & Anagnostou, G. (2018). Elastic deformation modulus for estimating convergence when tunnelling through squeezing ground. *Géotechnique, 68(8),* 713-728.

Wang, X., Lai, J., Garnes. R.S. & Luo, Y. (2019). Support system for tunnelling in squeezing ground of Qingling-Daba mountainous area: a case study from soft rock tunnels. *Advances in Civil Engineering, 1,* 1-23.

Whyte, R. J. "A study of progressive hanging-wall caving at Chambishi copper mine in Zambia using the base friction model concept." PhD Thesis, University, Imperial College, 1973: 5-25.

Wiesmann, E. (1912). Mountain pressure. *Switz J Struct, 60,* 7-12.

Wood, A.M.M. (1972). Tunnels for roads and motorways. *Quarterly Journal of Engineering Geology and Hydrogeology, 5(1-2),* 111-126.

Yassaghi, A. & Salari-Rad, H. (2005). Squeezing rock conditions at an igneous contact zone in the Taloun tunnels, Tehran–Shomal freeway, Iran: a case study. *International Journal of Rock Mechanics and Mining Sciences, 42*, 95–108.

Yuen, C.M.K. (1980). Rock-structure time interaction in lined circular tunnels in high horizontal stress field. *Doctoral Thesis, University of Western Ontorio, Canada*, 24-36.

Zhang, R.J., Santoso, A.M., Tan, T.S. & Phoon, K.K. (2013). Strength of high water-content marine clay stabilized by low amount of cement. *Journal of Geotechnical and Geoenvironmental Engineering, 139(12)*, 2170-2181.

Zwilsky, K.M. & Langer, E.L. (2001). Vol. 2-Properties and Selection: Nonferrous Alloys and Special-Purpose Mater. *ASM International*, 1119-1124.

APPENDIX A - DATA FROM THE PROJECT

Table A-1 Description of the squeezing level for different value of squeezing number

Class number	**Squeezing number, *S***	**Squeezing level**	**Hoek and Marinos (2000)**	
			Squeezing level	**Tunnel strain (%)**
1	$S < 1$	Light to no squeezing	Few support problem	$\varepsilon_t < 1.0$
2	$1 < S < 2$	Light squeezing	Minor squeezing	$1.0 < \varepsilon_t < 2.5$
3	$2 < S < 7$	Fair to moderate squeezing	Severe squeezing	$2.5 < \varepsilon_t < 5.0$
4	$7 < S < 17$	High to very high squeezing	Very severe squeezing	$5.0 < \varepsilon_t < 10.0$
5	$S > 17$	Extremely high squeezing	Extreme squeezing	$\varepsilon_t > 10$

Table A-2 Mix proportion for the synthetic mudstone prepared in the laboratory.

Component (unit)	Cement content, *C*	Water to cement ratio by weight, *w*/*c*	Quantity required for 1 m^3 of the mix			
			Clay (kg)	Cement (kg)	Water (kg)	Superplasticizer, MasterGlenium 7920 (litres)
Quantity	0.3	1.5	859.79	368.48	552.72	45

Table A-3 Physical and mechanical properties of synthetic mudstone after 28 days of curing.

Property	Saturated unit weight, Υ_{sat} (kN/m^3)	Dry unit weight, Υ_{dry} (kN/m^3)	Void ratio, *e*	Water content, w_w (%)	At strain rate = 10^{-5} s^{-1}		
					UCS, σ_c (MPa)	Elastic modulus, E_{50} (GPa)	Poisson's ratio, ν
Value	18.12	12.93	1.20	45	4.47 ± 0.15	0.65 ± 0.02	0.13

Table A-4 Burger's model parameters for the creep behavior of synthetic mudstone

Stress level	**Burger's model parameters**			
	E^M **(MPa)**	E^K **(MPa)**	η^M **(MPa.hour)**	η^K **(MPa.hour)**
$0.40\sigma_c$	680	93	1.93×10^5	3.81×10^3
$0.50\sigma_c$	701	91	1.38×10^5	3.86×10^3
$0.75\sigma_c$	695	95	1.50×10^5	3.51×10^3
Average value	692	93	1.60×10^5	3.73×10^3

Table A-5 Curve fitting parameters for the four-loading stage and different X.

p_o/σ_c	$X = x_f/R$	Proposed model parameters $(u/R = a - b(d)^t)$			Coefficient of determination R^2
		a	b	d	
0.5	0	0.45	0.27	0.62	0.99
	0.8	0.80	0.24	0.67	0.98
	1.6	1.64	0.63	0.72	0.99
	2.4	1.84	0.43	0.72	0.99
	3.2	2.05	0.25	0.75	0.95
	4.0	2.46	0.36	0.48	0.99
	4.8	2.42	0.31	0.57	0.95
1.0	0	1.64	0.62	0.96	0.93
	0.8	2.21	0.95	0.97	0.97
	1.6	3.30	1.00	0.95	0.96
	2.4	3.39	1.26	0.96	0.96
	3.2	3.90	1.25	0.97	0.96
	4.0	3.93	1.05	0.96	0.93
	4.8	4.35	1.31	0.96	0.93
1.5	0	4.46	2.31	0.98	0.99
	0.8	5.52	2.51	0.97	0.98
	1.6	6.38	2.29	0.98	0.98
	2.4	6.32	2.01	0.98	0.95
	3.2	6.82	2.27	0.98	0.98
	4.0	7.02	2.41	0.98	0.98
	4.8	7.54	2.40	0.99	0.96
2.0	0	10.76	5.33	0.99	0.97
	0.8	10.81	4.53	0.98	0.99
	1.6	13.29	6.35	0.99	0.99
	2.4	13.06	5.53	0.99	0.99
	3.2	13.18	5.42	0.99	0.99
	4.0	13.21	5.39	0.99	0.99
	4.8	13.95	5.66	0.99	0.99

Table A-6 LDP model parameters for supported and unsupported tunnel.

p_o/σ_c	$X = x_f/R$	Supported tunnel $(u/R = a_s - b_s(d_s)^t)$				Unsupported tunnel*		
		a_s	b_s (x 10^{-3})	d_s	Coefficient of determination	a	b	d
1.0	0.90	0.02	0.85	0.76	0.87	2.43	1.22	0.98
	1.80	0.05	2.21	0.87	0.96	2.92		
	2.70	0.08	3.02	0.66	0.89	3.41		
	3.60	0.09	4.10	0.50	0.88	3.90		
	4.50	0.09	2.68	0.85	0.88	4.39		
1.5	0.90	0.13	82.96	0.99	0.99	5.45	2.65	
	1.80	0.13	49.49	0.98	0.99	5.95		
	2.70	0.25	112.78	0.94	0.98	6.46		
	3.60	0.39	86.37	0.94	0.99	6.97		
	4.50	0.42	180.89	0.92	0.98	7.48		
2.0	0.90	0.17	34.51	0.96	0.95	11.65	4.59	
	1.80	0.30	86.70	0.95	0.94	12.22		
	2.70	0.40	64.07	0.95	0.94	12.80		
	3.60	0.51	56.85	0.93	0.94	13.37		
	4.50	0.64	102.31	0.95	0.93	13.94		
2.5	0.90	0.31	76.97	0.98	0.99	20.65	7.04	
	1.80	0.41	149.99	0.98	0.99	21.30		
	2.70	0.61	131.83	0.98	0.97	21.94		
	3.60	0.77	156.29	0.97	0.98	22.59		
	4.50	0.92	187.74	0.99	0.99	23.24		
3.0	0.90	0.46	92.09	0.98	0.99	32.76	9.98	
	1.80	0.58	84.65	0.94	0.96	33.51		
	2.70	0.93	251.48	0.98	0.92	34.27		
	3.60	1.31	401.45	0.99	0.95	35.02		
	4.50	1.36	366.36	0.98	0.96	35.78		

* The value presented in the Table are extracted from the LDP model for the unsupported tunnel proposed in Chapter 5

APPENDIX B – TECHNOLOGY TRANSFER ACTIVITIES

1 Accomplishments

1.1 What was done? What was learned?

We developed an experimental setup to study tunnels in squeezing ground conditions. The scale physical model studies important features of tunnel construction such as tunnel boring machine (TBM) excavation, three-dimensional effect of tunnel excavation, damages and deformations around the tunnel boundary, and time-dependent behavior of the tunnel boundary at field stress level. Based on the observations during the experiments an equation to determine the longitudinal displacement profile (LDP) with time was developed for supported as well as unsupported tunnels. A criterion for the selection of the tunnel support system in squeezing ground was also proposed based on the case studies and experimental results.

1.2 How have the results been disseminated?

Dissemination through 4 journal paper and 4 international conference presentations. Furthermore, Ketan Arora's Ph.D. thesis was funded by UTC-UTI and is archived at Colorado School of Mines Library.

2 Participants and Collaborating Organizations

Name: Colorado School of Mines
Location: Golden, CO, USA
Contribution: All research performed on campus

3 Outputs

Journal publications

Arora, K., Gutierrez, M., and Hedayat, A. Tunnels in squeezing clay-rich rocks, Underground Space, 2020 (In press). DOI: https://doi.org/10.1016/j.undsp.2020.07.001

Arora, K., Gutierrez, M., and Hedayat, A., New physical model to study tunnels in squeezing clay-rich rocks, Geotechnical Testing Journal (Under revision- Manuscript ID: GTJ-2020-0081.R1).

Arora, K., Gutierrez, M., Hedayat, A, and Cruz, E.C., Time-dependent Behavior of the Tunnels in Squeezing Ground: An Experimental Study, Rock Mechanics and Rock Engineering (Under review- Manuscript ID: RMRE-D-20-00712).

Arora, K., Gutierrez, M., and Hedayat, A., Rock-Support Interaction and Methodology for the Support Selection for the Tunnel in Squeezing Ground (Submission Pending).

Presentations

Arora, K., Gutierrez, M., and Hedayat, A., (2018) Experimental setup for studying tunnels in squeezing ground conditions, In World Tunneling Congress (WTC), 3515-3524, Naples, Italy.

Arora, K., Gutierrez, M., and Hedayat, A., (2019), Miniature Tunnel Boring Machine for Simulating Tunnel Excavation in Squeezing Ground Conditions, 4th International Conference on Tunnel Boring Machine in Difficult Ground: TBM Digs, Denver, CO, USA.

Arora, K., Gutierrez, M., and Hedayat, A. (2020), Physical Modeling of Lined Tunnel in Squeezing Ground Conditions, In Geo-Congress 2020: Engineering, Monitoring, and Management of Geotechnical Infrastructure, 335-344, Minneapolis, Minnesota, 2020.

Arora, K., Gutierrez, M., and Hedayat, A. (2020), Characterization of Synthetic Mudstone for Physical Model Studies, In 54th US Rock Mechanics/Geomechanics Symposium: American Rock Mechanics Association, Golden, Colorado, 2020.

4 Outcomes

The designed experimental setup has been successful in studying the time-dependent behavior of the tunnels constructed in squeezing ground conditions. Further, the proposed equation of LDP with time can be helpful in the estimation of the tunnel wall deformation prior to excavation and valuable for the appropriate design of the tunnel support system in squeezing ground.

5 Impacts

The research contained in this report, submitted journal publications, conference presentations and Ph.D. thesis provides the basis for the time-dependent behavior of tunnels in squeezing ground. The new approach will allow for a more scientific, data driven, and logical evaluation of the interaction between the tunnel support system and the squeezing ground.